



UNIVERSIDADE FEDERAL DO CEARÁ
CENTRO DE TECNOLOGIA
DEPARTAMENTO DE ENGENHARIA DE TRANSPORTES
PROGRAMA DE PÓS-GRADUAÇÃO EM ENGENHARIA DE TRANSPORTES

RENAN SANTOS MAIA

**CONTRIBUTIONS TO THE TIRE-PAVEMENT FRICTION CHARACTERIZATION
FROM THE TRAFFIC SAFETY PERSPECTIVE**

FORTALEZA

2020

RENAN SANTOS MAIA

CONTRIBUTIONS TO THE TIRE-PAVEMENT FRICTION CHARACTERIZATION
FROM THE TRAFFIC SAFETY PERSPECTIVE

M.Sc. Thesis presented to the Graduate Program in Transport Engineering of the Universidade Federal do Ceará, as a partial fulfillment of the requirements for the Master's Degree in Transport Engineering. Concentration Area: Transport Infrastructure.

Advisor: Verônica Teixeira Franco Castelo Branco, Ph.D.

FORTALEZA

2020

Dados Internacionais de Catalogação na Publicação
Universidade Federal do Ceará
Biblioteca Universitária

Gerada automaticamente pelo módulo Catalog, mediante os dados fornecidos pelo(a) autor(a)

M188c Maia, Renan Santos.

Contributions to the Tire-pavement Friction Characterization from the Traffic Safety Perspective / Renan Santos Maia. – 2020.

151 f.: il. color.

Dissertação (mestrado) – Universidade Federal do Ceará, Centro de Tecnologia, Programa de Pós-Graduação em Engenharia de Transportes, Fortaleza, 2020.

Orientação: Profa. Dra. Verônica Teixeira Franco Castelo Branco.

1. Tire-pavement friction. 2. Traffic Safety. 3. Digital Image Processing. 4. Microscopic Simulation. 5. Urban Environment. I. Título.

CDD 388

RENAN SANTOS MAIA

CONTRIBUTIONS TO THE TIRE-PAVEMENT FRICTION CHARACTERIZATION
FROM THE TRAFFIC SAFETY PERSPECTIVE

M.Sc. Thesis presented to the Graduate Program in Transport Engineering of the Universidade Federal do Ceará, as a partial fulfillment of the requirements for the Master's Degree in Transport Engineering. Concentration Area: Transport Infrastructure.

Approved in: ___/___/____.

COMMITTEE

Verônica Teixeira Franco Castelo Branco, Ph.D. (Advisor)
Universidade Federal do Ceará (UFC)

Flávio José Craveiro Cunto, Ph.D.
Universidade Federal do Ceará (UFC)

Ramez Muhammad Hajj, Ph.D.
University of Illinois at Urbana-Champaign (UIUC)

Elisabete Fraga de Freitas, D.Sc.
Universidade do Minho (UMINHO)

To my family and friends, for their support and love.

Words are not enough to express my gratitude.

ACKNOWLEDGEMENTS

These acknowledgements will be written partially in English and partially in Portuguese.

Em primeiro lugar, quero agradecer à minha orientadora, professora Verônica Castelo Branco, por seu apoio em todos os momentos. Gratidão por todas as oportunidades que foram abertas a mim e mudaram minha vida.

Thanks to the members of this committee, professors Flávio Cunto, Ramez Hajj, and Elisabete Freitas, for accepting this invitation and dedicating their time to contribute to this research. Also, many thanks to the members of my qualification committee, professors Flávio Cunto, Marcelo Medeiros, and Ramez Hajj, for their contributions to this work.

A todos do Programa de Pós-Graduação em Engenharia de Transportes (PETRAN) e do Departamento de Engenharia de Transportes (DET), alunos, funcionários, servidores e professores, pelo trabalho e dedicação para dar a nós, estudantes da universidade pública, estrutura e educação de qualidade.

Aos professores Marcelo Medeiros e Lucas Babadopulos, pela parceria na condução dos estudos envolvendo o método de modelagem tridimensional. Aos amigos Sued Costa, Victor Mosca, Aldaianny Maia e Rômulo Mesquita, pela parceria na condução dos ensaios de campo. Estendo este agradecimento à Insttale Engenharia LTDA e ao Laboratório de Mecânica dos Pavimentos (LMP/DET/UFC), pela estrutura disponibilizada para a realização deste trabalho.

A todos os amigos do grupo de Caracterização Avançada de Materiais para a Pavimentação (CAMP), pela troca de experiências e conhecimentos.

À CAPES, pelo apoio financeiro ao longo deste Mestrado.

Finalmente, à minha família e aos meus amigos. Dos mais novos aos mais velhos, dos mais antigos aos mais recentes, vocês sempre foram meu porto seguro. Juntos, compartilhamos os bons momentos e fazemos os momentos difíceis parecerem mais fáceis. Guardo cada um de vocês em um lugar muito especial. Nunca haverá palavras suficientes para expressar a minha gratidão por tudo que vocês fizeram e fazem por mim.

“O mundo é uma escola
A vida é o circo
Amor: palavra que liberta
Já dizia o profeta”
(Marisa Monte)

O presente trabalho foi realizado com apoio da Coordenação de Aperfeiçoamento de Pessoal de Nível Superior - Brasil (CAPES) - Código de Financiamento 001

ABSTRACT

The WHO recognizes traffic-related crashes as a public health problem, caused by a complex set of factors, many of which are related to transportation engineering. When it comes to infrastructure, the Traffic Safety Performance (TSP) is a function of the tire-pavement friction. Even so, roadway operators and urban authorities generally ignore this property in the pavement design and construction practices, taking safety-related strategies and decisions only after the occurrence of crashes. The two first stages of this work aimed to employ Digital Image Processing (DIP) techniques such as the Aggregate Imaging Measurement System (AIMS) and the Close-Range Photogrammetry (CRP) to predict the tire-pavement friction coefficient (μ) in the laboratory and to measure it in the field. Firstly, this research applied a predictive model of μ from aggregate shape properties, mixture gradations, and traffic. In the second stage of this research, a typical airport pavement mixture was designed and compacted in full-scale sections using 8 different protocols. For the texture analysis, traditional tests (sand patch – SP, and British pendulum - BP) and DIP techniques (AIMS and CRP) were applied. As a result, models for estimating the post-construction μ were proposed from parameters obtained from the AIMS texture analysis (MPD), and from the analysis of three-dimensional CRP models (MPD and V_{mp}). Finally, the assessment of vehicular conflicts in different urban scenarios was performed using microscopic traffic simulation (VISSIM software) and Surrogate Measures of Safety (SMoS) to support the proposition of minimum and ideal requirements of μ based on TSP parameters. TSP indicators are used to compare two main conditions: the necessary deceleration rates for vehicles to avoid a crash (DRAC), and the maximum available deceleration rates (MADR). DRAC was obtained using microscopic traffic simulation and vehicle trajectory analysis tools (SSAM3 software). MADR is a function of μ , vehicles' speeds, as well as road characteristics. Typical corridors of Fortaleza were represented in this simulation effort, resulting in the definition of the μ limits of 0.20 (minimum) and 0.65 (ideal) for the Fortaleza urban scenarios. Based on this analysis, material selection can be assessed in terms of the suitability for use in the urban environment. The main framework of this thesis can be summarized as follows: once a traffic simulation is performed, the TSP analysis using the SSAM tool and applying SMoS allows the estimation of required μ limits. The DIP tools presented (AIMS and CRP) can support the assessment of the estimated μ limits through contactless protocols. Furthermore, μ prediction based on material characteristics integrated into a database can indicate the suitability of construction or maintenance strategies for use in the urban environment.

Keywords: Tire-pavement friction; Traffic Safety; Digital Image Processing; Microscopic Simulation; Urban Environment.

RESUMO

A OMS reconhece os acidentes de trânsito como um problema de saúde pública, causado por um conjunto complexo de fatores, muitos dos quais relacionados à engenharia de transportes. Quando se trata de infraestrutura, o Desempenho de Segurança de Tráfego (TSP) é função do atrito pneu-pavimento. Mesmo assim, os operadores rodoviários e autoridades urbanas geralmente ignoram essa propriedade nas práticas de projeto e construção de pavimentos, tomando decisões e estratégias relacionadas à segurança somente após a ocorrência de acidentes. As duas primeiras etapas deste trabalho tiveram como objetivo empregar técnicas de Processamento Digital de Imagens (DIP), como o *Aggregate Imaging Measurement System* (AIMS) e a *Close-Range Photogrammetry* (CRP) para prever o coeficiente de atrito pneu-pavimento (μ) em laboratório e medi-lo em campo. Primeiramente, esta pesquisa propôs a utilização de um modelo preditivo de μ a partir das propriedades de forma de agregados, granulometrias de misturas e características do tráfego. Na segunda etapa desta pesquisa, uma mistura aeroportuária típica foi projetada e compactada em pistas em escala real, aplicando-se 8 diferentes protocolos. Para a análise de textura, foram aplicados testes tradicionais (Mancha de Areia - SP e Pêndulo Britânico - BP) e técnicas de DIP (AIMS e CRP). Como resultado, modelos para estimar μ na fase pós-construção foram propostos a partir de parâmetros obtidos na análise de textura a partir do AIMS (MPD), bem como de parâmetros obtidos na análise de modelos tridimensionais (MPD e V_{mp}). Por fim, a avaliação de conflitos veiculares em diferentes cenários urbanos foi realizada por meio de simulação microscópica de tráfego (*software VISSIM*) e *Surrogate Measures of Safety* (SMoS) para a proposição de requisitos mínimos e ideais de μ com base nos parâmetros do TSP. Os indicadores de TSP podem ser usados para comparar duas condições principais: as taxas de desaceleração necessárias para os veículos evitarem uma colisão (DRAC) e as taxas de desaceleração máximas disponíveis (MADR). O DRAC foi obtido usando ferramentas de simulação microscópica de tráfego e análise de trajetória de veículos (*software SSAM3*). Já o MADR é uma função de μ , velocidades dos veículos, bem como características da via. Corredores típicos de Fortaleza (Brasil) foram representados neste esforço de simulação, resultando na definição dos limites de μ de 0,20 (mínimo) e 0,65 (ideal) para os cenários urbanos de Fortaleza. Desta forma, as múltiplas possibilidades de seleção de materiais podem ser avaliadas em termos da sua adequação quanto ao uso no ambiente urbano. O principal arcabouço de contribuição desta dissertação pode ser resumido da seguinte forma: uma vez realizada uma simulação de tráfego, a análise do TSP usando a ferramenta SSAM3 e aplicando SMoS permite estimar os limites de μ a serem

cumpridos no cenário simulado. As ferramentas de DIP apresentadas (AIMS e CRP) permitem a avaliação do cumprimento dos limites de μ estimados a partir de procedimentos que não demandam a utilização de equipamentos de contato. Além disso, a previsão de μ baseada em características dos materiais oriundas de um banco de dados pode indicar a adequação das estratégias de construção ou manutenção a serem utilizadas no ambiente urbano.

Palavras-Chave: Atrito pneu-pavimento; Segurança de Tráfego; Processamento Digital de Imagens; Simulação microscópica; Ambiente urbano.

LIST OF FIGURES

Figure 1 - Paved area used for leisure in São Paulo, Brazil (a), and solar panels installed on a roadway in China (b).....	2
Figure 2 - Specific objectives' framework	6
Figure 3 - Forces developed at the tire-pavement interface with vehicles' motion.....	8
Figure 4 - Adhesion and hysteresis mechanisms of friction.....	9
Figure 5 - AIMS surface texture variation with time of Micro-Deval polishing.....	16
Figure 6 - Slabs compaction and polishing devices	19
Figure 7 - Predicted <i>versus</i> measured IFI by Kassem <i>et al.</i> (2013) model	20
Figure 8 - Predicted <i>versus</i> measured IFI by the Aldagari <i>et al.</i> (2020) model.....	21
Figure 9 - Predicted <i>versus</i> measured MPD by the Aldagari <i>et al.</i> (2020) model.....	22
Figure 10 - Chapter 2 method framework	29
Figure 11 - TMF over the years for different traffic volumes in the city of Fortaleza	33
Figure 12 - Initial IFI (F60) prediction (average, SD, and CV) for different gradations	34
Figure 13 - Boxplots of predicted initial IFI(F60) for different gradations.....	34
Figure 14 - Influencing points according to residuals' analysis (constant Leverage graph)	36
Figure 15 - Initial IFI (F60) prediction (average, SD, and CV) for different aggregates.....	38
Figure 16 - Boxplots of predicted F60 for different aggregates' sources	38
Figure 17 - Influencing points according to residuals analysis (Constant Leverage graph)	39
Figure 18 - Terminal IFI results in terms of the different gradations and mineral aggregates .	41
Figure 19 - Predicted MPD values trough 20 years in service	43
Figure 20 - Variation of IFI for different aggregate sources.....	44
Figure 21 - Analysis of different maintenance strategies according to gradation and aggregate source.....	45
Figure 22 - Comparison between predicted IFI _{final} and worn section in field.....	47
Figure 23 - AIMS asphalt mixture texture analysis process	53
Figure 24 - Representation of image taking of a target surface using the CRP technique	57
Figure 25 - 3D models of two asphalt mixtures	58
Figure 26 - Comparison between an actual and a CRP-measured profiles	58
Figure 27 - Aachen Polishing Machine	60
Figure 28 - Processing method performed in MoutainsMap.....	62
Figure 29 - Chapter 3 method framework	64
Figure 30 - Size distribution and design parameters of the asphalt mixture	66

Figure 31 - Comparison between gradations	67
Figure 32 - Construction of the full-scale experimental runways	67
Figure 33 - Upper view of the runways	68
Figure 34 - Macrotexture parameters obtained from an AIMS-processed profile	70
Figure 35 - AIMS stone matrix surface texture and asphalt mixture microtexture results (classification limits from IBIAPINA, 2018)	70
Figure 36 - Extraction, preparation and analysis of cores in AIMS	71
Figure 37 - CRP analysis method	73
Figure 38 - Friction ~ AIMS MPD parameter model 95% confidence and prediction interval	76
Figure 39 - MTD (SP test) ~ MPD (AIMS) parameter model 95% confidence interval	77
Figure 40 - Friction models obtained through the analysis of CRP parameters	79
Figure 41 - MTD results obtained using different techniques	82
Figure 42 - Correlation between ISO and the unified MTD parameters from different techniques	83
Figure 43 - Statistical analysis of compaction significance for macrotexture results	87
Figure 44 - Friction coefficient obtained through different techniques	89
Figure 45 - Safety continuum concept	93
Figure 46 - Heat maps for footage-observed (left) and simulator-predicted (right) vehicular conflicts	98
Figure 47 - Chapter 4 simplified method framework	100
Figure 48 - Wiedemann (1974) model	100
Figure 49 - Road networks to be evaluated in this work	102
Figure 50 - Speed reduction simulation in VISSIM	104
Figure 51 - Fortaleza city selected typical arterial corridor	105
Figure 52 - MADR variation for different μ values	107
Figure 53 - Assessment of materials' suitability to urban environments in terms of friction and traffic safety	110
Figure 54 - Analysis of μ limits for PFC (DNER 386/1999 – ES, Range II – Lower) and NE aggregates	117
Figure 55 - Analysis of μ limits for DG (DNIT 031/2006 – ES, Range C - Upper) and South-east Brazil aggregates	117
Figure 56 - Assessment of the maintenance strategy of replacement of aged asphalt wearing course with PFC	121
Figure 57 - Summary of the research contributions	124

LIST OF TABLES

Table 1 - CMF examples for roadways' friction improvement	4
Table 2 - Texture scales	8
Table 3 - Adjustment constants for Sp obtention from the use of different macrotexture measurement equipment	11
Table 4 - Adjustment constants for obtaining IFI obtention from friction tests	11
Table 5 - American and Brazilian aggregate shape properties classification systems.....	27
Table 6 - Weibull distribution parameters for different standardized mixture gradations.....	30
Table 7 - Aggregates' parameters database.....	32
Table 8 - ANOVA results for IFI predicted from different gradations.....	35
Table 9 - Tukey HSD test results for gradations.....	36
Table 10 - ANOVA results for IFI predicted from different aggregate groups.....	39
Table 11 - Tukey HSD test results for the Northeast aggregates	40
Table 12 - Tukey HSD test results for the Southeast aggregates	40
Table 13 - ANOVA analysis assessment of “gradation” and “aggregate source” significance in the IFI _{final} results	42
Table 14 - Texture measurement tests	51
Table 15 - Friction measurement tests	51
Table 16 - Classification systems for aggregates surface texture (AIMS parameter)	55
Table 17 - Aggregates shape properties	65
Table 18 - Summary of compaction and texture results	68
Table 19 - Texture parameters from ISO 25178-2 (2012)	74
Table 20 - Correlation matrix between texture, friction and AIMS-obtained parameters	75
Table 21 - Friction ~ AIMS MPD parameter model statistics	75
Table 22 - MTD (SP test) ~ MPD (AIMS) parameter model statistics	76
Table 23 - Microtexture results (AIMS) for the sections 1 to 8	78
Table 24 - Levelled 3D model parameters' correlation matrix.....	81
Table 25 - R ² values between ISO parameters and microtexture results	85
Table 26 - Paired Tukey test for comparison between compaction solutions	88
Table 27 - Tukey test matrix for verification of statistical differences between methods	89
Table 28 - Conflicts' classification according to angle and trajectory.....	93
Table 29 - Summary of proxy indicators' meanings.....	94
Table 30 - Typical values for driving behavior parameters	101

Table 31 - Expressway calibration parameters	103
Table 32 - MADR inputs	107
Table 33 - Gradations of different Brazilian traditional mixtures	108
Table 34 - Aggregates' database	109
Table 35 - Conflicts and proxy indicators results for an expressway	111
Table 36 - Summary of speed results for conflicts in an expressway.....	111
Table 37 - Minimum μ requirements for an expressway.....	112
Table 38 - Conflicts and proxy indicators results for deceleration waves in an expressway .	113
Table 39 - Summary of speed results for conflicts in deceleration waves in an expressway .	113
Table 40 - Minimum μ requirements for deceleration waves in an expressway	113
Table 41 - Typical urban arterial corridor conflicts and proxy indicators results.....	114
Table 42 - Minimum μ requirements	115
Table 43 - Summary of speed results for conflicts in a typical urban corridor	115
Table 44 - ANOVA analysis for DRAC comparison in different scenarios	116
Table 45 - Proposed μ limits to inform materials' selection.....	116

LIST OF ACRONYMS

AADT:	Average Annual Daily Traffic
a_{agg} :	Terminal Surface Texture
$a_{agg} + b_{agg}$:	Initial Surface Texture
ABS:	Anti-lock Braking System
AC:	Asphalt Concrete
a_{GA} :	Aggregate Terminal Angularity
$a_{GA} + b_{GA}$:	Aggregate Initial Angularity
AIMS:	Aggregate Imaging Measurement System
AMD:	After Micro-Deval
a_{mix} :	Terminal IFI (F60)
$a_{mix} + b_{mix}$:	Initial IFI (F60)
ANOVA:	Analysis of Variance
APM:	Aachen Polishing Machine
ASTM:	American Society for Testing and Materials
a_{TX} :	Aggregate Terminal Surface Texture
$a_{TX} + b_{TX}$:	Aggregate Initial Surface Texture
ax :	Standstill distance in front of static obstacles
BMD:	Before Micro-Deval
BP:	British Pendulum
bx_{add} :	Additive Factor of Security Distance
bx_{mult} :	Multiplicative Factor of Security Distance
c_{agg} :	Aggregate rate of change in texture
CD:	Compaction Degree
c_{GA} :	Aggregate rate of change in angularity
CMF:	Crash Modification Factor
c_{mix} :	Mixture rate of change in IFI (F60)
CNT:	Confederação Nacional do Transporte (Brazil's National Transport Confederation)
CPI:	Crash Potential Index
CRP:	Close-Range Photogrammetry
CTMeter:	Circular Texture Meter

CTV:	Cumulative Traffic Volume
CTX:	Aggregate rate of change in surface texture
CV:	Coefficient of Variation
D ₉₀ :	Diameter immediately higher than 90% of particles' gradation
DAC:	Gneiss aggregate from Ceará, Brazil
DBI:	Phonolite aggregate from Ceará, Brazil
DBJ:	Phonolite aggregate from Ceará, Brazil
DCC:	Gneiss aggregate from Ceará, Brazil
DDC:	Gneiss aggregate from Ceará, Brazil
D _f :	Aggregate fractal dimension
DFT:	Dynamic Friction Tester
DG:	Dense-graded
DIP:	Digital Image Processing
DIRENG:	Diretoria de Engenharia Aeronáutica (Brazilian Aeronautic Engineering Directory)
DNER:	Departamento Nacional de Estradas de Rodagem (Former Brazilian National Department of Roadways)
DNIT:	Departamento Nacional de Infra-Estrutura de Transportes (Brazilian National Department of Transport Infrastructures)
DRAC:	Deceleration Rate to Avoid a Crash
EBC:	Empresa Brasil de Comunicação (Brazilian Public Communication Company)
ESAL:	Equivalent Single Axle Load
ET:	Encroachment Time
F(S):	Friction-speed function
F60:	Harmonized Friction Coefficient at 60 Km/h
FFS:	Free Flow Speed
FG:	Fine-graded
FHWA:	Federal Highway Administration
Gradation A:	Dense-graded Roadway Mixture - DNIT 031/2006 - ES - Range C - Lower Limit
Gradation B:	Dense-graded Roadway Mixture - DNIT 031/2006 - ES - Range C - Upper Limit

Gradation C:	Fine-graded Roadway Mixture - DNIT 032/2005 - ES - Range A - Lower Limit
Gradation D:	Fine-graded Roadway Mixture - DNIT 032/2005 - ES - Range A - Upper Limit
Gradation E:	Porous Friction Course Roadway/Airport Mixture - DNER 386/1999 - ES - Range II - Lower Limit
Gradation F:	Porous Friction Course Roadway/Airport Mixture - DNER 386/1999 - ES - Range II - Upper Limit
Gradation G:	Porous Friction Course Roadway/Airport Mixture - DNER 386/1999 - ES - Range V - Lower Limit
Gradation H:	Porous Friction Course Roadway/Airport Mixture - DNER 386/1999 - ES - Range V - Upper Limit
Gradation I:	Dense-graded Airport Mixture - DIRENG 04.05.610 (2002) - Range II - Lower Limit
Gradation J:	Dense-graded Airport Mixture - DIRENG 04.05.610 (2002) - Range II - Upper Limit
Gradation K:	Dense-graded Airport Mixture - DIRENG 04.05.610 (2002) - Range III - Lower Limit
Gradation L:	Dense-graded Airport Mixture - DIRENG 04.05.610 (2002) - Range III - Upper Limit
GT (Proxy Indicator):	Gap Time
GT (Equipment):	Grip Tester
HCM:	Highway Capacity Manual
HMA:	Hot-mix Asphalt
Hs:	Height of Sand
HSD:	Honestly Significant Difference
IFI:	International Friction Index
iPas:	Image Processing & Analysis System
ISO:	International Standardization Organization
k:	Weibull parameter (Shape)
LAA:	Los Angeles Abrasion
LLS:	Laser Profilometer
LPSD:	Logarithmic Power Spectral Density

MADR:	Maximum Available Deceleration Rate
MD:	Micro-Deval
MPD:	Mean Profile Depth (ASTM E1845-15, 2015)
MTD:	Mean Texture Depth (ASTM E965-15, 2015)
MTD _{est} :	Estimated Mean Texture Depth
NCAT:	National Center for Asphalt Technology
NMAS:	Nominal Maximum Aggregate Size
OG:	Open-Graded
OGFC:	Open-Graded Friction Course
PET:	Post-Encroachment Time
PFC:	Porous Friction Course
PG:	Performance Grade
PIARC:	Permanent International Association of Road Congresses
PSV:	Polishing Stone Value
PSV _{diff} :	Differential Polishing Stone Value
RGF:	Robust Gaussian Filter
RMS:	Root Mean Square (ISO 4287-97, 1997)
RSP:	Road Safety Performance
S _a :	Arithmetic mean height - ISO 25178-2 (2012)
SD:	Standard Deviation
S _{dv} :	Average valleys volume - ISO 25178-2 (2012)
SF:	Saturation Flow
SH:	Saturation Headway
S _{hv} :	Average peaks volume - ISO 25178-2 (2012)
SMoS:	Surrogate Measures of Safety
SN:	Skid Number
SP:	Sand Patch
Sp (IFI Method):	Speed Constant
S _p :	Peak height - ISO 25178-2 (2012)
S _{pd} :	Peaks density - ISO 25178-2 (2012)
S _q :	Average height - ISO 25178-2 (2012)
SRV:	Skid Resistance Value
SRV35:	Skid Resistance Value at 35°C

SSAM:	Surrogate Safety Assessment Model
S_v :	Maximum valley depth - ISO 25178-2 (2012)
S_z :	Maximum height - ISO 25178-2 (2012)
TA:	Time to Accident
TBA:	Basalt aggregate from São Paulo, Brazil
TGN:	Migmatic gneiss aggregate from Rio de Janeiro, Brazil
TGR:	Granitoid aggregate from Rio de Janeiro, Brazil
TLE:	Leucosome aggregate from Rio de Janeiro, Brazil
TMC:	Meta-limestone aggregate from Minas Gerais, Brazil
TMF:	Traffic Multiplication Factor
TML:	Melanosome aggregate from Rio de Janeiro, Brazil
TPA:	Paleosome aggregate from Rio de Janeiro, Brazil
TPE:	Pegmatite aggregate from Rio de Janeiro, Brazil
TSP:	Traffic Safety Performance
TTC:	Time to Collision
UTBWC:	Ultra-Thin Bonded Wearing Course
VFA:	Voids Filled with Asphalt
V_m :	Total material volume - ISO 25178-2 (2012)
V_{mc} :	Core material volume - ISO 25178-2 (2012)
V_{mp} :	Peak volume (10% Threshold) - ISO 25178-2 (2012)
vph:	Vehicles per Hour
VUC:	Urban Cargo Vehicle
VV:	Air Voids
V_v :	Total voids volume - ISO 25178-2 (2012)
V_{vc} :	Core void volume - ISO 25178-2 (2012)
V_{vv} :	Valley volume (80% Threshold) - ISO 25178-2 (2012)
W/S:	Wehner/Schulze Equipment
WHO:	World Health Organization
XRD:	X-Ray Diffraction
XRF:	X-Ray Fluorescence Spectrometry
λ :	Weibull parameter (Scale)
λ_w :	Texture Wavelengths
μ :	Friction Coefficient

LIST OF CONTENTS

1	INTRODUCTION	1
1.1	Research problem	1
1.2	Research justification	2
1.3	Research questions	4
1.4	Research objectives	4
1.4.1	Main objective	4
1.4.2	Specific objectives	5
1.5	Thesis structure	6
1.6	Theoretical background	7
1.6.1	Tire-pavement interaction concepts	7
1.6.2	Texture and friction harmonization	10
2	A REVIEW OF TIRE-PAVEMENT FRICTION PREDICTION MODELS FROM ADVANCED LABORATORY CHARACTERIZATION OF MATERIALS	13
2.1	Initial considerations	13
2.2	Specific objective	14
2.3	Friction prediction models	14
2.3.1	Masad et al. (2007).....	14
2.3.2	Masad et al. (2009).....	16
2.3.3	Masad et al. (2010).....	18
2.3.4	Kassem et al. (2013).....	18
2.3.5	Chowdhury et al. (2017) and Aldagari et al. (2020).....	20
2.3.6	Siriphun et al. (2016).....	22
2.3.7	Siriphun et al. (2017).....	23
2.3.8	Chen et al. (2017)	24
2.4	The Aggregate Imaging Measurement System (AIMS)	25
2.5	Materials and methods	28
2.5.1	IFI prediction and measurement.....	29
2.5.2	Aggregate gradations.....	30
2.5.3	Aggregates' shape properties database by Diógenes (2018) and Trotta (2020)	31
2.5.4	Traffic consideration.....	32
2.6	Results and discussion	33

2.6.1	Analysis of initial IFI: Gradations.....	33
2.6.2	Analysis of initial IFI: Aggregates	37
2.6.3	Analysis of final IFI	41
2.6.4	Analysis of MPD and traffic	42
2.6.5	Field analysis.....	44
2.7	Partial conclusions.....	47
3	ADVANCES IN THE ANALYSIS OF ASPHALT PAVEMENTS' SURFACE TEXTURE AND FRICTION USING THE AGGREGATE IMAGING MEASUREMENT SYSTEM (AIMS) AND 3D COMPUTER VISION.....	49
3.1	Initial considerations.....	49
3.2	Specific objective	49
3.3	Literature review	50
3.3.1	Ordinary characterization of texture and friction	50
3.3.2	The Aggregate Imaging Measurement System (AIMS).....	52
3.3.3	The Close-Range Photogrammetry (CRP).....	55
3.4	Materials and methods.....	63
3.4.1	Full-scale test sections.....	64
3.4.2	Aggregate Imaging Measurement System (AIMS) analysis.....	69
3.4.3	Close-range photogrammetry (CRP) analysis.....	72
3.5	Results and discussion.....	74
3.5.1	AIMS.....	74
3.5.2	3D computer vision	78
3.5.3	Analysis of results from different techniques.....	81
3.5.4	Compaction assessment.....	86
3.5.5	Tire-pavement friction analysis.....	88
3.6	Partial conclusions.....	89
4	USING MICROSCOPIC SIMULATION TO ASSESS ASPHALT PAVEMENTS' TIRE-PAVEMENT FRICTION REQUIREMENTS	91
4.1	Initial considerations.....	91
4.2	Specific objective	92
4.3	Literature review	92
4.3.1	Proactive approach to Traffic Safety	92
4.3.2	Tire-pavement friction influence on TSP	95
4.3.3	Microscopic traffic simulation and safety analysis	96

4.3.4	Practical application of microscopic traffic simulation for TSP analysis.....	97
4.4	Materials and methods.....	99
4.4.1	Simulation framework.....	100
4.4.2	Case study one: default network – expressway.....	103
4.4.3	Case study two: forced speed reduction in an expressway	103
4.4.4	Case study three: typical urban arterial corridor	105
4.4.5	Traffic safety analysis considering tire-pavement friction.....	106
4.5	Results and discussion.....	110
4.5.1	Case study one: default network – expressway.....	110
4.5.2	Case study two: forced speed reduction in an expressway	112
4.5.3	Typical urban arterial corridor.....	113
4.5.4	Selecting asphalt materials for urban environments.....	116
4.6	Partial conclusions.....	118
5	CONCLUSIONS AND RECOMMENDATIONS FOR FUTURE WORKS	119
5.1	Practical application of this work	119
5.2	Final considerations	121
5.3	Recommendations for future works	125
	BIBLIGRAPHICAL REFERENCES	127
	Chapter 1	127
	Chapter 2	130
	Chapter 3	132
	Chapter 4	136
	APPENDIX 1 IFI HARMONIZATION	141
	APPENDIX 2 μ SUGGESTED LIMITS	146

1 INTRODUCTION

1.1 Research problem

According to official data records, from January to June 2018, 19,398 deaths and around 20,000 cases of permanent disability were recorded resulting from traffic crashes in Brazil. Such crashes represent a loss of 96.5 billion BRL (more than 20.0 billion USD) to the country (EBC, 2018). Estimates made by different sectors of civil society in Brazil point out that, in the last 10 years (2009 to 2018), 1.6 million citizens were hurt in traffic-related crashes. Also, rates of approximately 5 deaths and 20 injuries per hour are estimated to occur in the country because of such events.

Only on Brazilian federal highways, 5,332 deaths were recorded in 2019, the first increase in 7 years. According to data from the National Transport Confederation (CNT), the crash rate per 100 km of federal highways is approximately 5 times higher for roads subjectively classified as “in worst conditions”, compared to “in excellent conditions” roads (CNT, 2019). Based on the latest data from the official insurance company for traffic-related crashes in Brazil, a person dies in these events every 15 minutes in the country (SEGURADORA LÍDER, 2019).

Nowadays, traffic-related crashes are recognized as a public health problem. According to a report published by the World Health Organization (WHO, 2018), the number of traffic-related deaths is growing continuously in the world. This is an effect of the population and motorization growth occurring in many regions. Among the 5-29 years old population, traffic-related crashes are the leading cause of death worldwide. When it comes to all age groups, these events occupy the 8th position among the causes of deaths. In Brazil, WHO data (WHO, 2018) showed a rate of approximately 20 traffic-related deaths per 100,000 inhabitants, which remained stable over 10 years. On the other hand, countries such as Germany, France, and the United Kingdom achieved a decrease in this rate, which is now below 6 deaths per 100,000 inhabitants.

1.2 Research justification

As mentioned, traffic-related crashes have become a public health problem, caused by a deeply complex set of factors, many of which are part of the transport engineering areas of study (including transport infrastructures). The importance of transport infrastructures for society is obvious based on their large area in the urban environment and throughout all the Brazilian territory, which has the 4th largest road network in the world (ROAD TRAFFIC TECHNOLOGY, 2014). For example, the city of São Paulo alone is cut by 16,000 km of paved streets and avenues (SÃO PAULO CITY HALL, 2017). It has become an increasingly important pursuit by scientists and technicians to propose innovative uses of paved areas to meet objectives that go beyond vehicle traffic. These structures may also be the focus of efforts to mitigate social, environmental, and economic costs related to transportation, for example: the use of waste from different industries (LOPES *et al.*, 2015; CHOUDHARY *et al.*, 2020), energy harvesting (DUARTE and FERREIRA, 2016; JIANG *et al.*, 2017), atmospheric depollution (photocatalytic pavements) (ROCHA SEGUNDO *et al.*, 2018), and the promotion of the use of paved areas for leisure (GOMES *et al.*, 2011), as shown in Figure 1.

Figure 1 - Paved area used for leisure in São Paulo, Brazil (a), and solar panels installed on a roadway in China (b)



Sources: (a) Catraca Livre (2015); (b) Business Insider (2018).

The risk of traffic crashes is an issue related to the social costs of transportation. When it comes specifically to infrastructure studies, the Road Safety Performance (RSP) (or Traffic Safety Performance - TSP) is very much influenced by the quality of the friction developed at the tire-pavement interface. There is a logical trend that the higher the friction, the better the vehicles' deceleration performance to avoid crashes. Nevertheless, pavement design and construction practices generally ignore surface friction in favor of structural performance.

One exception is the design and construction of overlays, which require from engineers more attention to texture and friction properties. Furthermore, other factors also impair a better understanding of traffic safety issues, such as reduced regulatory rigor and the misperception that safety issues derive only from drivers' imprudence. In general, roadway operators and authorities make safety-related strategies and decisions only after the occurrence of crashes. Such reactive behavior is an ethical issue. An illustrative fact of such a lack of proactivity is that important information about TSP, such as the occurrence and severity of vehicular conflicts obtained from traffic microscopic simulations, is generally disregarded in the design, construction, and maintenance/rehabilitation phases of pavement service life analyses.

Part of the complexity of tire-pavement friction analysis is the fact that this phenomenon is not yet fully understood. Predicting this property in the laboratory and measuring it in the field is, therefore, a difficult task. However, the use of Digital Image Processing (DIP) has been potentializing the scientific development of many fields, including surface condition evaluation. One way to approach the tire-pavement friction phenomenon is to apply prediction models of frictional properties based on the characteristics of the materials used in asphalt pavements. Besides, some approaches aim to establish relationships between surface parameters obtained using the DIP and those obtained from standardized protocols, resulting in the combination of data for the estimation of tire-pavement friction in the field. These techniques may be applied both in a pre-construction and in a post-construction analysis. In this work, special attention is given to the use of the Aggregate Imaging Measurement System (AIMS) (MASAD, 2005; REZAEI *et al.*, 2011; ARAUJO *et al.*, 2015; CHOWDHURY *et al.*, 2017, ARAUJO *et al.*, 2019; ALDAGARI *et al.*, 2020), and three-dimensional surface modeling from the Close-Range Photogrammetry (CRP) (KOGBARA *et al.*, 2016; KOGBARA *et al.*, 2018).

Lyon and Persaud (2008) highlight the importance of tire-pavement friction, and its impact on the anti-skidding properties of asphalt surfaces. The authors employed an empirical Bayes before-after study to analyze the impact of improving friction at points with a high frequency of vehicular crashes in wet weather conditions in New York State (USA). The authors calculated the Crash Modification Factors (CMF) associated with the reduction in crash rates (e.g., a 0.8 CMF represents 20% fewer crashes than the expected for a specific location according to its crash prediction model). Table 1 shows general CMF values, which indicate that improving texture and friction (skid resistance) is, at a final stage of observation, a way to reduce crashes and save human lives.

Table 1 - CMF examples for roadways' friction improvement

CMF	Unadjusted Standard Error of CMF	Traffic Control Type	Crash Type	Area Type
0.799	0.028	-	All	All
0.667	0.050	Signalized	All	All
0.819	0.048	Stop-controlled	All	All
0.590	0.114	Yield sign	All	All

Source: adapted from Lyon and Persaud (2008) (Available on: <http://www.cmfclearinghouse.org>).

1.3 Research questions

In Brazil, generally, only when it comes to pavement maintenance and rehabilitation, texture and friction properties of the pavement surface are considered. However, it would be prudent to consider the impact of any pavement-engineering decisions on TSP in all phases of asphalt pavements' lifecycle, not only after construction. Because of this perception, transport engineers must proactively consider traffic safety. As mentioned, DIP and traffic microscopic simulation emerge as tools that may contribute to the proactive traffic safety approach. Therefore, the following research questions will be addressed in this work:

First research question: Is it possible to introduce a more proactive approach of tire-pavement friction and traffic safety consideration in the asphalt mixture design phase (pre-construction) using DIP for advanced materials characterization?

Second research question: Is it possible to improve the characterization of the tire-pavement conditions in post-construction assessments using DIP techniques such as AIMS and CRP?

Third research question: How can TSP analysis based on traffic microscopic simulation be used to set tire-pavement friction requirements, therefore guiding the rational selection of asphalt mixture materials from the perspective of their suitability for improving traffic safety in the urban environment?

1.4 Research objectives

1.4.1 Main objective

This thesis aims to provide contributions to the integration of knowledge between physical infrastructure and traffic planning/operation studies. Therefore, the main objective of this research is to integrate advanced, practical, and low-cost methods for the analyses of tire-pavement friction and TSP throughout the service life of asphalt pavements.

1.4.2 Specific objectives

As mentioned, the main objective of this research refers to the integration of knowledge from two different fields of transportation engineering studies to provide a safety-based assessment of tire-pavement friction throughout pavement service life. Hence, the structure of this thesis will be divided into two general parts: (i) transportation infrastructure, and (ii) transportation planning/operation.

The part one (transportation infrastructure) specific objectives are:

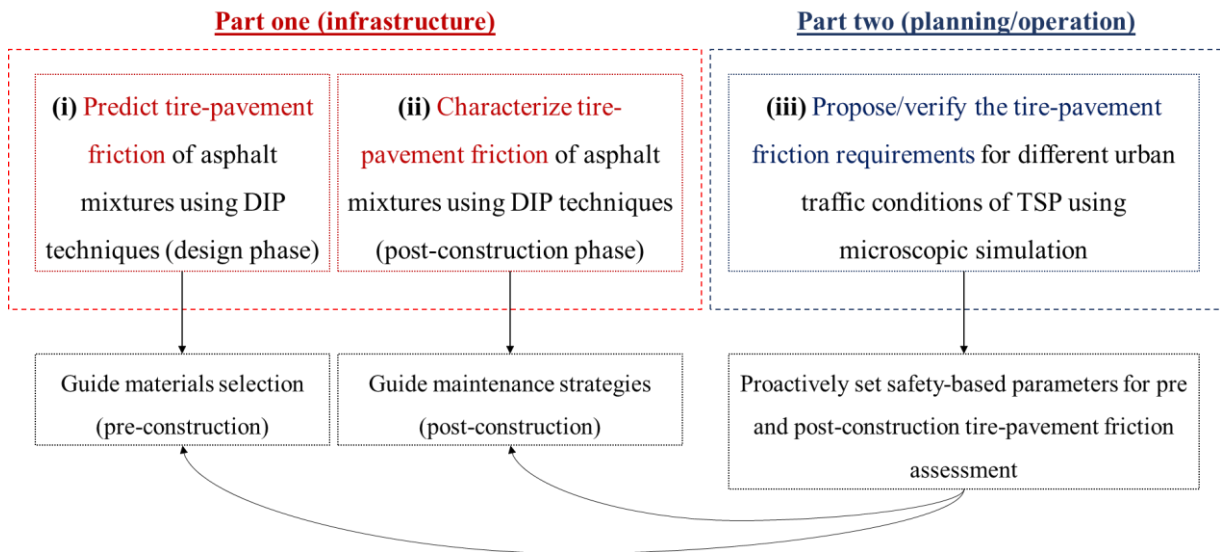
(i) To review and propose the use of models for tire-pavement friction coefficient (μ) prediction for asphalt pavements. The scope of this objective focuses on laboratory-advanced characterization of materials in the asphalt mixture design phase (pre-construction).

(ii) To advance the existing body of knowledge in the characterization of the tire-pavement friction coefficient (μ) in post-construction assessments. The scope of this objective focuses on the use of DIP techniques and measurement tools (AIMS and CRP) to provide a reliable and low-cost surface analysis during the pavement service life.

The part two (planning/operation) specific objective is:

(iii) To propose/verify tire-pavement friction requirements based on information derived from traffic microscopic simulation. The scope of this objective focuses on the integration of transport planning and operation tools, such as traffic microscopic simulation and Surrogate Measures of Safety (SMoS), with materials selection and maintenance strategies (pre-construction and post-construction). Figure 2 presents the framework of objectives to be addressed in this thesis.

Figure 2 - Specific objectives' framework



Source: the author.

1.5 Thesis structure

This thesis is divided into 5 chapters. Chapter 1 presents a general introduction to this research, which focuses on the definition of research problem, justification, and objectives. This chapter also contains a basic theoretical background (item 1.6) to support the understanding of non-specialist readers concerning some general concepts. Chapters 2, 3, and 4 are dedicated to the specific objectives of parts one (infrastructure) and two (planning/operation). More specifically, chapters 2 and 3 focus on the processes of using DIP tools (AIMS and CRP) and their relationships with texture and friction parameters of pavement surfaces. These parameters define, afterward, the Maximum Available Deceleration Rate (MADR) of an asphalt surface. Chapter 4 details the process of obtaining, by using traffic microscopic simulation and vehicular conflict analysis tools, the Deceleration Rate to Avoid a Crash (DRAC). $DRAC > MADR$ situations reflect therefore higher crash potential. Chapter 5 summarizes the general conclusions of this work and underlies the future perspectives for this work. In summary:

- i. Chapter 1: “Introduction” (research problem, justification, questions, objectives, and basic theoretical background);

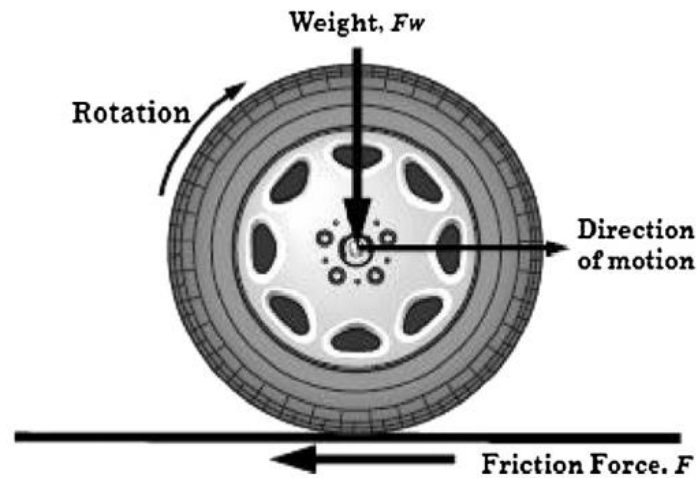
- ii. Chapter 2: “A review of tire-pavement friction prediction models from laboratory advanced characterization of materials”;
- iii. Chapter 3: “Advances in the analysis of asphalt pavements’ surface texture and friction using the Aggregate Imaging Measurement System (AIMS) and the 3D Computer Vision”;
- iv. Chapter 4: “Using microscopic simulation to assess asphalt pavements’ tire-pavement friction requirements”;
- v. Chapter 5: “Final considerations” (conclusions and recommendations for future research);
- vi. Bibliographical references and appendix.

1.6 Theoretical background

1.6.1 Tire-pavement interaction concepts

This section aims to define concepts related to the tire-pavement friction phenomenon. This includes terms like texture, tire-pavement friction, skid resistance, and road safety, as used in this work. Here, the concept of texture will always be related to the variation of the z-axis (height) of a surface at different scales: irregularities, megatexture, macrotexture, and microtexture. The concept of friction, on the other hand, will always refer to the physical response represented by the forces developed at the interface between a solid and its sliding surface (Figure 3).

Figure 3 - Forces developed at the tire-pavement interface with vehicles' motion



Source: Kogbara *et al.* (2016).

When it comes to transport engineering, it is worth highlighting that the friction concept directly refers to the so-called tire-pavement friction. This property is an attribute resulting from two distinct and independent surface texture characteristics: micro and macrotexture. These terms derive from a traditional classification of texture scales based on texture wavelengths (λ_w) and vertical dimensions (A) (Table 2). Different knowledge areas investigate texture and friction questions from different perspectives. For example, mechanical engineering focuses on machines and lubricants, which is a different point of view when compared to transportation infrastructure engineering, dedicated to the tire-pavement interface and traffic safety.

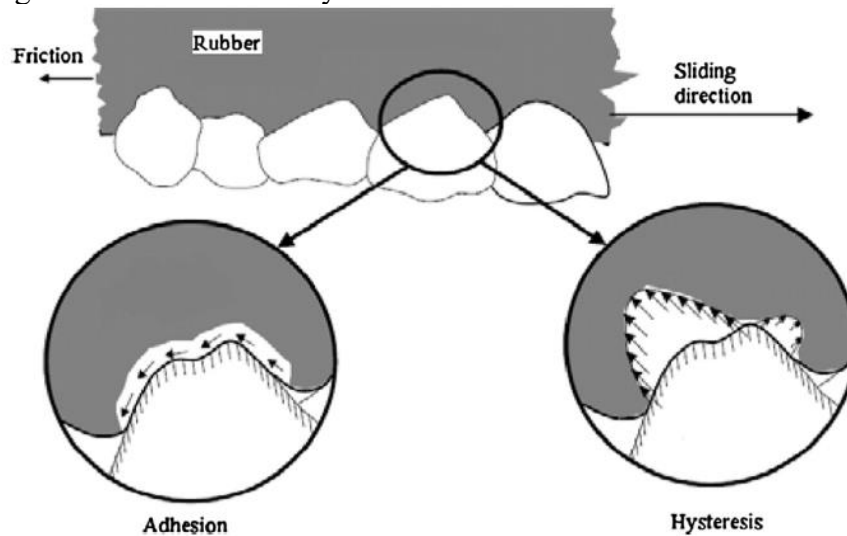
Table 2 - Texture scales

Scale	Limits
Microtexture	$\lambda_w < 0.5 \text{ mm}$ ($A < 0.5 \text{ mm}$)
Macrotexture	$0.5 \text{ mm} < \lambda_w < 50 \text{ mm}$ ($0.1 \text{ mm} < A < 20 \text{ mm}$)
Megatexture	$50 \text{ mm} < \lambda_w < 500 \text{ mm}$ ($0.1 \text{ mm} < A < 50 \text{ mm}$)
Unevenness	$500 \text{ mm} < \lambda_w < 50 \text{ m}$

Source: adapted from Wambold *et al.* (1995) and Wang *et al.* (2014).

The combination of two mechanisms governs the tire-pavement friction: adhesion and hysteresis (Figure 4). Adhesion occurs at a molecular level in which there is a bonding between areas of the tire-pavement intermedium subjected to high-pressure levels. Hysteresis represents energy losses resulting from tire rubber deformation as an effect of the existence of hills and valleys on the pavement surface (KOGBARA *et al.*, 2016; WANG *et al.*, 2018).

Figure 4 - Adhesion and hysteresis mechanisms of friction



Source: Kogbara *et al.* (2016).

This work is concentrated on asphalt pavements; therefore, it is important to note that the real effects of each texture scale on asphalt pavement friction and skid resistance are still not fully understood. Skid resistance is a more restricted concept which refers specifically to the texture/friction conditions which help to avoid hydroplaning. This knowledge gap justified the development of research from different scientific groups worldwide. In the last few decades, DIP methods potentialized the development of innovative approaches to surface conditions evaluation.

In general, these studies rely on premises such as macrotexture (a characteristic governed by aggregates' grain size distribution, 3D form, angularity, and asphalt mixture volumetric parameters) as a factor that contributes to the water drainage and the loss of energy governed by tire deformations (hysteresis). Higher macrotexture values mean more available space for pressurized water to escape from the tire-pavement contact area, preventing this fluid to act as a lubricant. Macrotexture is fundamental to the pavement drainage capacity and the development of high-speed friction. On the other hand, microtexture reflects the adhesion mechanisms and is a result of the aggregates' capacity to resist polishing over time. Microtexture governs skid resistance at low traffic speeds (< 20 km/h) (HENRY, 2000; HALL *et al.*, 2009; WANG *et al.*, 2018).

This work will use the broad term TSP because the reader will better associate it with urban environments. When it comes to transport systems planning and operation, both micro and macrotexture scale parameters are important for the TSP evaluation. However, relating TSP to texture and friction is a complex task because one cannot fully comprehend the

combined effects of friction and driving behavior, especially for wet conditions. In this context, texture and friction characteristics relate not only to skid resistance but also to drivers' behavior. Depending on the surface characteristics, drivers may need to perform evasive maneuvers because of a lack of friction to develop the necessary vehicle deceleration rate. Therefore, texture and friction impact on greater maneuverability and vehicle control for drivers.

1.6.2 Texture and friction harmonization

Friction and texture have always been measured using tests which are different in principles. Therefore, the Permanent International Association of Road Congresses (PIARC) found it necessary to develop harmonization methods to represent different measures in a single parameter. Thus, as part of an effort to achieve the mentioned objective, the PIARC proposed the International Friction Index (IFI) (WAMBOLD *et al.*, 1995). This method defines the parameters Sp (speed constant) and F60 (friction value) to estimate the coefficient of friction (μ) at different speeds. Macrotexture measurements determine the Sp parameter (Equation 1). Then, the Sp value is employed to adjust the friction parameter to a normalized speed of 60 km/h (Equation 2). Finally, Sp and F60 values are reported as the IFI. Therefore, the friction value F(S) can be computed at any other slip speed (S) of interest (Equation 3).

$$Sp = A + B \times Tx \quad (1)$$

$$F60 = A + B \times FRS \times e^{\frac{(S-60)}{Sp}} + C \times Tx \quad (2)$$

$$F(S) = F60 \times e^{\frac{(60-S)}{Sp}} \quad (3)$$

In which: Sp: speed constant;
 A and B: constants defined for different texture-measurement devices;
 Tx: texture measure.
 F60: friction value converted to a 60 km/h measurement;
 A, B and C: device constants;
 FRS: the friction reading of a device at slip speed;
 S = {for locked wheel testers: S = Vehicle Velocity (V); for fixed slip testers: S = V × percent slip/100; for SFC (a = slip angle): S=V × sin (a)}.

The Brazilian Asphalt Pavements Restoration Manual (DNIT, 2006) standardizes that asphalt mixtures with μ higher than 0.30 for speeds of 60 km/h will be considered satisfactory concerning friction. The documents that guide the calculation of IFI values (ASTM and PIARC) do not present parameters A and B for the definition of Sp by applying tests such as AIMS and CRP. In general, correction factors are provided only for tests whose applications date back to the '90s. Table 3 and Table 4 present the adjustment factors for both macrotexture and friction tests.

Table 3 - Adjustment constants for Sp obtention from the use of different macrotexture measurement equipment

Equipment	Speed (km/h)	Measure	a	b
Laser profilometer (LLS)	0	MPD**	9.74081	81.67568
LLS	0	RMS***	21.1784	158.69943
Sand Patch (SP)	0	MTD*	-11.5981	113.63246
CT Meter (CTM)	0	MPD**	14.2	89.7

* MTD: mean texture depth (ASTM E965-15, 2015)

** MPD: mean profile depth (ASTM E1845-15, 2015)

*** RMS: root mean square (ISO 4287-97, 1997)

Source: the author.

Table 4 - Adjustment constants for obtaining IFI obtention from friction tests

Equipment	Speed (km/h)	Macrotexture measure	A	B	C
GripTester (GT) (UK)	5, 30, 65, 90	MPD	0.08209	0.91040	0
GT (UK)	5	MPD	0.05852	0.92036	0
GT (UK)	5	MTD	0.08317	0.84639	0
British Pendulum (BP)	10	MTD	0.05626	0.00756	0
Dynamic Friction Tester (DFT)	20	MPD	0.081	0.732	0

Source: the author.

The complex relations between texture and friction (also between the different techniques of texture/friction measurement) are subjects of interest of several recent studies. For example, seeking a better understanding of these questions, Kouchaki *et al.* (2018) traced a parallel between texture measured by the laser profilometer (LLS) and the circular-track meter (CTM), and friction measured by GT and DFT. Test sections older than 5 years were analyzed: one open-graded (OG) mixture, a porous friction course (PFC) in section with daily average traffic of 13,972 vehicles) and two dense-graded (DG) mixtures, asphalt concrete (AC) with two different gradations, with traffic volume of 5,843 and 57,386 vehicles, respectively. Satisfactory compatibility of MPD measurements from LLS and CTM was observed, and the LLS device was the one that showed lower standard deviations regarding MPD measurements from the same surface. Also, a satisfactory correlation was observed between the coefficients

of friction obtained from the use of GT and DFT (R^2 greater than 0.90).

Kouchaki *et al.* (2018) found that the relations between GT and DFT measurements (50 km/h) presented R^2 values lower than 0.70 (from 0.57 to 0.69). The authors pointed out that this happened essentially because OG mixtures present higher MPD values due to the lack of fine aggregates. This gradation characteristic leads to higher hysteresis dependence for friction development, but DG AC mixtures depend upon the combination of adhesion and hysteresis to tire-pavement friction development. One should observe, however, that there were also differences in traffic: the low values of friction found for the PFC sections may reflect their higher daily traffic volume and more severe polishing processes. Therefore, one may have this in mind: every comparison involving texture and friction (and afterward TSP) must account for the existing differences between measurement methods (even with the significant advance represented by the IFI method proposition) and the differences in the conditions (traffic and environment, for example) that each analyzed section is subjected to.

Many other factors may influence the magnitude of the friction developed at the tire-pavement interface. These factors include the effects of temperature and, as a consequence, the viscoelastic behavior of asphalt binders (COLONY, 1992; HENRY, 2000; WILSON, 2013), surface contamination by fine particles (DO *et al.*, 2014), the occurrence of precipitation after periods of drought and the continuous effect of precipitation and the resulting wet-dry condition of the surfaces (VEITH, 1983; KOKKALIS and PANAGOULI, 1998; FWA and ONG, 2008; DAN *et al.*, 2017). Veith (1983) also analyzed the speed effects on skid resistance, observing a 70% reduction in this property with an increase in the vehicle's speed from 30 km/h to 96 km/h.

The presented conceptualization is valuable for the achievement of this work's objectives. In chapter 2, important findings will be presented as a derivation from the application of the Chowdhury *et al.* (2017) and Aldagari *et al.* (2020) friction prediction models, associating material characteristics with DFT-measured friction. Furthermore, chapter 3 refers, among other discussions, to the post-construction friction assessment model proposed by Kogbara *et al.* (2018), which uses parameters from 3D model processing to predict friction of AC surfaces originally measured using the GT equipment.

2 A REVIEW OF TIRE-PAVEMENT FRICTION PREDICTION MODELS FROM ADVANCED LABORATORY CHARACTERIZATION OF MATERIALS

2.1 Initial considerations

Surface characteristics are variables that must be taken into consideration when assessing pavements' performance for management and rehabilitation. Such characteristics are deeply important not only to determine the ride quality, but also because they play an important role in safety, durability, comfort, and appearance of rigid and flexible pavements. Furthermore, the pavement surface characteristics determine tire wear, rolling resistance, road noise, and water drainage. Skid resistance depends on several factors, such as rubber tire properties, environmental conditions, and pavements' surface texture, specifically micro and macrotexture. Micro and macrotexture represent different scales of the pavement profile frequency spectrum.

Microtexture (determined by aggregates' surface texture) provides the mechanism of adhesion at the tire-pavement interface. However, we usually do not measure such property directly. In general, performing friction tests provides an indirect microtexture parameter. Macrotexture (highly influenced by aggregates' shape properties and size) is responsible for the hysteresis mechanism and for creating micro-channels for water to flow (HALL *et al.*, 2009). These are the main scales of profile irregularities seen as essential to increase tire-pavement friction, hence preventing vehicles' hydroplaning (WAMBOLD *et al.*, 1995; KOKKALIS and PANAGOULI, 1998)

Although an essential activity, the assessment of surface characteristics depends, by one side, on simplified empirical tests. On the other hand, achieving precision in this assessment depends on complex and expensive tests. This issue reflects the fact that the most accessible tests provide static measurements of pavement conditions at one point in time. However, traffic and environmental pressures occur under varying conditions over the service life of the pavement. These conditions vary in terms of vehicle weights and speeds, temperature, pollution, and several complex characterization-factors, as previously stated.

In general, the focus of asphalt mixture design methods is on volumetric parameters and mechanical properties only (CHEN *et al.*, 2017). Therefore, predicting texture and friction during materials selection and the mixing processes is not a common protocol followed by technicians. In this context, Digital Image Processing (DIP) techniques such as the Aggregate Imaging Measurement System (AIMS) are important tools that can potentialize the

development of new practical, precise, and low-cost methods for surface conditions evaluation. This can happen not only after construction but also in a proactive approach, in the design phase.

2.2 Specific objective

The objective of this chapter is to review and apply models to predict the friction coefficient (μ) of asphalt pavements from the laboratory advanced materials characterization using DIP techniques. This is an effort to contribute to introduce a more proactive approach of considering tire-pavement friction and traffic safety at hot-mix asphalt (HMA) design phase.

2.3 Friction prediction models

In the first stage of this literature review, studies carried out over the past few years in different regions of the world were selected to trace a recent evolution of tire-pavement friction prediction models. The starting point of this review was based on the initial studies of DIP application to understand the influence of aggregate shape characteristics, especially surface texture, on the formation of asphalt pavements' skid resistance. Research done in this direction were more frequent in the first decade of the 2000s, but remain in development and improvement until today.

2.3.1 Masad et al. (2007)

This study pioneered the development of experimental and analytical methods for the evaluation of the relationship between coarse aggregate texture and tire-pavement friction. The authors introduced a new measuring method of aggregate shape properties resistance to polishing based on the Micro-Deval (MD) and the Aggregate Imaging Measurement System (AIMS) equipment. The authors also selected different aggregate sources and mixture gradations for the conduction of laboratory and field tests in terms of materials characteristics and tire-pavement friction after construction.

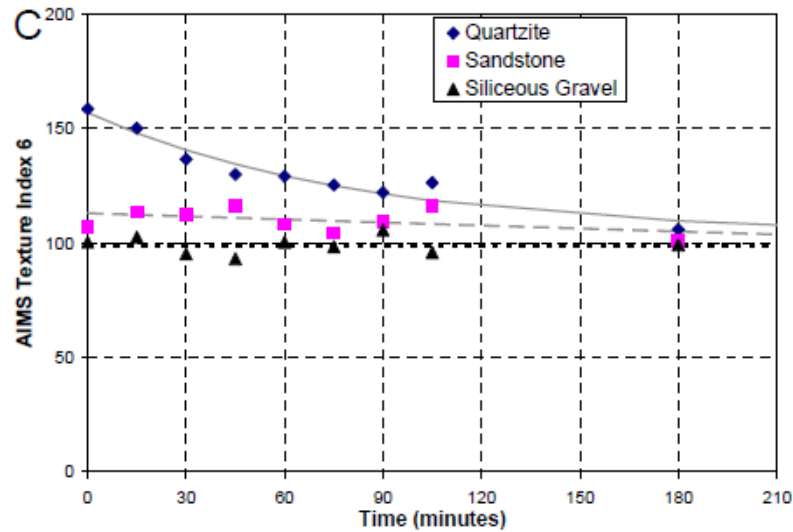
In the laboratory, the surface texture of coarse aggregates retained on sieve #4 (4.75 mm) was measured using AIMS before and after the polishing process in MD. The AIMS surface texture parameter results from the digital analysis of grayscale images of aggregate

surfaces using the wavelet method. After the AIMS analysis of initial conditions, 1,500 g of aggregates underwent polishing through the MD equipment: 750 g retained on #3/8 (9.5 mm), 375 g on #1/4 (6.3 mm), and 375 g on #4 (4.75 mm). The analyses covered a range of 62 samples of gravel, sandstone, and limestone aggregates. From all samples, 56 particles from each size were measured in terms of AIMS surface texture. Statistically, no significant difference was found in the texture results between the particle sizes. However, before-MD (BMD) average texture values were indeed higher than the after-MD (AMD) values, even with a wide range of variation in texture among the different aggregate samples.

In the field, tire-pavement friction was assessed in 9 test sections. The construction of these sections used three different aggregate types: quartzite, sandstone, and siliceous gravel. The aggregates were combined in three different dense-graded mix types. All sections used PG 76-22 asphalt in the mix production and the average asphalt layer thickness was 2 inches. Furthermore, the mixtures were designed to carry 30 million Equivalent Single Axle Loads (ESAL). To measure skid resistance, a skid trailer (ASTM E274-97) was used in two sets of measurements, taken in 2004 and 2005. The result of the test was shown in terms of Skid Number (SN), which represents the relative force required to pull a trailer in locked-wheel and wet surface conditions.

Analyses of variance (ANOVA) (0.05 significance level) assessed the significance of the aggregate mineralogy and mixture gradation on SN values. Only the aggregate mineralogy variable was reported to be a statistically significant factor impacting SN values (mixture gradation was found not to be statistically significant). The authors pointed out that the evaluated mixture gradations did not present significant differences between each other (all DG AC). When it comes to aggregates' polishing, the different particle sources (quartzite, sandstone, and siliceous gravel) underwent the Micro-Deval polishing for 15, 30, 60, 75, 90, 105, and 180 minutes. AIMS texture after each interval of polishing at the largest texture scale (6th level of decomposition) led to the conclusion that the quartzite aggregate had the most rapid decrease in texture. Sandstone and siliceous gravel aggregates, although they initially had lower surface texture, did not lose much of this property over time (Figure 5).

Figure 5 - AIMS surface texture variation with time of Micro-Deval polishing



Source: Masad *et al.* (2007)

2.3.2 Masad *et al.* (2009)

After the observation of aggregates mineralogy influence on tire-pavement friction (Masad *et al.*, 2007), the project conducted by Masad *et al.* (2009) aimed to develop a method to predict tire-pavement friction based on aggregates' characteristics and gradation. To do so, the authors prepared, in the laboratory, slabs in which asphalt mixtures with different combinations of aggregate sources and mixture gradations. Five different types of aggregates were selected, from different locations in Texas (United States), and petrography analyses were performed using thin sections. The aggregates had mineralogy classified as (i) sandstone/limestone, (ii) granite/dolomite/limestone/sandstone, (iii) sandstone/limestone/dolomite, (iv) limestone, and (v) 100% calcite-limestone.

The slabs' skid resistance was measured after different polishing intervals using the wheel-polishing device developed by the National Center for Asphalt Technology (NCAT). Sand patch (SP), British Pendulum (BP), Dynamic Friction Tester (DFT), and Circular Texture Meter (CTMeter) were the methods used to evaluate friction characteristics of slabs. Furthermore, aggregates' surface texture was measured using AIMS after different polishing intervals in MD.

Based on the proposed model, the International Friction Index (IFI) (WAMBOLD *et al.*, 1995) could be predicted as a function of aggregates' surface texture (before and after

MD polishing) and gradation. The surface texture was incorporated in the model by the parameters of the fitted curve of aggregate surface texture data in the function of polishing time in MD (Equation 4). The aggregate gradation was incorporated in the model by the Weibull distribution parameters, which provided the optimum fit to the gradation curve. Equation 5 presents the Weibull characteristic function. Equations 6 to 8 present the IFI (F60) predictive model.

$$\text{AIMS}_{\text{texture}} = a_{\text{agg}} + b_{\text{agg}} \times e^{(-c_{\text{agg}} \times t)} \quad (4)$$

In which: a_{agg} : Terminal surface texture;
 $a_{\text{agg}} + b_{\text{agg}}$: Initial surface texture;
 c_{agg} : Rate of change in texture;
 t : time of polishing (minutes).

$$F(x, k, \lambda) = 1 - e^{-\left(\frac{x}{\lambda}\right)^k} \quad (5)$$

In which: x : Aggregate size in millimeters;
 k and λ : Weibull parameters (shape and scale parameters, respectively).

$$a_{\text{mix}} = \frac{18.422 + \lambda}{118.936 - 0.0013 \times (\text{AMD})^2} \quad (R^2 = 0.96) \quad (6)$$

$$a_{\text{mix}} + b_{\text{mix}} = 0.4984 \times \ln[5.656 \times 10^{-4} \times (a_{\text{agg}} + b_{\text{agg}}) + 5.846 \times 10^{-2} \times \lambda - 4.985 \times 10^{-2} \times k] + 0.8 \quad (R^2 = 0.82) \quad (7)$$

$$c_{\text{mix}} = 0.765 \times e^{\left(\frac{-7.297 \times 10^{-2}}{c_{\text{agg}}}\right)} \quad (R^2 = 0.90) \quad (8)$$

In which: a_{mix} : Terminal IFI (F60);
 $a_{\text{mix}} + b_{\text{mix}}$: Initial IFI (F60);
 c_{mix} : IFI (F60) rate of change;
AMD: Terminal aggregate texture after polishing in the MD equipment.

2.3.3 Masad *et al.* (2010)

The Masad *et al.* (2009) model became more robust one year later. The authors developed a way to relate traffic to the decrease of friction, assuming Equation 9 accurately represents the phenomenon of friction variation with polishing cycles.

$$\text{IFI (N)} = a_{\text{mix}} + b_{\text{mix}} \times e^{(-c_{\text{mix}} \times N)} \quad (9)$$

In which: N: number of loading cycles of polishing using the NCAT equipment (in 1,000 cycles).

Data recorded over the years using the Texas skid trailer was analyzed to determine the change in skid resistance with time. DFT and CTMeter were also used to evaluate field sections constructed guided by findings developed in previous phases of the project, including aggregate characterization. As a result, Equation 10 was proposed, achieving the objective of including traffic data (Equation 11) to the model for IFI change with polishing.

$$N = \text{TMF} \times 10^{\frac{1}{A+B \times c_{\text{mix}} + \frac{c}{c_{\text{mix}}}}} \quad (10)$$

$$\text{TMF} = \frac{\text{AADT} \times \text{years in service} \times 365}{1000} \quad (11)$$

In which: TMF: Traffic multiplication factor;
 AADT: Average annual daily traffic;
 A, B, and C: -0.452 , -58.95 , and 5.834×10^{-6} , respectively.

2.3.4 Kassem *et al.* (2013)

Based on the previous findings published by Masad *et al.* (2009) and Masad *et al.* (2010), Kassem *et al.* (2013) developed a model whose objective was to relate parameters including aggregate shape properties, aggregate resistance to abrasion/polishing, aggregate gradation, and polishing cycles to the friction prediction. The authors selected one asphalt binder type and three aggregate sources (two limestones and one sandstone) to produce asphalt

hot mixtures with four different gradations, compacted in squared slabs (Figure 6, a). This study used a polisher device containing three wheels with pneumatic rubber tires attached to a turntable polished the squared slabs by applying a 105 lb load (50 psi pressure in the tires) on their surface (Figure 6, b).

Figure 6 - Slabs compaction and polishing devices



(a) compaction

(b) polishing

Source: Masad *et al.* (2010)

This polishing equipment simulates more precisely what occurs at pavement surfaces under traffic, including a water spray system to simulate wet conditions. Test slabs polished to 5,000, 10,000, 30,000, 50,000, and 100,000 cycles and friction characteristics were then examined using CTMeter and DFT. The statistical analysis resulted in a model (Equations 12 to 14) which demonstrated that aggregate shape properties and mixture gradation significantly impacts skid resistance over time. Figure 7 presents the graphical and statistical analysis of predicted *versus* measured IFI.

$$a_{\text{mix}} = \frac{47.493 + \lambda}{307.071 - 0.003 (\text{AMD})^2} \quad (12)$$

$$(a_{\text{mix}} + b_{\text{mix}}) = 0.308 \times \ln \left[\frac{1.438 \times (a_{\text{TX}} + b_{\text{TX}}) + 46.893 \times \lambda + 333.491 \times k}{2.420 \times (a_{\text{GA}} + b_{\text{GA}})} \right] + 1.008 \quad (13)$$

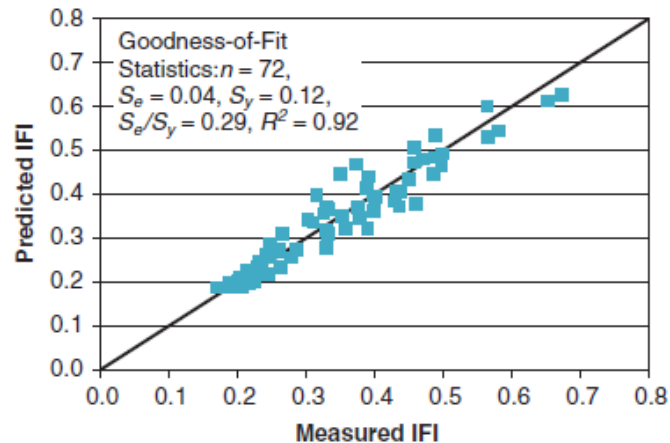
$$c_{\text{mix}} = 0.052 + 2.284 \times 10^{-14} \times e^{\left(\frac{0.523}{c_{\text{TX}}}\right)} + 2.008 \times 10^{-47} \times e^{\left(\frac{1.708}{c_{\text{GA}}}\right)} \quad (14)$$

In which: a_{TX} : Terminal surface texture;

$a_{\text{TX}} + b_{\text{TX}}$: Initial surface texture;

c_{TX} : Rate of change in surface texture;
 a_{GA} : Terminal angularity;
 $a_{GA} + b_{GA}$: Initial angularity;
 c_{GA} : Rate of change in angularity;

Figure 7 - Predicted *versus* measured IFI by Kassem *et al.* (2013) model



Source: Kassem *et al.* (2013)

2.3.5 Chowdhury *et al.* (2017) and Aldagari *et al.* (2020)

One of the issues concerning the model proposed by Kassem *et al.* (2013) was the fact that higher numbers of aggregate sources were needed to provide a more comprehensive model. The objective of the studies published by Chowdhury *et al.* (2017) and Aldagari *et al.* (2020) was to validate and review the friction prediction model proposed in earlier projects and to develop a skid prediction model for seal coat surfaces. Also, lane distribution percentage of truck traffic was incorporated to improve the method of predicting friction loss as a function of traffic.

The authors aimed to develop a calibrated friction prediction model. 70 sections (including 35 hot-mix asphalt mixtures and 35 seal coat sections) were selected to represent the variety of materials across the Texas state (USA). Different equipment was used to measure friction: DFT, MPD using CTMeter, and the Texas skid trailer. In the laboratory, the resistance of aggregates to abrasion and polishing was quantified, based on their shape characteristics (texture and angularity). The selection process provided a wide variety of mixture gradations, aggregate sources (limestone, gravel, granite, sandstone, dolomite, rhyolite, traprock, and quartzite), and climatic zones of Texas, in which friction was measured over time. It is worth

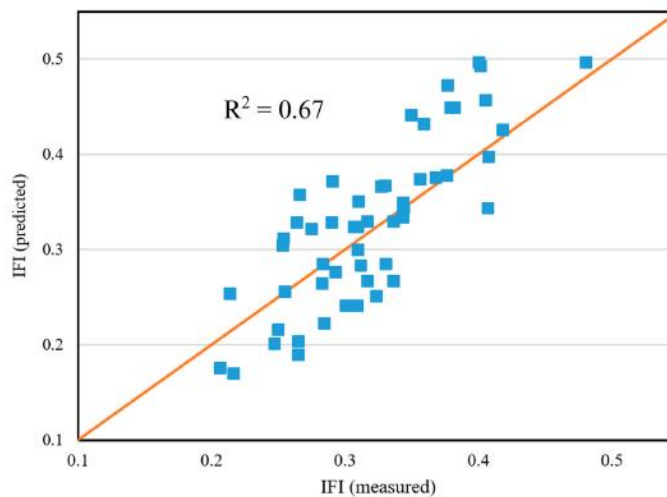
mentioning that sections with heavy traffic were able to provide a better understanding of polishing within a short time. Equations 15 to 17 present the resulting model. Considering more variables, R^2 of IFI predicted versus IFI measured (Figure 8) was lower than that obtained by Kassem *et al.* (2013), but the model was more robust.

$$a_{\text{mix}} = \frac{49.3144 + \lambda}{351.289 - 0.00193 (\text{AMD})^2} \quad (15)$$

$$a_{\text{mix}} + b_{\text{mix}} = 0.33 \times \ln\left(\frac{1.43757 \times (a_{\text{TX}} + b_{\text{TX}}) + 46.8933 \times \lambda + 333.491 \times k}{2.42031 \times (a_{\text{GA}} + b_{\text{GA}})}\right) + 1.00801 \quad (16)$$

$$c_{\text{mix}} = 0.018 + 1.654 \times c_{\text{TX}} + 1.346 \times c_{\text{GA}} \quad (17)$$

Figure 8 - Predicted *versus* measured IFI by the Aldagari *et al.* (2020) model



Source: Aldagari *et al.* (2020)

The researchers also developed a predictive model for MPD as a function of aggregate gradation and polishing cycles (or traffic level). The purpose of this model was to predict MPD if such information is not available for a given mixture. Equations 18 to 21 present the resulting model for MPD and the influence of traffic. Figure 9 shows the R^2 of predicted MPD versus measured MPD.

$$\text{MPD} = \left(\frac{\lambda}{34.180}\right) - \left(\frac{0.398}{k}\right) + (k^{0.416}) - 0.003N \quad (18)$$

$$N = \text{TMF} \times 10^{\frac{1}{A+B \times c_{\text{mix}} + \frac{C}{c_{\text{mix}}}}} \quad (19)$$

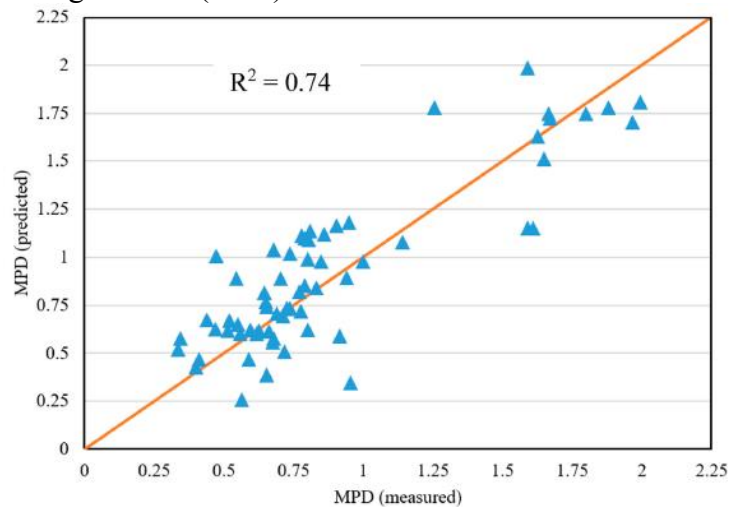
$$\text{TMF} = \frac{\Delta T \times \text{AT}}{1000} \quad (20)$$

$$\text{AT} = \frac{\text{AADT} \times (100 - \text{PTT}) \times \text{DL}_{\text{AADT}}}{100} + \frac{\text{AADT} \times \text{PTT} \times \text{DL}_{\text{truck}} \times 20}{100} \quad (21)$$

In which:

- MPD: Mean profile depth (m);
- AT: Adjusted traffic;
- ΔT : Number of days between construction and field testing;
- DL_{AADT} : Design lane factor (function of number of lanes and type of road);
- DL_{truck} : Design lane factor of trucks;
- PTT: percentage of trucks (%).

Figure 9 - Predicted *versus* measured MPD by the Aldagari *et al.* (2020) model



Source: Aldagari *et al.* (2020)

2.3.6 Siriphun *et al.* (2016)

The study conducted by Siriphun *et al.* (2016) proposed a model to predict tire-pavement friction during the aggregate selection and mixing processes (pre-construction). 14 locations in Thailand were selected to have their aggregate characteristics analyzed. Different combinations of asphalt mixtures were prepared. The asphalt binder content, air voids, and

mineral aggregates of asphalt concrete samples were defined based on Marshall mix design following Thai specifications.

The employment of different tests supported the analysis of mineral aggregate and mixture characteristics, including X-ray diffraction (XRD) and X-ray fluorescence spectrometry (XRF) for mineral composition identification. Different degradation tests were carried out for laboratory analysis of aggregates, such as the Los Angeles abrasion (LAA) and Polishing Stone Value (PSV). The PSV consists of determining friction using the BP test in surfaces with aggregates of size between 7.94 and 9.52 mm after polishing for 6 hours. The PSV_{diff} is the difference between the friction measured by BP before and after polishing. Finally, the authors defined the Weibull distribution parameters as the particles' size distribution variables.

106 sections were selected to cover a specific range of aggregates (limestone, granite, and basalt) and mix types (called AC 9.5 and AC 12.5). The selected projects had complete records of skid-resistance measurements and texture depths. The input parameter found to be suitable for representing microtexture characteristics was PSV_{diff} (the difference between PSV values of aggregate before and after polishing). MTD (from the sand patch method) and gradation (λ , κ) (model parameters of the Weibull distribution curve) represented the "macrotexture variables". Equation 22 presents the model proposed by the authors.

$$F_{60} = A_x MTD_x + B_x PSV_{diff} + C_x \lambda_x + D_x \kappa_x + E_x \quad (22)$$

In which: For $x = 9.5$: $A_x = 0.2699$; $B_x = 0.0087$; $C_x = 0.0113$; $D_x = -0.0904$; $E_x = 0.3346$.

For $x = 12.5$: $A_x = 0.4556$; $B_x = 0.0041$; $C_x = 0.0165$; $D_x = 0.0602$; $E_x = 0.1702$.

2.3.7 Siriphun *et al.* (2017)

The model proposed by Siriphun *et al.* (2016) was modified to consider the effect of cumulative traffic on skid resistance reduction. In the field, 12 sections in 6 Thai provinces had skid resistance value at 35 °C (SRV35) measured at every interval of 50,000 passenger car units (pcu) passes. Such sections presented aggregates' maximum nominal sizes (NMAS) of

12.5 and 9.5 mm and were evaluated in terms of SRV by the BP test value for 3 to 4 years after the end of construction.

Statistical analyses showed that from 0 to 300,000 pcu values of cumulative traffic volume (CTV), the mixture aggregates' maximum nominal sizes (12.5 and 9.5 mm) statistically influenced on skid resistance reduction (p-value lower than 0.04). For CTV between 300,000 and 2,000,000, the maximum nominal sizes were found not to be statistically relevant to the skid resistance reduction (p-value of approximately 0.20). For this reason, the authors proposed a model of loss of friction depending on traffic and aggregate maximum nominal sizes in 3 conditions of CTV, represented by Equations 23 to 25, with R² values higher than 0.915.

$$\frac{SRV_{35^\circ}}{SRV_{initial}} = 1.00 - 1.83 \times 10^{-6} \text{ CTV (If } 50,000 < \text{CTV} < 300,000 \text{ pcu and MNS } 12.5 \text{ mm)} \quad (23)$$

$$\frac{SRV_{35^\circ}}{SRV_{initial}} = \exp(-2.67 \times 10^{-6} \text{ CTV}) \text{ (If } 50,000 < \text{CTV} < 300,000 \text{ pcu and MNS } 9.5 \text{ mm)} \quad (24)$$

$$\frac{SRV_{35^\circ}}{SRV_{initial}} = -0.46 - 3.00 \times 10^{-8} \text{ CTV (If } 300,000 < \text{CTV} < 2,000,000 \text{ pcu)} \quad (25)$$

2.3.8 *Chen et al. (2017)*

The objective of the study conducted by *Chen et al. (2017)* was to optimize the design of asphalt mixtures considering surface texture, as opposed to traditional design methods which focus on volumetric and mechanical properties and pay little attention to skid resistance. The authors believed that incorporating a friction prediction evaluation would aid in a more rational selection of materials for both mechanical and functional properties of asphalt mixtures. Given the development of new vehicle industry technologies (such as the ABS systems), *Chen et al. (2019)* proposed a modification of the model presented two years before, calibrating the model to represent an optimum slip ratio of 15% (based on the ABS breaking principle).

In that study, the authors analyzed 2 mixture types (Asphalt Concrete, AC, and Open Gradation Friction Course, OGFC), 5 aggregate sources with different mineralogical compositions (diorite, limestone, granite, gneiss, and diabase), and 4 aggregates NMAS (16, 12.5, 9.5, and 4.75 mm). Mixture samples were compacted in the laboratory using a small road roller on squared slabs in ranges of different temperatures and compaction degrees. Core samples were then extracted from the slabs and analyzed in terms of volumetric parameters. 2D-ITAM software was used to obtain the surface profile of asphalt mixture from the scanned

image of mixture cross-section based on image analysis techniques, to identify the different levels of mixture surface texture at different wavelengths. Wavelengths ranging from 0.125 to 0.5 mm represent microtexture, and wavelengths range from 0.4 to 50 mm represent macrotexture (CHEN *et al.*, 2015).

The authors aimed to propose a model using fundamental characteristics of (i) mixture volumetric design, (ii) aggregates properties, and (iii) asphalt binder rheology. The volume of air voids (VV) and the voids filled with asphalt (VFA) represented the volumetric properties of asphalt mixtures according to the traditional design methods. D_{90} (diameter higher than the particles' 90% threshold) represented the aggregates' gradation, given the fact that this parameter best correlated with the level of characteristic wavelength (related to friction). Also, iPas software was employed to detect the internal structure parameters of the asphalt mixtures: the fractal dimension of aggregate gradation (D_f), the direction angle, and shape properties of aggregates in the mixture (iPas analysis results) were also selected as model parameters. The authors stated that contact length amongst aggregate particles per 100 cm² area of a core section (Σ CLAP) determined using iPas can indicate the viscosity of asphalt binder/mastic. The rheological properties of binders contribute to the density of the mixture and influence the formation of mixture surface texture during compaction. As a result, the multivariate regression model presented in Equation 26 includes variables that were statistically significant to estimate the properties of mixture surface texture.

$$L_{TX}(\lambda_i) = c_1 + c_2 \times \frac{VV}{VFA} + c_3 \times \frac{D_{90}}{D_f \Sigma \sin \theta \Sigma \Phi} + c_4 \times \frac{1}{\Sigma CLAP} \quad (26)$$

In which: $L_{TX}(\lambda_i)$: surface texture level at the central texture wavelength (λ_i) in octave band (mm), measured by 2D-ITAM (dB);

θ : aggregates direction angle (summation of sines for each 100 cm²);

Φ : regulation degree of aggregates per 100 cm²;

c_1 , c_2 , c_3 , and c_4 : model coefficients.

2.4 The Aggregate Imaging Measurement System (AIMS)

In addition to aggregate shape properties (AL ROUSAN, 2004; MASAD, 2005; BESSA, 2012; DIÓGENES, 2018; IBIAPINA, 2018), AIMS equipment may provide asphalt mixtures texture indicators analysis (REZAEI *et al.*, 2011; ARAUJO *et al.*, 2015). Macrotexture

evaluation results from reading of the distance between a camera and an asphalt mixture sample surface. Microtexture evaluation employs the analysis of captured image pixels. For the texture analysis, AIMS equipment performs 5 imaging scans of each sample at different zoom magnitudes. The first scan takes place at the maximum zoom magnitude. The microscope lenses move vertically at each image until detecting a high-resolution grayscale image. This process results in a 2D reconstruction of the macrotexture profile (Rezaei *et al.* 2011). The microtexture analysis happens at the last 3 sweeps. The equipment works at the same magnitudes of aggregate surface texture evaluation (4.75 mm, 9.5 mm, and 19 mm sizes).

The main aggregates' shape properties evaluated using AIMS which were found to be significant in friction prediction models are angularity and surface texture. Angularity is obtained for coarse and fine particles, measured by means of the gradient method (Equation 27), in which black & white images are used to calculate changes in gradient along the particle outline. Angularity ranges range from 0 to 10,000, with angular materials being the ones with higher angularity values.

$$\text{Angularity} = \frac{1}{\frac{n}{3}-1} \sum_{i=1}^{n-3} |\theta_i - \theta_{i+3}| \quad (27)$$

In which: θ : Orientation angle between each edge-point;
 n : Total number of points;
 i : The i^{th} point on the edge of the particle.

Also, the mixture microtexture processing technique employs the wavelet method, which is a function of the average and the standard deviation of pixel values of the processed images (Equation 28) (MASAD, 2005). The results might vary from 0 to 1,000, and rough surfaces have values closer to 1,000.

$$\text{Surface Texture} = \frac{1}{3n} \sum_{i=1}^3 \sum_{j=1}^N (D_{i,j}(x,y))^2 \quad (28)$$

In which: D : decomposition function;
 n : level of image decomposition;
 N : total number of coefficients in a detailed image;
 i : texture direction;
 j : wavelet index;

x, y: location of the coefficients in the transformed domain.

In Brazil, one of the most recent advances concerning the use of AIMS derived from the realization that a national database of aggregate shape properties was needed to set a national classification system (IBIAPINA, 2018). This finding stood out in studies conducted within the country from the beginning of the 2010s. In general, analysis previously performed in AIMS resulted in different aggregates being similarly classified when using the American classification system proposed by Al Rousan (2004). These indications raised the hypothesis that the Brazilian aggregate sources would have significantly different characteristics when compared with those of the aggregates that made up the American database. Table 5 shows both the American and Brazilian classification systems of aggregates' shape properties. In terms of the asphalt mixture cores texture analysis, the general practice within Brazil is to apply the AIMS classification systems (AL ROUSAN, 2004; IBIAPINA, 2018) for aggregate surface texture also to the mixture microtexture assessment.

Table 5 - American and Brazilian aggregate shape properties classification systems

Shape property	System	Limits				
2D Form	Al Rousan (2004)	<6.5	6.5-8.0	8.0-10.5	>10.5	
	Ibiapina (2018)	<4.0	4.0-11.0	11.0-15.5	>15.5	
	Classification	Circular	Semicircular	Semi-elongated	Elongated	
Angularity	Al Rousan (2004)	<2100	2100-4000	4000-5400	>5400	
	Ibiapina (2018)	<1260	1260-4080	4080-7180	>7180	
	Classification	Rounded	Sub-rounded	Sub-angular	Angular	
Sphericity	Al Rousan (2004)	<0.6	0.6-0.7	0.7-0.8	>0.8	
	Ibiapina (2018)	<0.5	0.5-0.7	0.7-0.9	>0.9	
	Classification	Flat/Elongated	Low Sphericity	Moderate Sphericity	High Sphericity	
Surface Texture	Al Rousan (2004)	<165	165-275	275-350	350-460	>460
	Ibiapina (2018)	<260	260-440	440-600	600-825	>825
	Classification	Polished	Smooth	Low Roughness	Moderate Roughness	High Roughness

Source: the author.

When it comes to the analysis of asphalt mixtures' texture and the relation between this characteristic and the multiple factors that influence it, the use of AIMS increased the level of understanding of this phenomenon. There are indications that different mixtures (concerning gradation and design method) may have similar macrotexture when compacted by the same type of roller. Also, similar mixtures may have different macrotexture values when compacted by different rollers (it is worth mention that tandem rollers used as finishing equipment may lead to general macrotexture reduction) (ARAUJO *et al.*, 2020). On the other hand, the type of

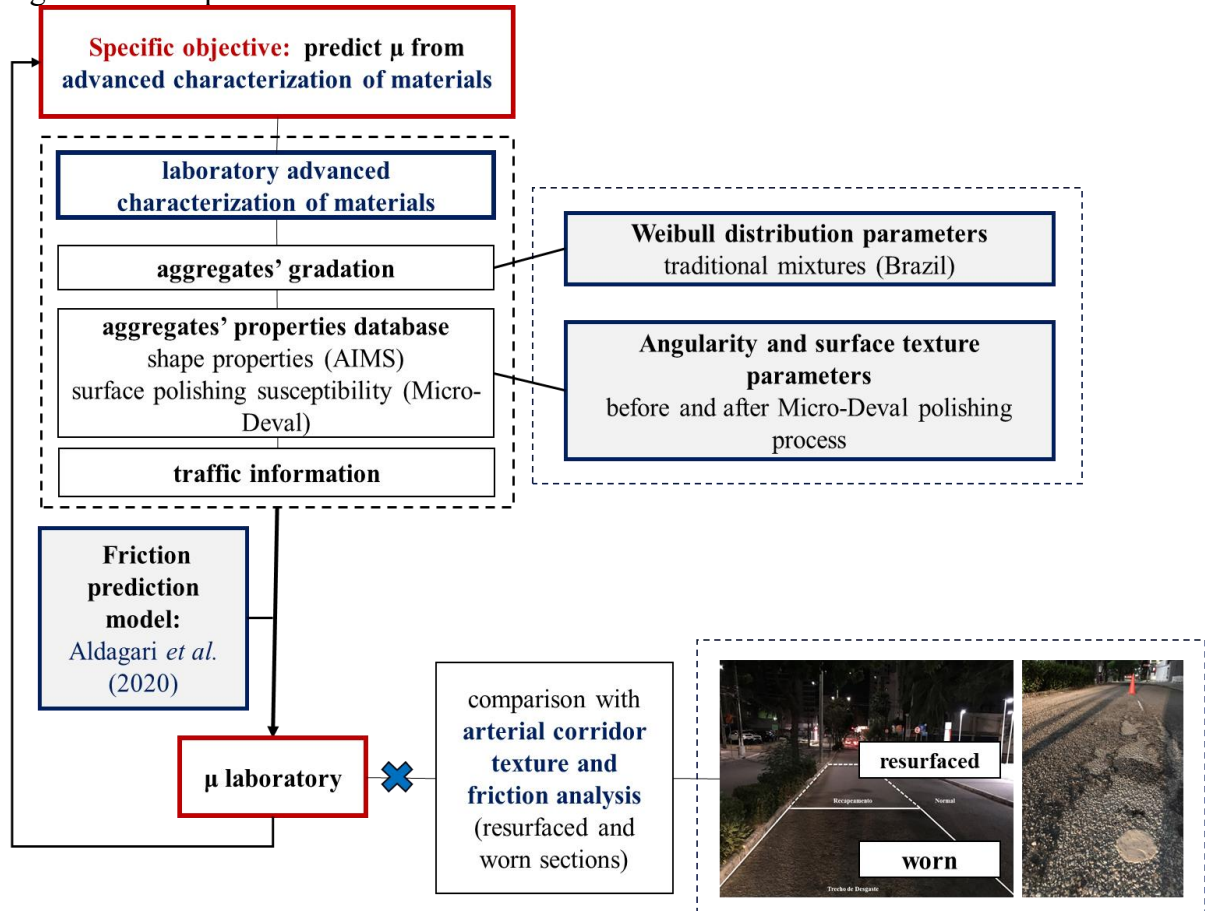
roller does not cause significant changes in microtexture, evaluated according to AIMS and indirectly by BP, because this property is more strongly influenced by the aggregates' surface texture (HALL *et al.*, 2009; ARAUJO *et al.*, 2020).

Besides compaction, reports of the AIMS use also suggest that the aggregates' manufacturing can be optimized to improve the properties of materials in terms of their shape. Such work depends on the understanding of a complex set of relationships between shape properties, crushing processes, and mineralogical analysis. For example, the use of impact crushers may generate more angular aggregates. Also, aggregates with granitic/gneissic composition tend to have less reduction in surface texture due to the polishing processes, especially when they have higher biotite content (BESSA *et al.*, 2011; BESSA, 2012; DIÓGENES, 2018).

2.5 Materials and methods

In this research, the scientific advances listed in the bibliographic review previously presented guided the definition of use of the friction prediction model detailed in the studies conducted by Chowdhury *et al.* (2017) and Aldagari *et al.* (2020). This choice was based on the possibility of use of parameters obtained in characterizations already consolidated (shape properties and degradation characterization) in Brazil. This consolidation means that the use of the AIMS and MD equipment has become increasingly widespread in the country, with vast data gathered in different recent studies. Based on works published in the last decade, a database of characteristics of mineral aggregates has been developed, which will be detailed in this section. Detailed information about gradation and traffic analysis and field application will be shown in this section. Figure 10 presents the general framework of this method.

Figure 10 - Chapter 2 method framework



Source: the author.

2.5.1 IFI prediction and measurement

The study conducted in this chapter relies on the friction prediction model proposed in the studies conducted by Chowdhury *et al.* (2017) and Aldagari *et al.* (2020). From this application, it is possible to obtain values of friction coefficient (μ) for different speeds. Different asphalt mixture solutions had tire-pavement friction evaluated in terms of their IFI initial and IFI final (a_{mix} and $a_{\text{mix}} + b_{\text{mix}}$, see Equations 15 to 17). The IFI obtention resulted from the combination of (i) 12 different aggregate gradations from standardized Brazilian asphalt mixtures, and (ii) 13 aggregate sources from two regions of Brazil (northeast and southeast). In the statistical analysis of gradations, in each of the 12 groups, the variation occurred in terms of aggregate sources. Therefore, for the statistical analysis of aggregate sources, gradation varied.

For the field validation, 1.5 km of the *Senador Virgílio Távora* avenue (Fortaleza, Brazil) was assessed concerning general pavement conservation state. Previous works

identified two extreme conditions: (i) resurfaced asphalt (a fine-grained asphalt mixture used as a maintenance strategy), and (ii) deteriorated asphalt. The experimental framework proposed was expected to provide information about the different states of conservation. The sand patch (SP) test (ASTM E965, 2015) was performed for the macrotexture characterization, and the British pendulum (BP) test (ASTM E303, 2013) was performed to evaluate microtexture. By using the IFI method (ASTM E1960-07, 2015), macro and microtexture data were converted into a coefficient of friction (μ) for different vehicular speeds.

2.5.2 Aggregate gradations

As shown in Table 6, 12 Brazilian standardized gradations had tire-pavement friction predicted:

- (i) upper and lower limits of a dense-graded AC for roadways.
- (ii) upper and lower limits of a fine-graded AC mixture for roads and urban pavements.
- (iii) upper and lower limits of 2 porous friction course (PFC) gradations.
- (iv) upper and lower limits of 2 dense-graded asphalt mixtures for use in airport pavements.

Table 6 also shows the Weibull distribution parameters and the Brazilian standards of the evaluated asphalt mixtures size distributions. It is important to mention that airport mixtures were selected to represent mixtures with higher nominal maximum aggregate sizes (NMAS).

Table 6 - Weibull distribution parameters for different standardized mixture gradations

Code	Type of gradation	Type of use	Brazilian standard	Range/Limit	λ	k
A	Dense-graded	Roadway	DNIT 031/2006 - ES	C - Lower	7.668	1.078
B	Dense-graded	Roadway	DNIT 031/2006 - ES	C - Upper	2.917	0.682
C	Fine-graded	Roadway	DNIT 032/2005 - ES	A - Lower	2.472	0.970
D	Fine-graded	Roadway	DNIT 032/2005 - ES	A - Upper	0.525	1.496
E	Porous Friction Course	Roadway/Airport	DNER 386/1999 - ES	II - Lower	8.534	2.717
F	Porous Friction Course	Roadway/Airport	DNER 386/1999 - ES	II - Upper	5.928	2.127
G	Porous Friction Course	Roadway/Airport	DNER 386/1999 - ES	V - Lower	11.116	1.971
H	Porous Friction Course	Roadway/Airport	DNER 386/1999 - ES	V - Upper	7.200	1.768
I	Dense-graded	Airport	DIRENG 04.05.610 (2002)	II - Lower	9.343	0.798
J	Dense-graded	Airport	DIRENG 04.05.610 (2002)	II - Upper	5.752	0.684
K	Dense-graded	Airport	DIRENG 04.05.610 (2002)	III - Lower	6.320	0.808
L	Dense-graded	Airport	DIRENG 04.05.610 (2002)	III - Upper	3.949	0.737

Source: the author.

2.5.3 Aggregates' shape properties database by Diógenes (2018) and Trotta (2020)

Table 7 presents the aggregate sources selected for the development of this work. The consolidation of a database of mineral aggregates properties (from analyses performed in equipment such as AIMS and MD) can be remarkably valuable for infrastructure studies.

A consolidated database of materials' properties would support the selection of the most suitable aggregates for functional aspects such as tire-pavement friction.

Five aggregate sources (3 gneissic and 2 phonolytic) were obtained from the Fortaleza (northeast Brazil) region. In terms of shape properties, phonolytic aggregates presented greater angularity (see Table 7). On the other side, the values of surface texture vary heterogeneously according to the mineralogy. This perception reinforces the result highlighted by Diógenes (2018), which stated that factors such as the biotite content, as well as the percentage of knurled boundaries among mineral grains, would better describe the aggregate texture than the mineralogical classification itself.

The aggregates from the southeastern region of Brazil, exposed in the study conducted by Trotta (2020) were obtained in the states of São Paulo (basalt, TBA), Minas Gerais (meta-limestone, TMC) and Rio de Janeiro (migmatic gneiss of high compositional heterogeneity). The aggregate classified as migmatic gneiss can be divided into: migmatic gneiss (mixture of different lithotypes) (TGN), paleosome (TPA), melanosome (TML), leucosome (TLE), pegmatite (TPE) and granitoid (TGR). The TBA and TMC aggregates have higher texture values, both before and after wear on the MD. As for the heterogeneous gneiss mineral aggregate, the melanosome lithotype has the highest surface texture (BMD and AMD) value, however this lithotype has a preponderance of only approximately 10%, while the paleosome lithotype has a preponderance of approximately 60%.

Table 7 - Aggregates' parameters database

	Origin	Code	Mineralogy	a _{ga}	b _{ga}	c _{ga}	a _{tx}	b _{tx}	c _{tx}
Northeast Brazil	Ceará	DAC	Gneiss*	1950	933	0.020	269	153	0.019
	Ceará	DBI	Phonolite**	2574	773	0.019	252	110	0.017
	Ceará	DBJ	Phonolite**	2911	555	0.018	221	158	0.021
	Ceará	DCC	Gneiss*	1979	817	0.019	232	67	0.017
	Ceará	DDC	Gneiss*	1873	760	0.019	243	99	0.017
Southeast Brazil	São Paulo	TBA	Basalt	2105	1088	0.020	372	269	0.020
	Minas Gerais	TMC	Meta-limestone	2032	1030	0.020	311	143	0.017
	Rio de Janeiro	TGN	Migmatic gneiss***	2180	1038	0.020	235	76	0.017
	Rio de Janeiro	TPA	Paleosome,	2068	1111	0.020	244	52	0.022
	Rio de Janeiro	TML	Melanosome	1521	1376	0.022	634	150	0.029
	Rio de Janeiro	TLE	Leucosome	2184	1062	0.020	102	-5	0.003
	Rio de Janeiro	TPE	Pegmatite	2379	1010	0.020	143	28	0.018
	Rio de Janeiro	TGR	Granitoid	2207	845	0.019	265	36	-0.015

* Aggregates DAC, DCC, and DDC were obtained from different quarries, but all from conic crushers.

** Aggregate DBI was obtained from impact crusher and DBJ from jaw crusher.

*** Aggregate TGN is the mixture of the 5 lithotypes that originated aggregates TPA, TML, TLE, TPE, and TGR.

Source: adapted from Diógenes (2018) and Trotta (2020).

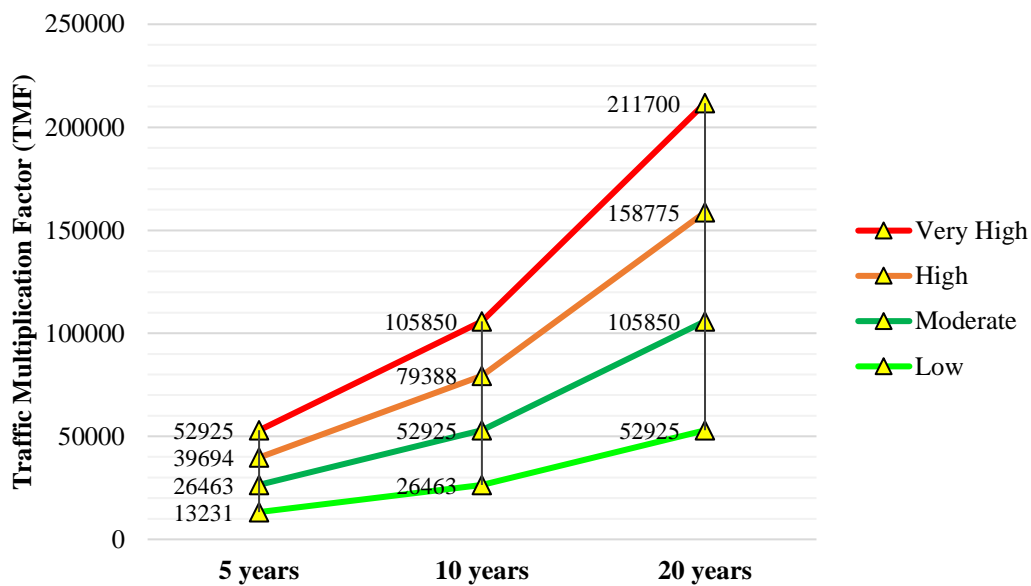
2.5.4 Traffic consideration

The data collected by Costa (2017) and Maia *et al.* (2019) at 20 different points of the city of Fortaleza (Brazil) based the estimation of 4 vehicular traffic volumes for representing a typical arterial road:

- (i) high traffic volume: 1200 vph;
- (ii) intermediate traffic volume: 900 vph;
- (iii) low traffic volume: 600 vph;
- (iv) very low traffic volume: 300 vph.

The division of the traffic flow between 90% of cars and 10% of heavy vehicles was found to accurately represent traffic in the city. Figure 11 shows the representation of these characteristics in terms of TMF, the parameter incorporated into the Chowdhury *et al.* (2017) and Aldagari *et al.* (2020) models.

Figure 11 - TMF over the years for different traffic volumes in the city of Fortaleza



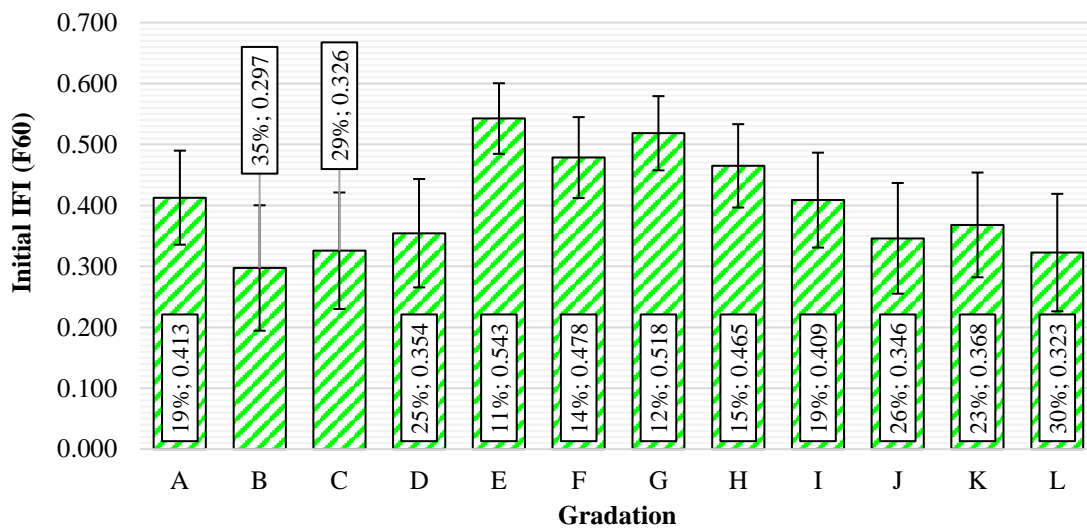
Source: the author.

2.6 Results and discussion

2.6.1 Analysis of initial IFI: Gradations

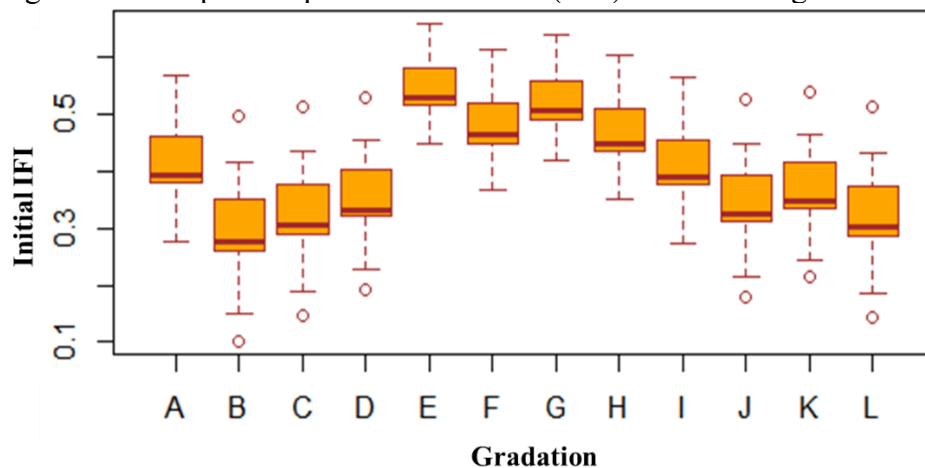
According to Hall *et al.* (2009), the gradation of aggregate particles directly impacts the macrotexture formation of asphalt mixtures. Among the particle gradations evaluated in this study, the highest $IFI_{initial}$ averages (F60) were obtained from PFC mixtures (E, F, G, H), as expected. Fine-graded mixtures of AC for roadways (B) and airport mixtures (J, L) resulted in the lowest values of F60. Figure 12 and Figure 13 summarize these results. In Figure 13, it is possible to observe the presence of outliers: for example, selecting gradations B, C, D, J, K, and L may improve predicted friction values, using the aggregate TML.

Figure 12 - Initial IFI (F60) prediction (average, SD, and CV) for different gradations



Source: the author.

Figure 13 - Boxplots of predicted initial IFI(F60) for different gradations



Source: the author.

It is worth observing that, among the dense-graded mixtures, the ones with higher percentages of coarse particles present better average predicted friction. The lowest initial IFI value (0.297), for the upper limit of range C (DNIT 031/2006 - ES), is lower than the limit considered ideal for road courses, according to Aps (2006) ($F_{60} > 0.35$) and the Asphalt Pavement Restoration Manual (DNIT, 2006a) ($F_{60} > 0.30$). The same is true for fine-graded mixtures (DNIT 032/2005 - ES), which are used for maintenance services (stop-gap) in urban areas in Brazil. It is also worth mentioning that, depending on the mineral aggregate used, this

value may be even lower, as can be seen by the value of -1 Std and the boxplots (mixtures B, C, and D).

Regarding the airport mixtures evaluated (DIRENG 04.05.610-2002 standard), the coarser limit of range II (average 0.409 - mixture "I") presents the highest average value predicted for F60. However, as shown in Figure 12, the variation coefficients for mixtures I, J, K, and L are high (from 19 to 30%), suggesting that a higher value of F60 will be obtained from better aggregate characteristics, especially surface texture. One option to guarantee better tire-pavement friction conditions on airport pavements is the adoption of PFC (E, F, G, and H mixtures) as wearing courses. In airports, authorities require stricter maintenance operations for runways' texture and friction. Therefore, as PFC mixtures present the highest predicted average F60, as well as the lowest coefficients of variation (less than 15%), this solution seems to be appropriate. In recent years, the Rio de Janeiro Santos Dumont (O GLOBO, 2019) and the São Paulo Congonhas (G1, 2020) airports received a PFC treatment on their main runways.

The perception of a pattern among the initial IFI values from the 12 evaluated gradations suggested the need for a more robust statistical analysis. Table 8 presents the results of an analysis of variance (ANOVA). The size distribution of particles was found to be statistically significant on the predicted initial IFI, based on the p-value (lower than 0.05).

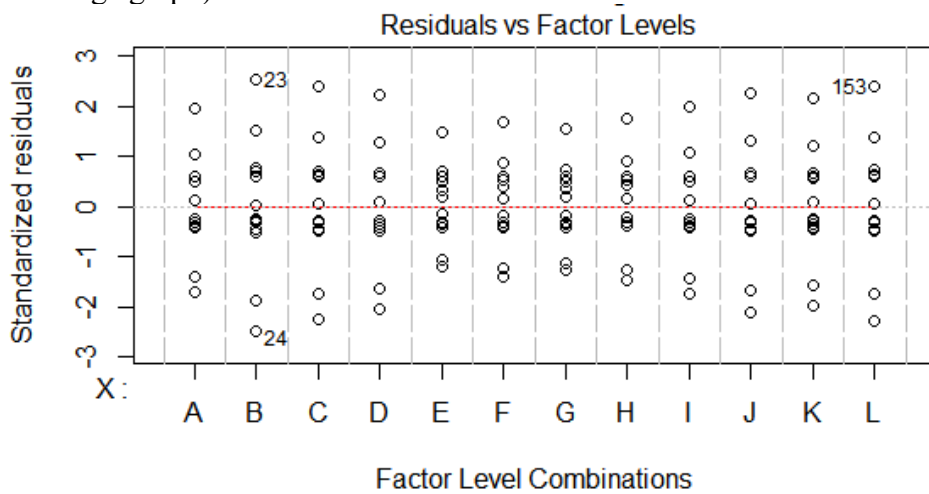
Table 8 - ANOVA results for IFI predicted from different gradations

Multiple R²	Adjusted R²	F-statistic	p-value
0.49	0.46	12.81	2.2E-16

Source: the author.

The analysis of the residuals allows for identifying gradation-aggregate combinations that tend to potentialize the positive and negative effects on the tire-pavement friction (Figure 14). The Leverage graph indicates the presence of influencing points, such as the combination of gradation B with the TML aggregate (the high aggregate surface texture raises the predicted F60 value) (point 23). The same happens for the gradation L and aggregate TML (point 153). As an example of a potentially unfavorable combination, we can mention the combination of gradation B and the TLE aggregate (point 24).

Figure 14 - Influencing points according to residuals' analysis (constant Leverage graph)



Source: the author.

Finally, to evaluate the difference between particle gradations, pair by pair, Tukey's post hoc test was performed. From the Tukey test, the null hypothesis is that the difference between the averages of the two evaluated gradations is equal to zero. In the case that the null hypothesis cannot be rejected, there is sufficient evidence to state that there are no statistically significant differences in the expected F60 value for the two-particle gradations evaluated, keeping the other sources of variation constant. Table 9 shows the Tukey post hoc analysis.

Table 9 - Tukey HSD test results for gradations

p-value	A	B	C	D	E	F	G	H	I	J	K	L
A	-											
B	0.022	-										
C	0.234	0.999	-									
D	0.808	0.829	0.999	-								
E	0.005	0.000	0.000	0.000	-							
F	0.662	0.000	0.000	0.009	0.699	-						
G	0.056	0.000	0.000	0.000	1.000	0.985	-					
H	0.898	0.000	0.002	0.036	0.404	1.000	0.881	-				
I	1.000	0.033	0.301	0.871	0.003	0.573	0.038	0.842	-			
J	0.641	0.935	1.000	1.000	0.000	0.004	0.000	0.016	0.726	-		
K	0.964	0.554	0.976	1.000	0.000	0.036	0.000	0.116	0.982	1.000	-	
L	0.191	1.000	1.000	0.998	0.000	0.000	0.000	0.001	0.250	1.000	0.960	-

(a) p-values matrix

Hypothesis	A	B	C	D	E	F	G	H	I	J	K	L	
A	-												
B		-											
C			-										
D				-									
E					-								
F						-							
G							-						
H								-					
I									-				
J										-			
K												-	
L													-
	<i>Gradations generate F60 values statistically different each other</i>												
	<i>Gradations do not generate F60 values statistically different each other</i>												

(b) Hypothesis statement matrix

Source: the author.

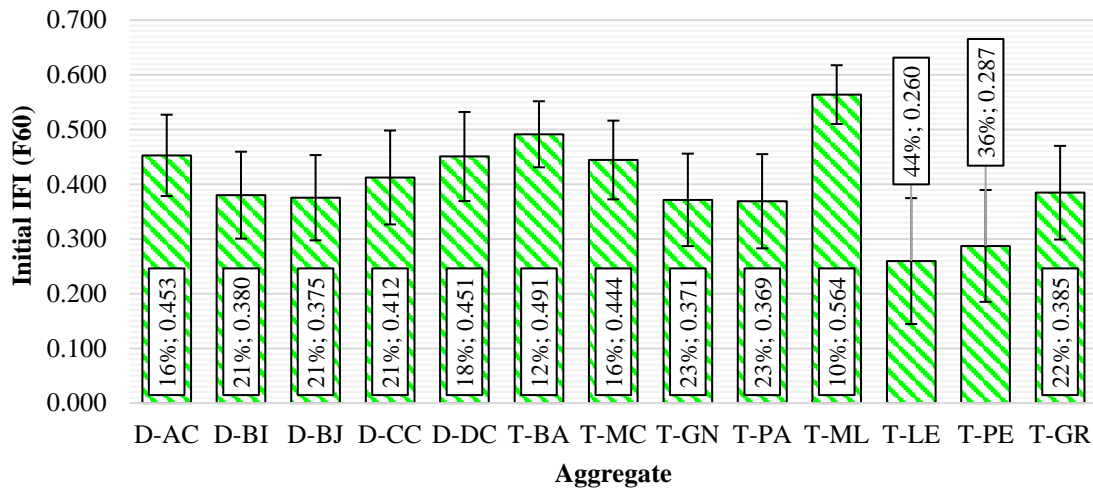
2.6.2 Analysis of initial IFI: Aggregates

An organized database of mineral aggregate properties parameters from two Brazilian regions (northeast and southeast) was used to obtain the results presented in this session. This database was structured from analyses of particle mineralogy and shape properties (before and after polishing in MD). Diógenes (2018) and Trotta (2020) presented similar results in recent years. Concerning the aggregates from the northeastern region, the gneissic ones (processed from cone crushers) presented initial IFI averages slightly higher than those obtained from phonolytic aggregates. The surface texture of northeastern aggregates varied without a specific pattern. However, the phonolytic aggregate particles had the highest angularities among the five analyzed materials, thus reflecting in a lower predicted IFI based on the model by Chowdhury *et al.* (2017) and Aldagari *et al.* (2020).

When it comes to aggregate sources from different states in southeastern Brazil (basalt, meta-limestone, and the six variations of a heterogeneous migmatic gneiss), TBA and TMC aggregates presented the highest average surface texture values. These averages are considerably higher than the TGN aggregate (a mixture of lithotypes with heterogeneous surface textures). As a result, the TBA and TMC aggregates presented an initial predicted IFI, on average, 26% higher than the one obtained from the TGN aggregate. As for the specific analysis of the heterogeneous migmatic gneissic aggregate, one may observe similar behavior

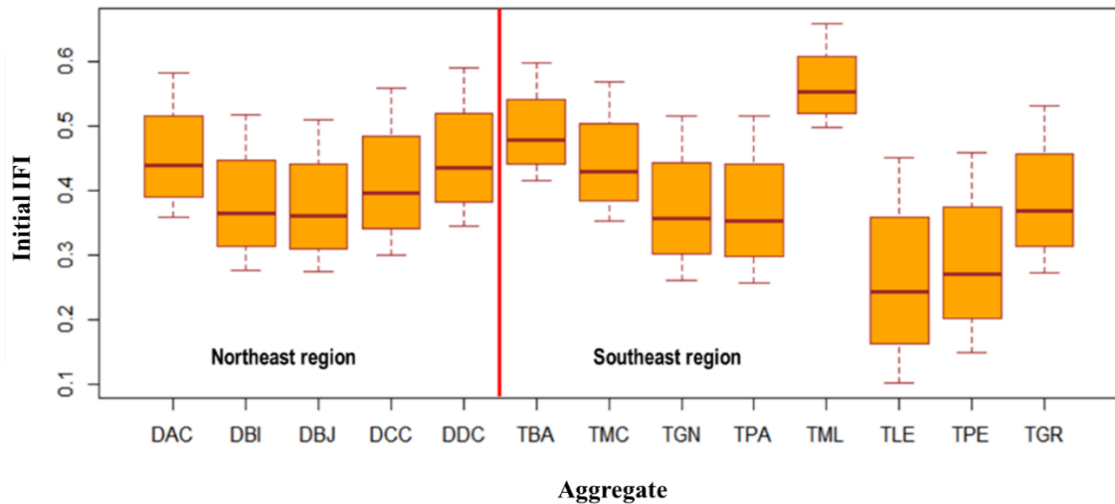
between the mixture of aggregates (TGN) and its predominant lithotype (TPA - paleosome). Furthermore, the heterogeneity in lithotypes reflects the presence of extreme behaviors, as in the case of the TML aggregate (higher IFI and lower CV), and the TLE aggregate (lower IFI and higher CV). Figure 15 and Figure 16 show the results for the different aggregate sources (with varying gradations).

Figure 15 - Initial IFI (F60) prediction (average, SD, and CV) for different aggregates



Source: the author.

Figure 16 - Boxplots of predicted F60 for different aggregates' sources



Source: the author.

It is important to note that there is a correlation ($R^2 = 0.88$) between the average predicted IFI value and the variation coefficient for aggregates classified according to the mineralogical origin (with varying particle sizes). Given the perception of considerable variation among the 13 aggregate sources, ANOVA analysis allowed the evaluation of the

statistical significance (Table 10). The mineral aggregate source variable can be considered statistically significant based on the p-value obtained (less than 0.05).

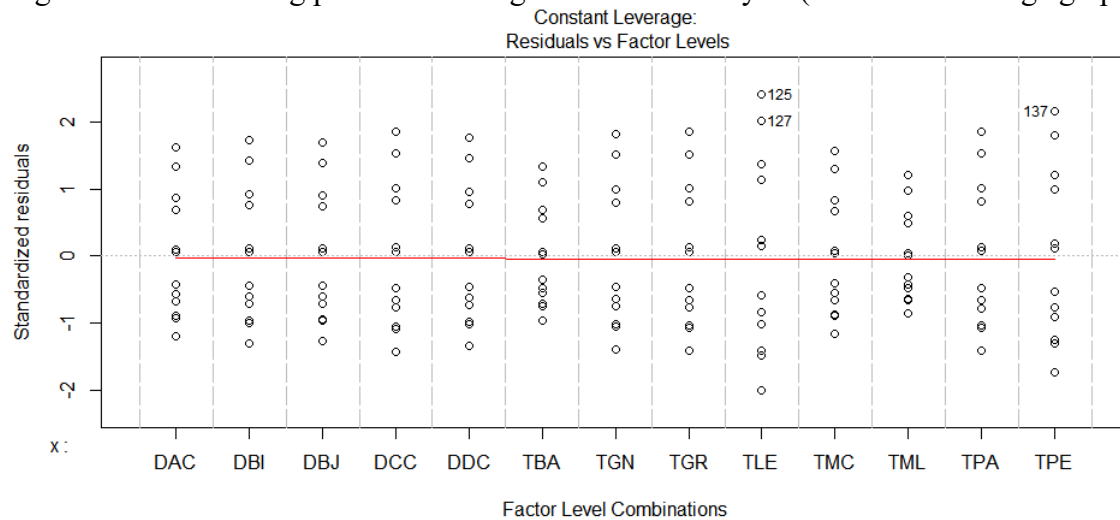
Table 10 - ANOVA results for IFI predicted from different aggregate groups

Multiple R ²	Adjusted R ²	F-statistic	p-value
0.49	0.44	11.35	9.4E-16

Source: the author.

The Constant Leverage graph (Figure 17) shows some points in which the gradation can “compensate” for the effects of lower surface texture values, providing better functional performance in terms of tire-pavement friction. One can predict, therefore, that combining PFC mixtures with higher coarse fraction contents with aggregates TLE and TPE would provide satisfactory predicted IFI, even though these aggregate sources presented the lowest averages in terms of surface texture.

Figure 17 - Influencing points according to residuals analysis (Constant Leverage graph)



Source: the author.

Running the Tukey post hoc hypothesis test allowed the assessment of the difference between mineral aggregates, pair by pair. The materials from the northeastern region of Brazil (more specifically from the Fortaleza region) (Table 11) do not show significant differences based on the quarry of origin of the aggregates (with specific mineralogical composition and manufacturing processes). This finding means that, if the same mixture gradation is maintained, the initial characteristics of IFI tend to be independent of the chosen mineral aggregate source. The evaluated aggregate sources from the southwest region showed

higher variability in terms of the Tukey test results, with several pairs presenting statistically significant differences between predicted initial IFI values.

Table 11 - Tukey HSD test results for the Northeast aggregates

<i>p-value</i>	DAC	DBI	DBJ	DCC	DDC
DAC	-				
DBI	0.630	-			
DBJ	0.531	1.000	-		
DCC	0.993	0.999	0.997	-	
DDC	1.000	0.673	0.575	0.996	-

(a) p-values matrix

Hypothesis	DAC	DBI	DBJ	DCC	DDC
DAC	-				
DBI		-			
DBJ			-		
DCC				-	
DDC					-

Aggregates generate F60 values statistically different each other

Aggregates do not generate F60 values statistically different each other

(b) Hypothesis statement matrix

Source: the author.

Table 12 - Tukey HSD test results for the Southeast aggregates

<i>p-value</i>	TBA	TGN	TGR	TLE	TMC	TML	TPA	TPE
TBA	-							
TGN	0.030	-						
TGR	0.091	1.000	-					
TLE	0.000	0.060	0.018	-				
TMC	0.975	0.626	0.861	0.000	-			
TML	0.630	0.000	0.000	0.000	0.030	-		
TPA	0.024	1.000	1.000	0.073	0.575	0.000	-	
TPE	0.000	0.392	0.183	1.000	0.001	0.000	0.440	-

(a) p-values matrix

Hypothesis	TBA	TGN	TGR	TLE	TMC	TML	TPA	TPE
TBA	-							
TGN		-						
TGR			-					
TLE				-				
TMC					-			
TML						-		
TPA							-	
TPE								-

Aggregates generate F60 values statistically different each other

Aggregates do not generate F60 values statistically different each other

(b) Hypothesis statement matrix

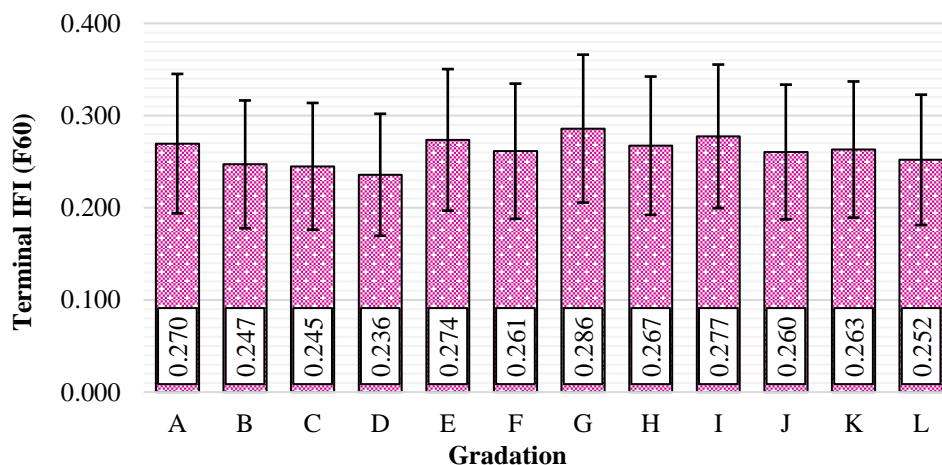
Source: the author.

2.6.3 Analysis of final IFI

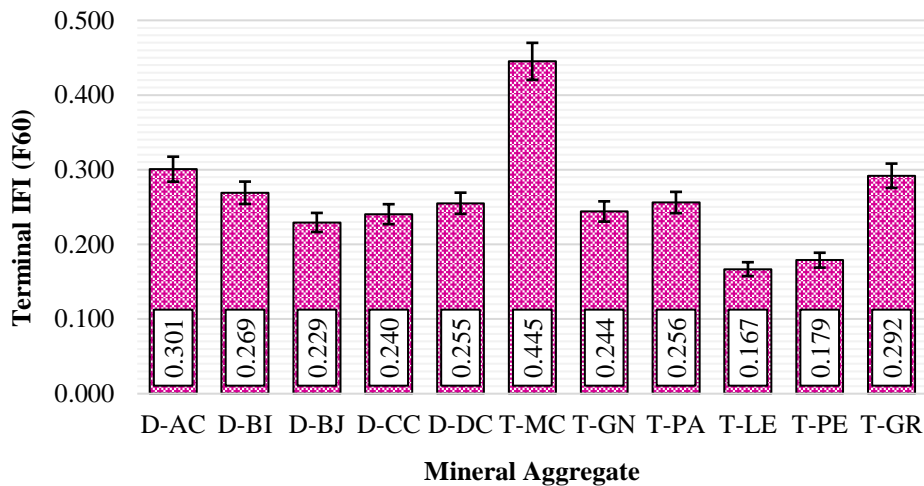
According to the model proposed in the study by Aldagari *et al.* (2020), the terminal value of IFI varies from a gradation parameter (λ) and the surface texture (AIMS) of the mineral aggregate after polishing in Micro-Deval (AMD). More specifically, the final IFI value is a quadratic function of the AMD parameter and a linear function of the gradation parameter (λ). However, in the database of aggregate characteristics (shape properties) that originated the model (Chowdhury *et al.*, 2017), there is no aggregate source whose a_{TX} parameter exceeds 300. Given that a_{TX} is a direct function of AMD, there is a limitation of the IFI_{final} model application in the analysis of some of the Brazilian aggregates presented in this research's database (TBA, TML, TMC). In this case, the AMD values are higher than any presented in the American database that originated the prediction model.

In terms of the IFI_{final} variation among the different selected gradations (Figure 18, a), there is a 21% difference between the lowest and the highest final IFI average value (D, 0.236, and G, 0.286). Furthermore, each class presented a 28% variation coefficient. When analyzing the final IFI average values for different aggregate sources (Figure 18, b), a more considerable variation was observed, as the higher is the IFI_{final} average, the higher the AMD value. The values obtained for the TMC aggregate were the highest ($IFI_{final} = 0.445$). However, as previously discussed, there is a limitation in the model application for AMD values higher than 300.

Figure 18 - Terminal IFI results in terms of the different gradations and mineral aggregates



(a) Results for different gradations



(b) Results for different aggregate sources

Source: the author.

The ANOVA analysis assessed the statistical significance of the two variables (“gradation” and “mineral aggregate source”) on the IFI_{final} average values (Table 13). One cannot reject the hypothesis that the “gradation” variable does not have statistical significance (if grouped in terms of the different gradations, with varying aggregate sources in each group). As for the “mineral aggregate source” variable, the ANOVA analysis shows a low p-value (2.2E-16), confirming its statistical significance (considering that each aggregate group has several gradations varying internally). It is worth remembering that the model of IFI_{final} derives from the aggregate surface texture after the polishing in the Micro-Deval test.

Table 13 - ANOVA analysis assessment of “gradation” and “aggregate source” significance in the IFI_{final} results

Variable	Multiple R ²	Adjusted R ²	F-statistic	p-value
Gradation	0.04	0.05	0.43	0.94
Aggregate	0.96	0.96	284.6	2.2E-16

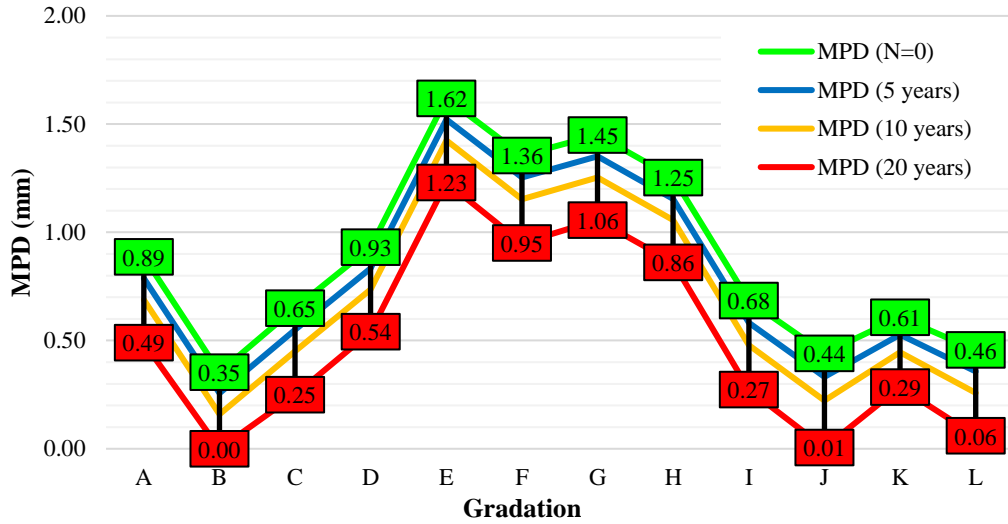
Source: the author.

2.6.4 Analysis of MPD and traffic

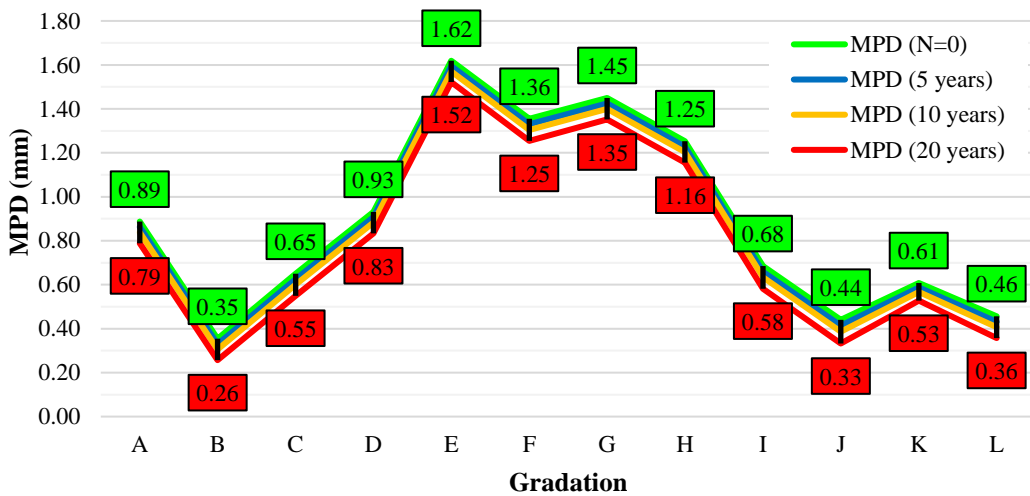
The model introduced by Aldagari *et al.* (2020) also presents a prediction equation for MPD based on gradation (Weibull distribution) and traffic levels. According to this model, there is a correlation between traffic volume and mineral aggregate degradation susceptibility (evaluated in terms of Micro-Deval). Figure 19 shows the MPD variation predicted for each gradation group. This result refers to the extreme traffic conditions (so-called “low” and “very heavy” traffic, with an average of 300 and 1,200 vph measured in the peak hour, respectively)

and the periods of 0, 5, 10, and 20 years of degradation. The higher MPD expected results were the ones from PFC gradations (E, F, G, H), while mixtures with higher levels of fine material (B, J, L) had the worst predicted performance.

Figure 19 - Predicted MPD values trough 20 years in service



(a) Very heavy traffic (1200 vph)



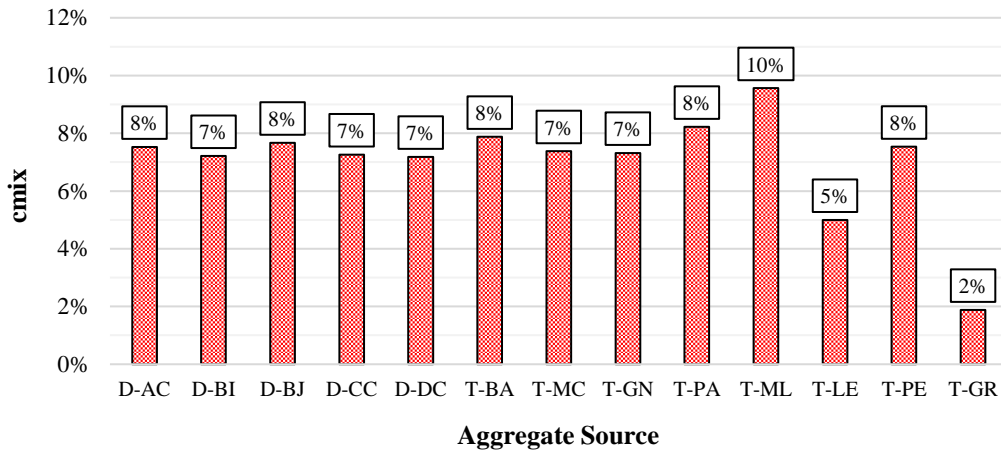
(b) Low traffic (300 vph)

Source: the author.

When it comes to the aggregate-traffic relationships, the rate of change in IFI (c_{mix}) is a function of angularity and texture before and after degradation using the MD equipment. The majority of the aggregate sources presented predicted c_{mix} values between 7 and 8%. The TML aggregate specifically showed the highest c_{GA} and c_{TX} values, resulting in a higher c_{mix} value. The TGR aggregate presented the lowest c_{GA} and c_{TX} values, which impacts on the lower susceptibility of this aggregate source to the loss of friction with time and traffic. The TLE aggregate, despite its behavior in terms of loss of angularity, presents resistant surface texture.

In this case, there is no expressive variation of this property evaluated in AIMS before and after 105 minutes of wear in the MD. Figure 20 presents a summary of these variation indexes.

Figure 20 - Variation of IFI for different aggregate sources



Source: the author.

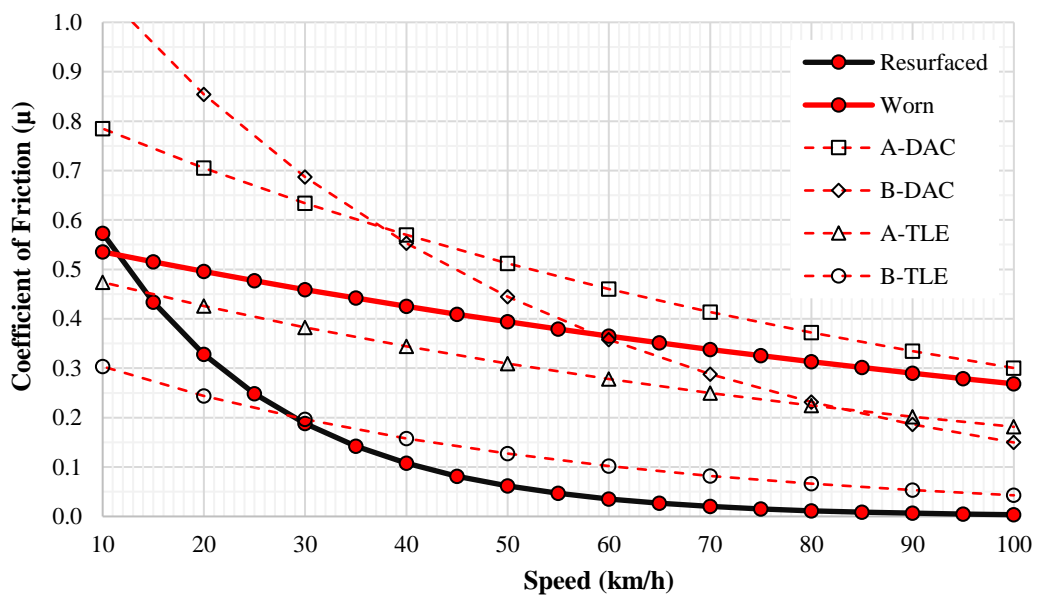
2.6.5 Field analysis

As mentioned in the method session, 120 tests were performed in the field, employing the SP and BP tests in areas of visible wear and areas treated with the maintenance strategy based on fine-graded mixtures of indefinite age (resurfaced). The results obtained at the *Senador Virgílio Távora* avenue (Fortaleza, Brazil) supported the traffic safety analyses published by Costa (2017) and Maia *et al.* (2020). Figure 21 presents the comparison between the tire-pavement friction parameters obtained in the field for real conditions (visible wear and resurfaced sections), and the ones predicted for maintenance strategies from different types of asphalt mixes. This analysis evaluated the "extreme" aggregate sources in terms of surface texture (DAC and TLE) and different gradations. The maintenance-strategy gradations analyzed were: (a) DG AC - DNIT 031/2006 – ES; (b)FG AC – DNIT 032/2005 - ES, and (c) PFC - DNER 386/1999 – ES. The continuous lines refer to the field results, and the dashed lines refer to the maintenance strategy (values of μ in initial service life). The Aldagari *et al.* (2020) model was employed to predict the μ values for different speeds, harmonized through the IFI method.

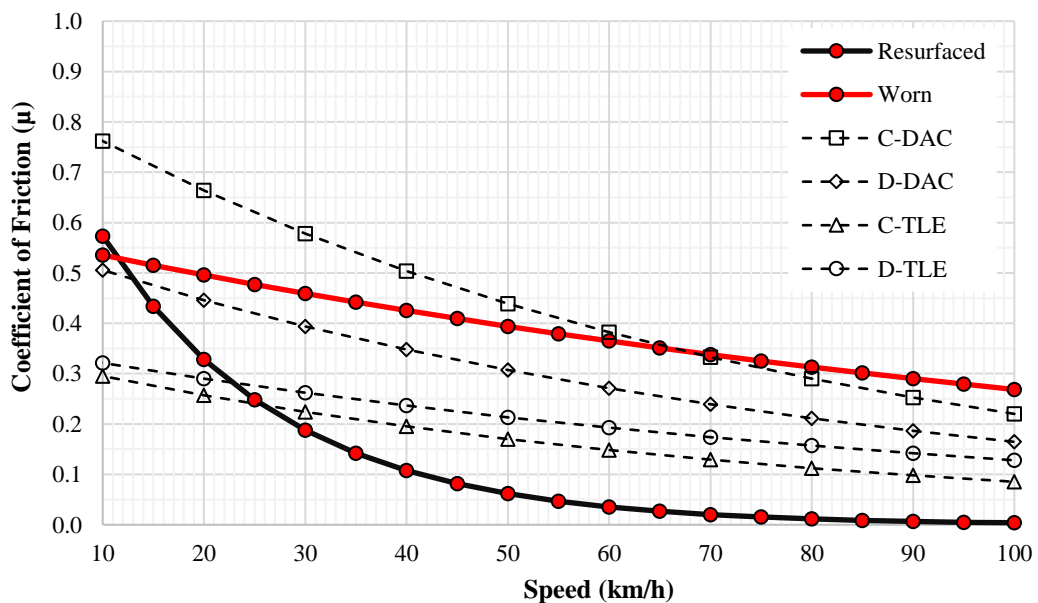
The Brazilian Asphalt Pavements Restoration Manual (DNIT, 2006) indicates IFI values (at 60 km/h) higher than 0.30 as optimal. According to Aps (2006), F60 values higher than 0.35 are satisfactory. As seen in Figure 21, only PFC-mixtures had optimal/satisfactory IFI value regardless of the selected mineral source. At low speeds, mixtures with a higher

content of fine aggregates, including the typical asphalt mixture used in Brazil for resurfacing purposes (fine-graded mixtures), have the worst performance when it comes to the predicted friction. The observation of Figure 21 also suggests that replacing worn surfaces by dense-graded or PFC mixtures may represent friction improvement, especially in lower-speed zones, such as near signalized crossings. For velocities above 40 km/h, PFC and DG AC mixtures with a higher content of coarser aggregates had a better performance in terms of predicted initial IFI.

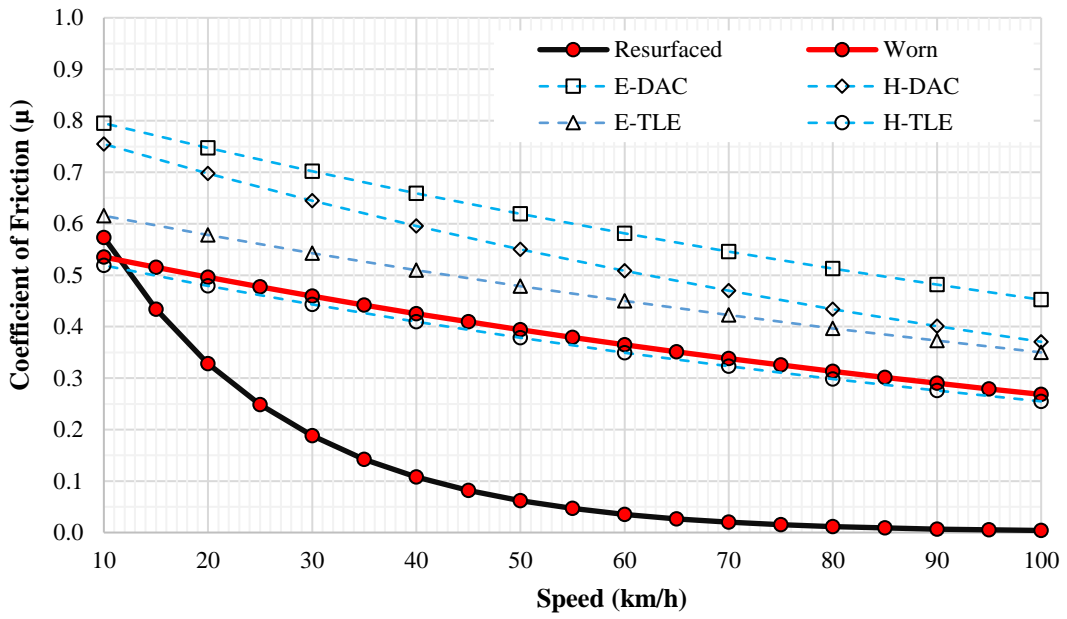
Figure 21 - Analysis of different maintenance strategies according to gradation and aggregate source



(a) Dense-graded asphalt concrete for roadways



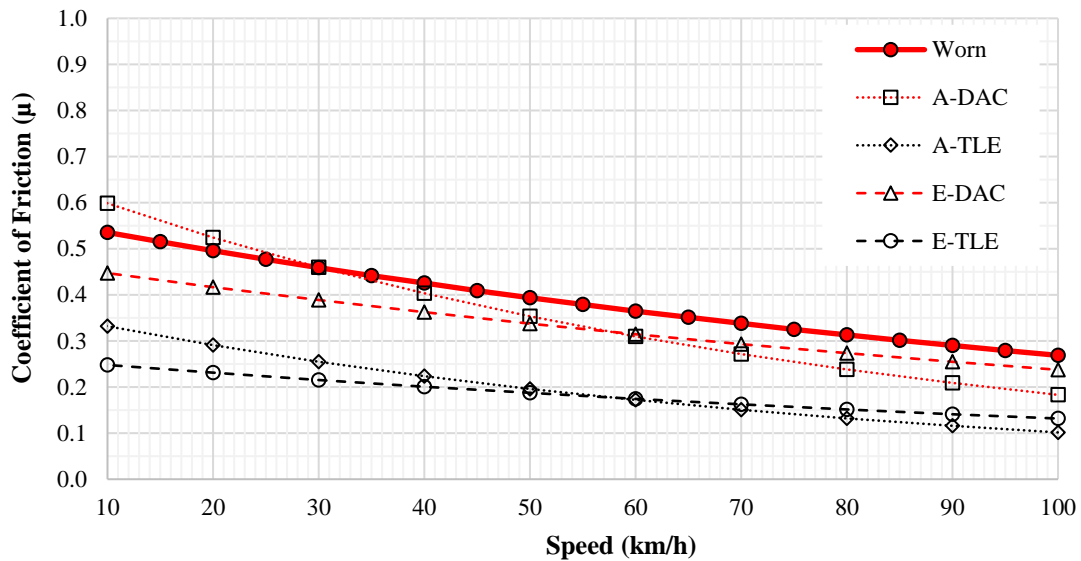
(b) Fine-graded asphalt concrete for roadways



(c) PFC for roadways

Source: the author.

Finally, the analysis presented in Figure 22 supports the verification and validation of the similarity of the predicted IFI values for a typical aggregate from the Fortaleza area. Regardless of the particle size distribution, the harmonized IFI curves predicted in the laboratory (dashed) and measured in the field (continuous) are close to each other for the DAC aggregate. This finding validates the hypothesis of similarity of behaviors between different aggregates from the same region (Northeast), regardless of the gradation used. In this case, at 60 km/h, the difference between the final IFI predicted for the DAC aggregate for different particle sizes (dense-graded and PFC, for example) showed a difference of less than 0.1 for the F60 measured in the field in the worn section.

Figure 22 - Comparison between predicted IFI_{final} and worn section in field

Source: the author.

2.7 Partial conclusions

Achieving a proactive approach to traffic safety in terms of infrastructure depends on the acquisition of data to predict some characteristics of pavements. Therefore, the possibility to use properties of asphalt mixture components to predict texture and friction becomes a valuable asset for transport engineers and public managers. The objective of this chapter was to review and to propose the utilization of models to predict the friction coefficient (μ) of asphalt pavements based on advanced laboratory materials characterization using DIP techniques. The model found to be the most adequate to the practical application of the purposes of this study (ALDAGARI *et al.*, 2020) required the integration of three inputs: (i) mineral aggregate shape properties; (ii) mixture gradation; and (iii) traffic parameters.

DIP techniques such as the ones applied using the Aggregate Imaging Measurement System (AIMS) can contribute to the generation of a robust database in terms of the mineral aggregate shape properties. Therefore, two mineral aggregate groups were selected to compose an initial structured Brazilian database in terms of aggregates shape properties and degradation over time (using the Micro-Deval equipment). Aggregates' data from northeast Brazil (DIÓGENES, 2018) and from southeast Brazil (TROTТА, 2020) comprised this work's database.

Statistical analysis confirmed the significance of both the "gradation" and the "mineral aggregate source" variables on the result of predicted tire-pavement friction at initial stages (IFI_{initial} , right after construction). On the other hand, for the tire-pavement friction

conditions at terminal service life, only the "mineral aggregate source" variable was found to be statistically relevant. It is worth highlighting that, according to the applied model, the more resistant to polishing in the MD equipment, the more the aggregate source can contribute to maintaining an adequate friction coefficient over time.

For speeds above 60 km/h, PFC-type and coarser DG mixtures showed better performance in terms of the predicted tire-pavement friction. This result highlights the importance of selecting an adequate mixture gradation when performing maintenance strategies. One example of such need is the fact that mixtures with a higher content of fine aggregates presented lower predicted friction coefficients at lower speeds. Therefore, this maintenance strategy may be risky at points such as signalized crossings, in which the friction at low speeds determine the safe deceleration to avoid the need for evasive maneuvers.

Regarding the analysis of the Northeast aggregates, this work highlights the importance of observing not only the initial aggregate properties, but also if it is susceptible to "lose" these shape properties after a polishing in equipment such as the Micro-Deval. Furthermore, the model used to predict friction considers angularity as a property that contributes to decreases in the friction value. Some findings, such as the ones presented by Diógenes (2018), suggest that angularity and surface texture depend on mineral characteristics (such as the heterogeneity of mineral grains, the preponderance of lithotypes, and the grain-to-grain contacts). This means that, even when aggregates have the same general mineral classification (such as what happens for the three gneissic aggregates and the two phonolytic aggregates), the internal structure of particles may influence on several characteristics, including the ones found by Aldagari *et al.* (2020) to govern the tire-pavement friction modeling.

The different predicted friction values were compared to actual field measurements of two section types: (i) worn surface areas, and (ii) resurfaced section (which received maintenance treatment with indefinite fine-graded asphalt mixture). This analysis validated the previous finding of the general similarity of behaviors between different aggregates from the same region (in this case, the Brazilian northeast). The harmonized IFI_{final} curves predicted in the laboratory and measured in the field were close to each other, regardless of the gradations used. In general terms, the findings presented in this chapter introduce a more proactive approach to the consideration of tire-pavement friction and traffic safety at the hot-mix asphalt (HMA) mix design phase.

3 ADVANCES IN THE ANALYSIS OF ASPHALT PAVEMENTS' SURFACE TEXTURE AND FRICTION USING THE AGGREGATE IMAGING MEASUREMENT SYSTEM (AIMS) AND 3D COMPUTER VISION

3.1 Initial considerations

Assessing texture and friction characteristics of asphalt pavements is an essential task, but the relationship between such characteristics is still not fully understood (KOUCHAKI *et al.*, 2018). Also, this assessment relies, by one side, on simplified and empirical tests. On the other hand, achieving precision in this assessment depends on advanced and expensive tests. Much of this is because the most accessible skid-resistance tests provide static measurements of pavement conditions at one point in time. However, traffic and environmental aspects (such as vehicle weight and speed, temperature, and pollution) occur under varying conditions over the pavements' service life (VEITH, 1983; FWA and ONG, 2008; DO *et al.*, 2014; DAN *et al.*, 2017). Some recently developed methods aim to establish a relationship between surface parameters obtained using Digital Image Processing (DIP) techniques and those obtained from standardized protocols. Combining such data supports the prediction of tire-pavement friction at the design and post-construction phases. These techniques include the use of the Aggregate Imaging Measurement System (AIMS) (REZAEI *et al.*, 2011; ARAUJO *et al.*, 2015; ALDAGARI *et al.*, 2020), and three-dimensional surface modeling from Close-Range Photogrammetry (CRP) (KOGBARA *et al.*, 2018; CHEN *et al.*, 2019).

3.2 Specific objective

The objective of this chapter is to advance the characterization of the tire-pavement friction in contactless post-construction assessments using DIP tools such as AIMS and CRP.

3.3 Literature review

3.3.1 Ordinary characterization of texture and friction

Many techniques support the assessment of asphalt pavements' surface texture, many of these recently reported by KOGBARA *et al.* (2016). There are two main types of texture measurements: static and dynamic. In general, static tests are more common: the sand patch (SP) for macrotexture and the British pendulum (BP) for microtexture (assessed through a friction parameter). The SP volumetric technique (ASTM E965-15, 2015) quantifies the average macrotexture depth. This parameter represents the depth of the pavement area that accommodates 25 cm³ of standard sand circularly spread by the operator over the pavement surface. The BP test (ASTM E303-93, 2018) represents the impedance imposed by a surface to the sliding of a standardized rubber pendulum. The impedance must be expressed in BPN (British pendulum number). The harmonization of different methods is relevant to ensure uniformity of texture and friction values. The proposition of the international friction index (IFI) (ASTM E1960, 2015) was the fundamental step for the mentioned objective (WAMBOLD *et al.*, 1995). In the last decade, tests have been performed in extreme conditions for macrotexture (from 0.16 to 2.50 mm) to evaluate the IFI method limitations. The literature converged to 1.50 mm as the upper limit of the macrotexture average depth for the IFI method (FUENTES *et al.*, 2012).

Three different types of techniques are used to measure macrotexture: (i) volumetric tests; (ii) profilometers; and (iii) drainability tests. Table 14 summarizes some texture measurement tests. It is important to mention that volumetric tests are associated with macrotexture ($0.5 \text{ mm} < \lambda_w < 50 \text{ mm}$) and techniques such as the Laser Profilometer may capture microtexture scales ($\lambda_w < 0.5 \text{ mm}$). Friction tests are performed for indirectly measuring microtexture of wet surfaces, to represent the condition that may be more significant for vehicular skidding, as seen in Table 15.

Table 14 - Texture measurement tests

Equipment/Method	Positive Aspects	Negative Aspects
Sand Patch (SP)	Standardized, quick and low-cost	Empiricism, result represented by only one parameter (statistic issue), besides problems such as segregation and small area evaluation
Laser Test	Good correlation with sand patch method, possibility of capturing wavelengths of microtexture scale	Expensive equipment, post-processing data needed, limitation of capture of microtexture scales (below 0.05 mm)

Source: adapted from Kogbara *et al.* (2016).

Table 15 - Friction measurement tests

Type of Measurement	Tests	Physical Principle	Speed
Longitudinal Friction	ADHERA, BV-11, GripTester, RoadSTAR, ROAR DK, ROAR NL, Skiddo-meter BV-8, SRM, TRT, SRT-3, IMAG, T2GO, VTI Portable Friction Tester (PFT)	Tire-pavement friction measurement at different Slip Ratios (SR) (a relation between tire and vehicle speeds)	Variable from 5 (GripTester) to 140 (TRT) km/h*
Sideway Friction	SCRIM, SKM	Tire-pavement friction measurement at different SR and a Slip Angle (set to the vehicles' travel direction)	50 km/h for both
Stationary Measurement	Pendulum Test (British Pendulum) (PB), DFT (Dynamic Friction Tester)	Device fixed at a reduced area (single-point friction measurement)	DFT: variable (10-80 km/h) BP: 10 km/h

* GripTester measurements may be performed at 5 to more than 100 km/h. TRT measurements may be performed at 40 to 100 km/h.

Source: adapted from Kogbara *et al.* (2016).

Several conventional tests for analysis of aggregates' shape and asphalt mixtures' texture properties use simple equipment. Nevertheless, such techniques may be time-consuming and determine only average indexes, disregarding the cumulative distribution of properties (MASAD, 2005). On the other side, pavement assessment may rely on sophisticated and expensive tests to overcome precision issues. Advanced techniques such as DIP use cameras or scanners to capture images, as well as computational packages that perform the statistical processing of data. AIMS and CRP are some examples which can create a balance between simple protocols and a robust analysis of data.

The obtention of surface conditions parameters may vary according to the applied test method. Factors that generate variability to the SP test include the wind conditions, as well as the operators' experience. The same is true for the BP test, which may vary depending on the equipment calibration, the accuracy of readings, and operator experience. Furthermore, there are influences in terms of the surfaces' irregularities scales (slope and macrotexture) and the dry/wet conditions (which also may vary in terms of the water film thickness).

3.3.2 The Aggregate Imaging Measurement System (AIMS)

Besides aggregates shape properties analysis (AL ROUSAN, 2004; MASAD, 2005; BESSA, 2012; DIÓGENES, 2018; IBIAPINA, 2018), the AIMS equipment may provide asphalt mixtures texture analysis (REZAEI *et al.*, 2011; ARAUJO *et al.*, 2015). Macrotexture evaluation results from readings of the distance between a camera and an asphalt mixture sample surface. Microtexture evaluation employs the analysis of captured pixels. For the texture analysis, the AIMS equipment performs 5 imaging scans of each sample at different zoom magnitudes. The first scan takes place at the maximum zoom magnitude. The microscope lenses move vertically at each image taking until detecting a high-resolution grayscale image. This process results in a 2D reconstruction of the macrotexture profile (REZAEI *et al.*, 2011). The microtexture analysis happens at the 3 last sweeps. The equipment works at the same magnitudes of aggregates' surface texture evaluation (4.75 mm, 9.5 mm, and 19 mm sizes). The microtexture processing technique employs the wavelet method, which is a function of the average and the standard deviation of pixel values of the processed images (Equation 29) (MASAD, 2005). Figure 23 presents part of the protocol for measuring texture of asphalt mixtures with the use of AIMS.

$$\text{Surface Texture} = \frac{1}{3n} \sum_{i=1}^3 \sum_{j=1}^N (D_{i,j}(x,y))^2 \quad (29)$$

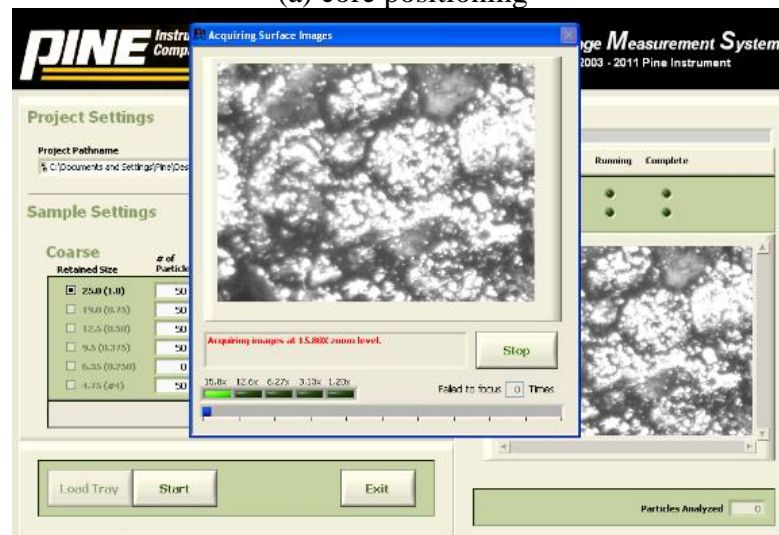
In which:

- D: decomposition function;
- n: level of image decomposition;
- N: total number of coefficients in a detailed image;
- i: texture direction;
- j: wavelet index;
- x, y: location of the coefficients in the transformed domain.

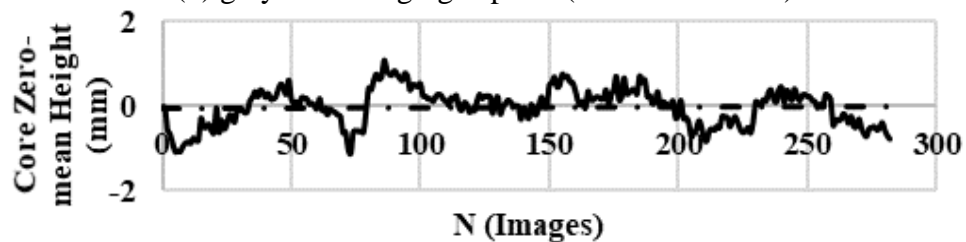
Figure 23 - AIMS asphalt mixture texture analysis process



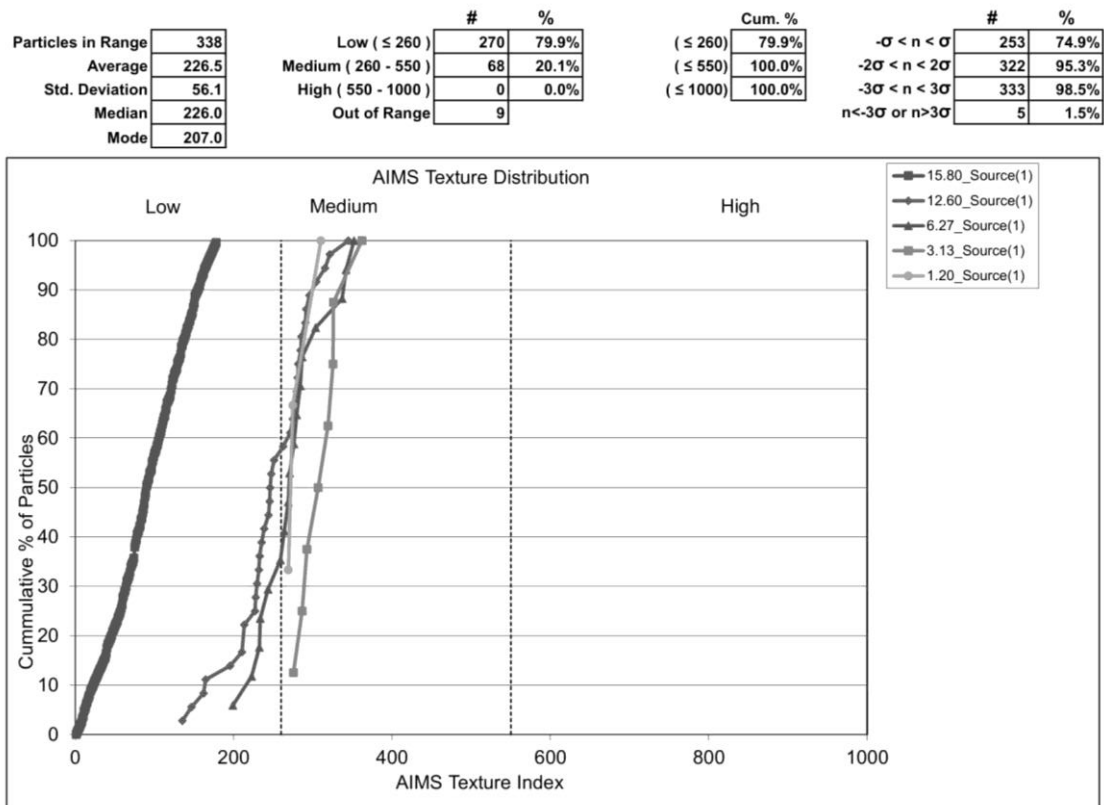
(a) core positioning



(b) grayscale imaging capture (maximum zoom)



(c) processed macrotexture profile (points captured at each 0.3 mm)



(d) processed microtexture results

Source: adapted from Araujo (2017).

The variability of the findings (REZAEI *et al.*, 2011; ARAUJO *et al.*, 2015; ARAUJO *et al.*, 2020) when it comes to the relationships between AIMS and more scientifically consolidated tests is one of the concerns of the use of AIMS for evaluating asphalt mixtures texture. It is necessary to emphasize, therefore, the need for extensive care when interpreting results in terms of correlation (R^2), because experiment frameworks may not provide proper variation of characteristics, as shown in Chapter 2, especially in terms of microtexture. As previously discussed, the use of the same mineral aggregate source (or aggregate sources from the same region), or the same aggregate particles' gradation in different experiments can make it hard to understand the relationship between AIMS texture parameters and those obtained through other tests, given the fact that the evaluated specimens may not be statistically different from each other.

One relevant aspect of the analysis of AIMS shape properties results is the application of specific classification systems. However, there is no system developed for asphalt mixtures surface texture specifically. Therefore, the direct application of the aggregates surface texture classification (AL ROUSAN, 2004; IBIAPINA, 2018) is frequently used for the

analysis of asphalt mixtures' microtexture. Table 16 shows surface texture classifications in two systems (North-American and Brazilian). It is worth mentioning the relative differences between the two systems: for example, an aggregate classified as "High Roughness" according to the Al Rousan (2004) system may be classified as "Low Roughness" according to the Ibiapina (2018) system. Also, it is important to highlight that these classifications derive from statistical analysis of a database, and there is no fundamental relationship between the surface texture classification in AIMS and the physical phenomenon of tire-pavement friction itself. Even so, these systems are essential for the comparison between different aggregates.

Table 16 - Classification systems for aggregates surface texture (AIMS parameter)

Shape property	System	Limits				
Surface Texture	Al Rousan (2004)	<165	165-275	275-350	350-460	>460
	Ibiapina (2018)	<260	260-440	440-600	600-825	>825
	Classification	Polished	Smooth	Low Roughness	Moderate Roughness	High Roughness

Source: the author.

3.3.3 The Close-Range Photogrammetry (CRP)

3.3.3.1 General view

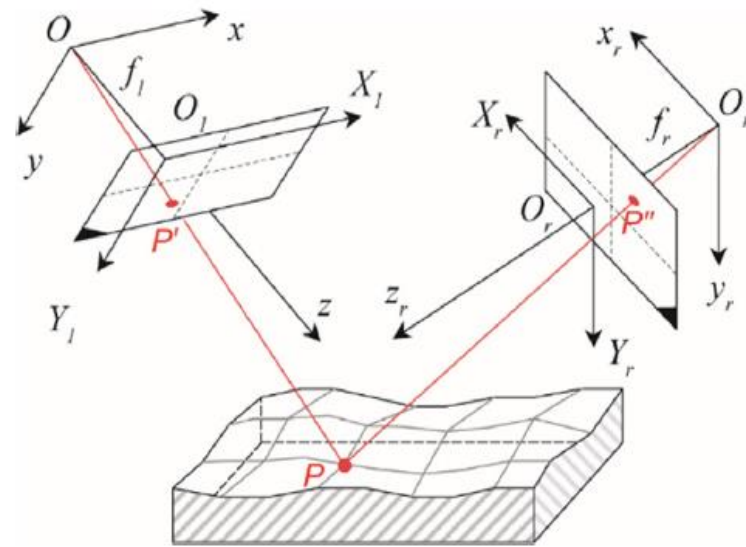
One of the DIP techniques that simplify and reduce the empiricism of state-of-practice texture evaluation methods is the 3D Computer Vision. This technique is based on the concepts of stereoscopy and photogrammetry. The stereophotogrammetry is the incorporation of multiple images from different angles to estimate 3D coordinates of a targeted surface points using the triangulation method (HARTLEY and STURN, 1997). Close-Range Photogrammetry (CRP) represents the use of ordinary cameras to surfaces' tridimensional reconstruction (MCQUAID *et al.*, 2014; CHEN *et al.* 2019). This method depends on camera parameters calibration and the overlapping processes, which will define the relative positions between subsequent image captures, applying scale factors and correcting lens distortions. Although complex, using computational tools simplifies this process by incorporating self-calibration algorithms if a considerable number of subsequent images is taken (TIGGS *et al.*, 2000). This way, computational packages may quickly generate a topographical map of the targeted surfaces. These packages automatize the steps of self-calibration, feature matching, triangulation, depth extraction, and 3D mesh generation.

3.3.3.2 Theoretical background

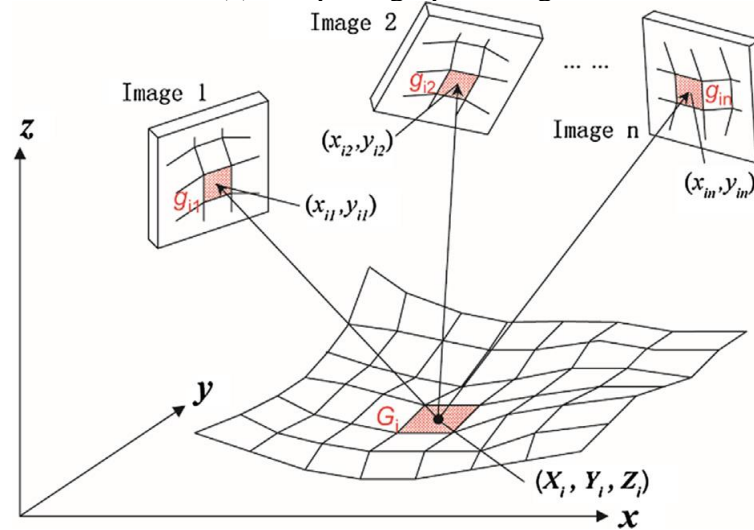
Figure 24 presents a simplified scheme representing the image-taking of a target surface. The cameras are positioned at the points O and O_r (which differ according to translation and rotation matrices). At each imaging, focal lengths are formed, leading to the representation of surface vision in two-dimensional planes (point P is captured at positions P' and P''). In the Close-Range Photogrammetry (CRP), images are taken within a coordinate system (x_c, y_c, z_c) from points where the cameras are positioned. By defining a specific focal length for each captured image (f_c), images are formed on a two-dimensional plane, where each point of the evaluated surface (x, y, z) will have a position (x_p, y_p) on the corresponding resulting plane. The images formed are a two-dimensional view, in which each point of the targeted surface will have a position (x_p, y_p) that will be defined as a function of x, y, z, x_c, y_c, z_c and f_c . At this moment, for each image taken, there is a set of complex solution systems of mathematical equations.

As new images are taken, from new angles and new positions, rotation and translation matrices are added to the mathematical systems, which will then represent new camera positions as a function of the starting one. Obtaining new images from different positions enables the estimation of x, y, z values, which become more accurate as taking more photographs. With the development of techniques of automated calibration of different parameters and hence the solution of equations, it is possible a better estimation of the coordinates of the points of a target surface from a more rational and practical process.

Figure 24 - Representation of image taking of a target surface using the CRP technique



(a) two photograph-takings



(b) multiple photograph-takings

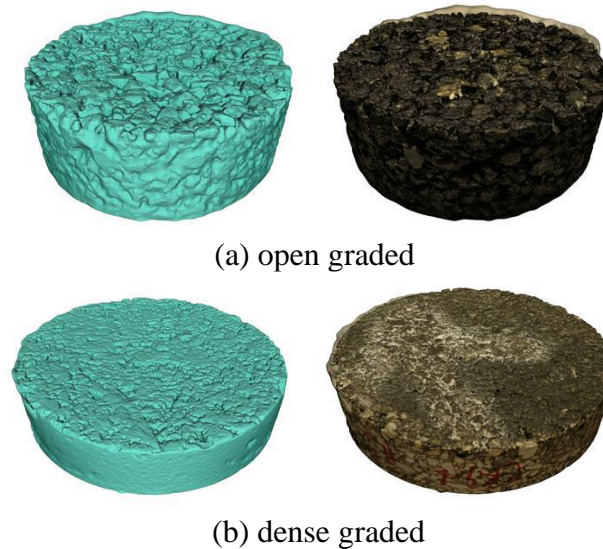
Source: adapted from Chen *et al.* (2019).

3.3.3.3 Macrotexture-related analysis

Medeiros *et al.* (2016) evaluated the macrotexture of different types of asphalt mixtures using CRP: dense-graded hot-mix asphalt, weathered hot-mix asphalt, open-graded friction course, and chip seal (see examples in Figure 25). Before the experimental framework, a calibration process was conducted to evaluate the feasibility of using CRP for this purpose. The authors compared a known profile from a calibration plate and the modeled profile obtained using the CRP technique, as shown in Figure 26. A similar calibration analysis was made by comparing CRP-based texture evaluations of HMA samples and the ones obtained through a

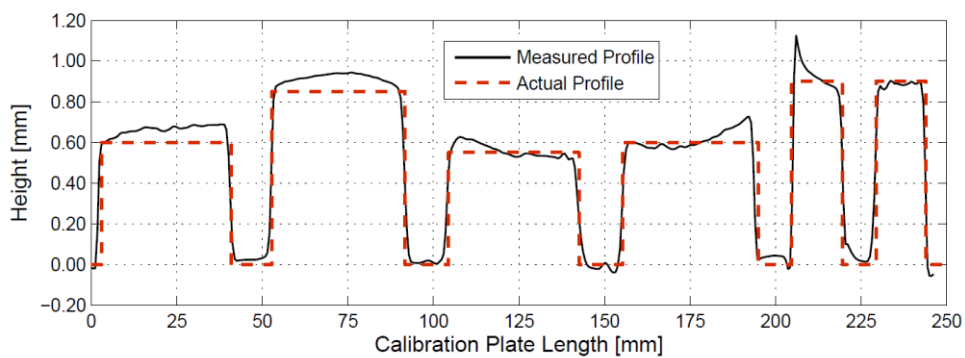
laser-scanning. The laser-scanning technique is a robust method of accurate surface profile evaluation. The authors concluded that CRP measurements were satisfactorily precise and accurate, highlighting its potential for evaluating pavement surface conditions.

Figure 25 - 3D models of two asphalt mixtures



Source: Medeiros *et al.* (2016).

Figure 26 - Comparison between an actual and a CRP-measured profiles



Source: Medeiros *et al.* (2016).

When pavements' surface is reconstructed by a three-dimensional model using the CRP technique, texture parameters such as the ones proposed by the American Society for Testing and Materials (ASTM) and the International Organization for Standardization (ISO) can be obtained from model processing. Parameters obtained from CRP have been reported to correlate well with SP test results (R^2 over 0.90), depending on factors such as equipment accuracy and software calibration (KOGBARA *et al.*, 2016). In the case of the study conducted by Medeiros *et al.* (2016), CRP-based calculated Mean Profile Depth (MPD) values of the different types of mixtures were found to be remarkably close to the SP Mean Topographical

Depth (MTD) values (no points outside a 95% prediction interval). Furthermore, the coefficient of correlation (R^2) of over 0.90 (MEDEIROS *et al.*, 2016; CASEY *et al.*, 2018) indicates that the CRP method can be adequately used as a static macrotexture measurement procedure.

Chen *et al.* (2019) conducted a study to compare macrotexture parameters from CRP and laser-scanning (ZGScan) methods. The results have also proven that texture data obtained by a CRP automatized system may present satisfactory accuracy and efficiency. In this case, mixed-language programming based on MATLAB and Python was applied to create a 3D surface reconstruction software that was able to control illumination and image acquisition processes in a platform specifically designed for such purpose. The authors also measured the time consumption of the different methods (CRP, laser-scanning, and sand patch) in 6 points, highlighting the potential to optimize efficiency on texture measurements by using an automatized CRP technique.

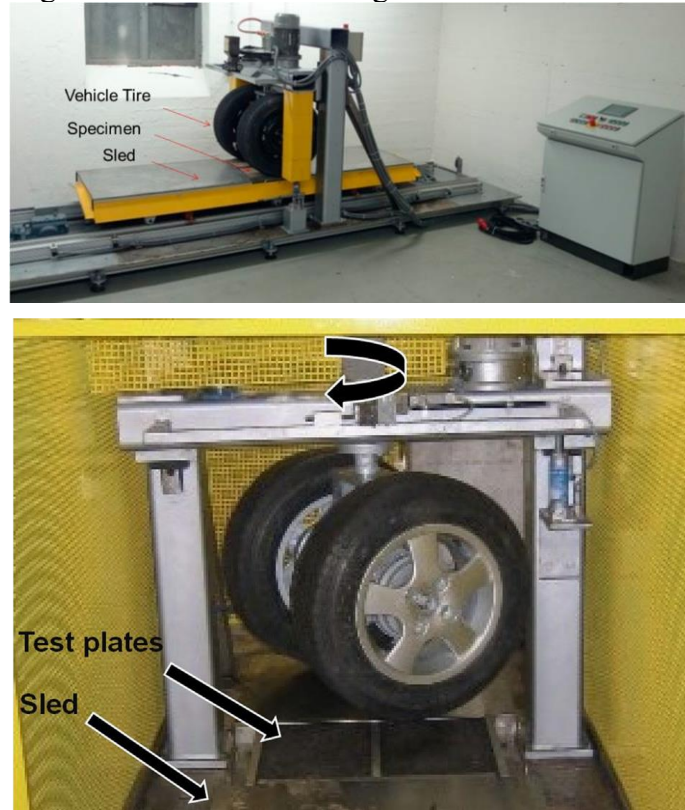
3.3.3.4 *Microtexture-related analysis*

One of the most recent studies regarding the understanding of the influence of the microtexture scale on tire-pavement friction was conducted by Wang *et al.* (2018). The authors grouped 11 aggregate types, each one characterized according to its mineralogy (3 graywacke; 2 diabase; 2 granite; 1 rhyolite; 1 gabbro; 1 basalt; 1 limestone). Mineral aggregate surface plates were manufactured under two conditions: before and after the aggregates were polished in the Micro-Deval (MD) equipment. According to the authors, although the test method in question adds characteristics common to the surface wear mode over its service life (dust and moisture, for example), abrasion does not occur from materials whose composition resembles tire rubber (given the abrasive material is made up of steel balls).

As an effort to bring the laboratory polishing process closer to the one observed in the field, the Aachen Polishing Machine (APM) (Figure 27) equipment was developed, providing a polishing process which occurs by the friction of the surface tested against a rubber-manufactured device from actual vehicle tires (0.2 MPa pressure and 200 kg load) (WANG *et al.*, 2014). The method applied for the friction measurement of the plates in such different conditions of polishing was based on the Wehner/Schulze (W/S) equipment, which reports the surface friction coefficient at a speed of 60 km/h. This equipment consists of rubber covered structures, which rotate sliding through the evaluated surface. In general, the plates whose material were not subjected to wear on MD had a friction coefficient 31% higher than those that were polished in the MD. Furthermore, the coefficient of friction was lower the longer the

surface polishing time in the APM equipment. As expected, aggregates from different mineralogical origins have different friction coefficient values, as well as different susceptibilities, both to MD wear and APM polishing.

Figure 27 - Aachen Polishing Machine



Sources: Wang *et al.* (2014) and Wang *et al.* (2018).

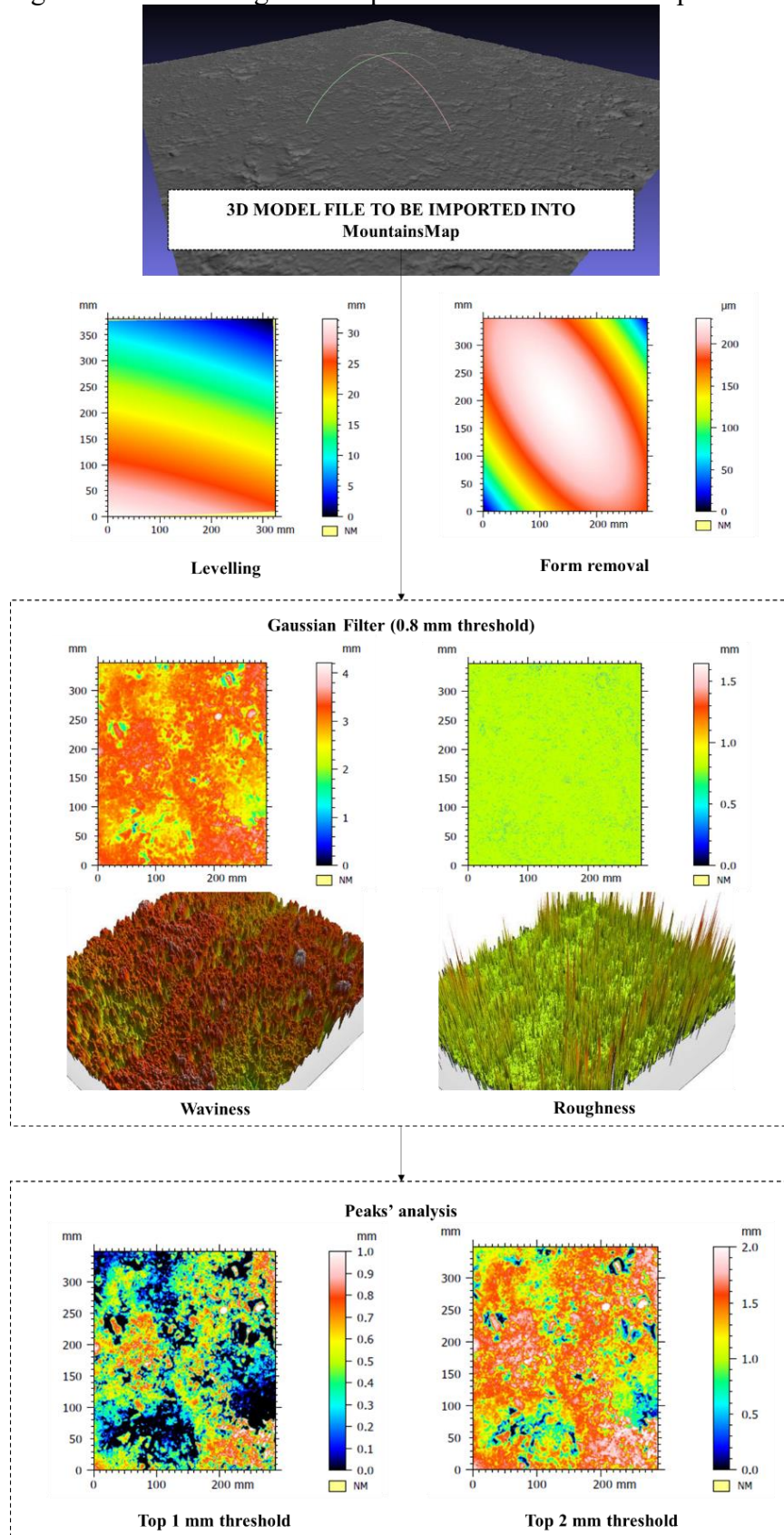
The mentioned method was performed to create different scenarios in which only the microtexture scale would vary. This way, the surfaces were evaluated concerning Mean Profile Depth (MPD) before and after the polishing process performed by APM, revealing that indeed macrotexture remained stable. The three-dimensional surfaces were evaluated using a high-resolution profilometer (accuracy of 6 nm and a lateral resolution of 3.3 μm). Spectral surface analysis was performed, segregated at different wavelength intervals, showing that the Logarithmic Power Spectral Density (LPSD) parameter (HARTIKAINEN *et al.*, 2014) presented a variable R^2 value when compared with friction coefficient values. Shorter wavelengths ($< 100 \mu\text{m}$) had the most influence on the change of the surface friction coefficient. The research indicated that friction properties (if maintained a stable macrotexture) depend on the mineral aggregate surface texture (specifically on the texture wavelengths range between 32 and 128 μm).

3.3.3.5 Friction-related analysis

One of the most recent models for tire-pavement friction related to texture relates ISO parameters obtained using CRP to friction measurements from the use of the GripTester (GT) equipment ($R^2 = 0.75$) (KOGBARA *et al.*, 2018). This model resulted from the analysis of 900 m of 2-lane road sections in Qatar. The North-South and South-North directions presented different daily traffic volumes, therefore different levels of polishing. Different dense-graded asphalt mixtures in the test sections were designed in 2010 using the Marshall methodology, gabbro (basaltic) aggregates, and different asphalt binders, including 40/50, 60/70 (1/100 mm) penetration, and polymer-modified asphalt (SADEK *et al.*, 2015). GT equipment measured georeferenced friction at 50 Km/h (15% fixed slip ratio on 0.5 mm water film wetted surface) at every 5 m of the section. The authors used a single-lens digital camera to capture around 12 images from 12 different locations under natural lighting and minimum overlap requirements.

The MountainsMap (DigitalSurf) software imported the 3D models generated through the CRP technique from the taken photographs. The surface leveling (using the minimum-squares method) and form removal (using a second-order polynomial function) represented the first processing. After that, a Robust Gaussian Filter (RGF) operator allows the "separation" of roughness and waviness, according to wavelengths magnitudes (0.08 mm cut-off length). Afterward, given the hypothesis that the equipment tire has contact only with the upper 2 mm depth of the wearing course, the operator has also applied the top of the 1- and 2-millimeters thresholds to the models. At the end of the process, one may obtain ISO parameters (ISO 25178-2 2012) for each of the processed models. Figure 28 summarizes this process.

Figure 28 - Processing method performed in MountainsMap



Source: the author.

The authors introduced a friction prediction equation from ISO 25178-2 (2012) standardized parameters obtained from the application of MountainsMap software. The friction coefficient (μ) (GN at 50 km/h) was found to be represented by the parameters V_{mp} (volume of material referring to the 10% highest peaks in the three-dimensional mesh) and S_{pd} (peak density of the evaluated surface) of the top 2 mm of the model. In summary, $GN_{predicted}$ can be calculated according to the model shown in Equation 30 (KOGBARA *et al.*, 2018).

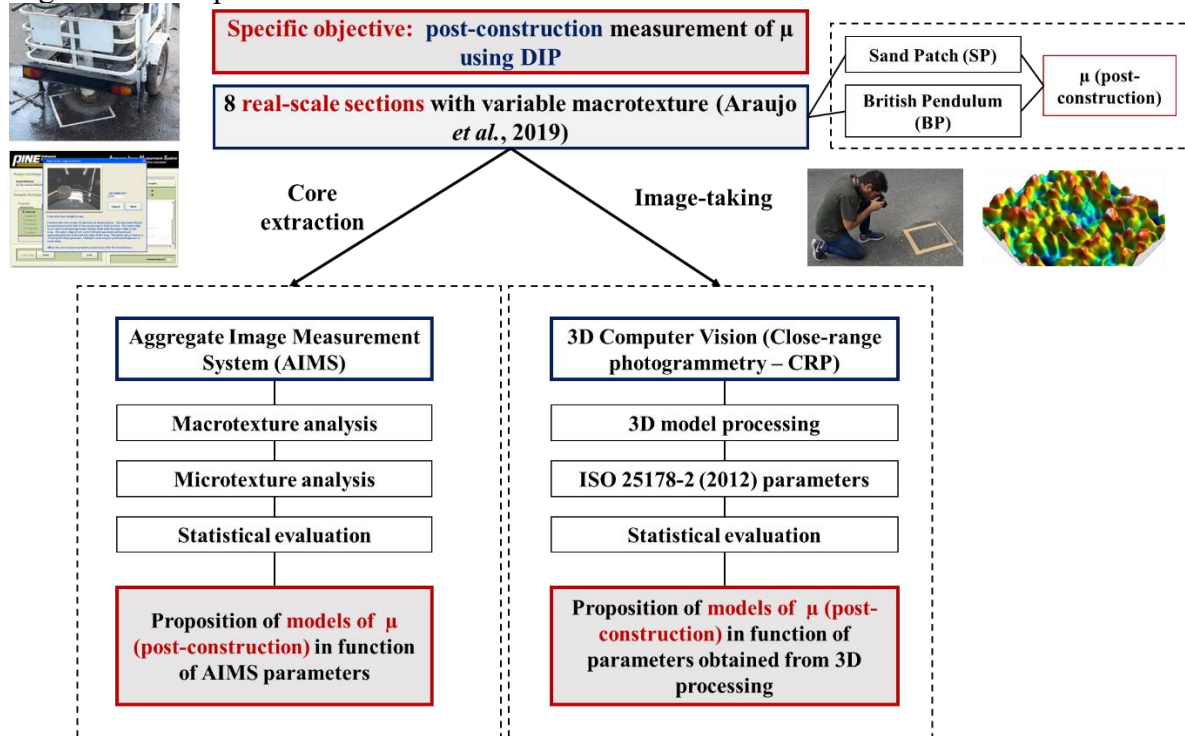
$$0.155 + 1.404V_{mp} + 1.092S_{pd} < GN_{predicted} \left(\frac{50km}{h} \right) < 0.187 + 2.656V_{mp} + 1.834S_{pd} \quad (30)$$

In which: V_{mp} : peak material volume (10% threshold) (surface's top 2 mm);
 S_{pd} : peaks' density (surface's top 2 mm).

3.4 Materials and methods

The objectives of this work include the review and application of a model for the phenomenon of tire-pavement friction, which consolidates the use of DIP techniques for such a purpose. These methods may be applied in the asphalt mixtures design phase (pre-construction) or the post-construction phase. This chapter is dedicated to the post-construction phase. To accomplish this objective, the DIP techniques evaluated in this chapter are the Aggregate Imaging Measurement System (AIMS) and 3D computer vision using the Close-range Photogrammetry (CRP). Figure 29 presents the method framework for the post-construction analysis of tire-pavement friction using DIP.

Figure 29 - Chapter 3 method framework



Source: the author.

As will be thoroughly discussed in the next chapter of this work, the fundamental analysis of the relationship between traffic safety and tire-pavement friction depends on some inputs, such as traffic volume and vehicle speeds. This analysis includes the friction coefficient (μ) of an analyzed surface, which defines its maximum available deceleration rate (MADR). When there is a vehicular conflict in which the needed deceleration rates to avoid the crash (DRAC) exceeds the surfaces' MADR, the potential to the occurrence of crashes soars.

3.4.1 Full-scale test sections

A complexity involved in asphalt mixtures materials selection and compaction is achieving satisfactory texture, tire-pavement friction, and mechanical performance at the same time. Given the importance of this balance for airports' runways projects, Brazilian airport specification (DIRENG 04.05.610/02) requires the construction of experimental full-scale runways before the main project. If materials and compaction methods satisfactorily accomplish standard requirements, regulators may allow the start of construction.

Understanding the relationships between compaction and texture of asphalt mixtures in airport pavements has been part of the Brazilian scientific community efforts. In

2017, researchers from Fortaleza (Brazil) analyzed 8 full-scale experimental runways constructed by applying different compaction methods (ARAUJO, 2017). The asphalt mixture design followed the Brazilian Air Force Infrastructure Directory specification (DIRENG 04.05.610/02).

For the asphalt mixture design, 50/70 (1/100 mm) penetration asphalt binder and granitic aggregates from the Fortaleza-Brazil region were selected. Standardized tests were performed to characterize aggregates (particle gradation; Los Angeles abrasion; density of coarse and fine aggregates; adhesiveness and sand equivalent). Additionally, aggregates shape properties were analyzed using AIMS. These results were then classified according to the systems proposed by Al Rousan (2004) and Ibiapina (2018). Table 17 shows the shape properties' results and classification.

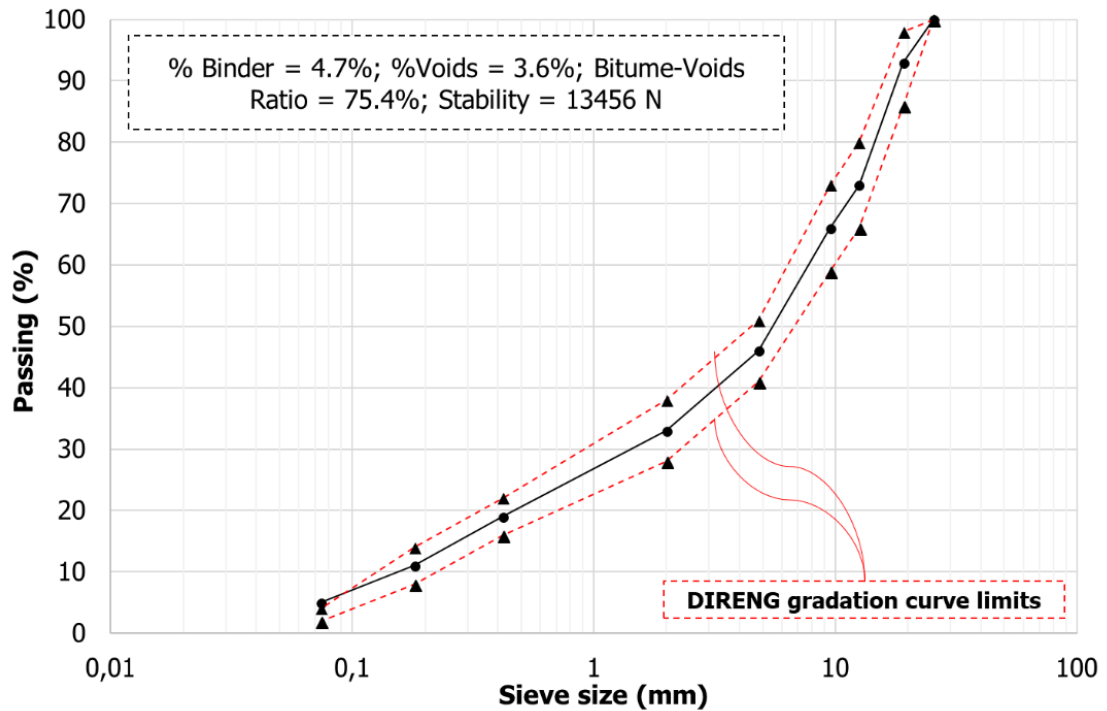
Table 17 - Aggregates shape properties

Shape property	Parameter/ Class. System	Aggregate's maximum nominal size			
		1"	3/4"	1/2"	Stone Dust
2D Form	Mean	-	-	8.10	8.29
	St. deviation	-	-	2.10	2.00
	CV (%)	-	-	25.93	24.25
	Al Rousan (2004)	-	-	<i>Semi-elongated</i>	<i>Semi-elongated</i>
	Ibiapina (2018)	-	-	<i>Semi-circular</i>	<i>Semi-circular</i>
Sphericity	Mean	0.69	0.68	0.69	0.62
	St. deviation	0.10	0.10	0.10	0.10
	CV (%)	15.75	14.31	12.92	15.11
	Al Rousan (2004)	Low sphericity	Low sphericity	Low sphericity	Low sphericity
	Ibiapina (2018)	Low sphericity	Low sphericity	Low sphericity	Low sphericity
Angularity	Mean	2,768.90	2,883.70	3,279.30	3,739.80
	St. deviation	656.20	634.20	787.00	1,151.50
	CV (%)	23.70	21.99	24.00	30.79
	Al Rousan (2004)	Sub-rounded	Sub-rounded	Sub-rounded	Sub-rounded
	Ibiapina (2018)	Sub-rounded	Sub-rounded	Sub-rounded	Sub-rounded
Texture	Mean	287.80	197.30	215.20	185.50
	St. deviation	153.38	113.90	136.10	111.00
	CV (%)	53.29	57.73	63.24	59.84
	Al Rousan (2004)	<i>Low roughness</i>	<i>Smooth</i>	<i>Smooth</i>	<i>Smooth</i>
	Ibiapina (2018)	<i>Smooth</i>	<i>Polished</i>	<i>Polished</i>	<i>Polished</i>

Source: the author.

The asphalt mixture was designed according to the Marshall method and the parameters adopted by the *Especificação Geral DIRENG 04.05.610 – CBUQ*, a specification from the Aeronautic Infrastructure Directory (Brazilian Air Force). The particles' gradation was fitted in the range II of the DIRENG standard. Figure 30 shows the gradation and the design parameters found in the laboratory for the asphalt mixture.

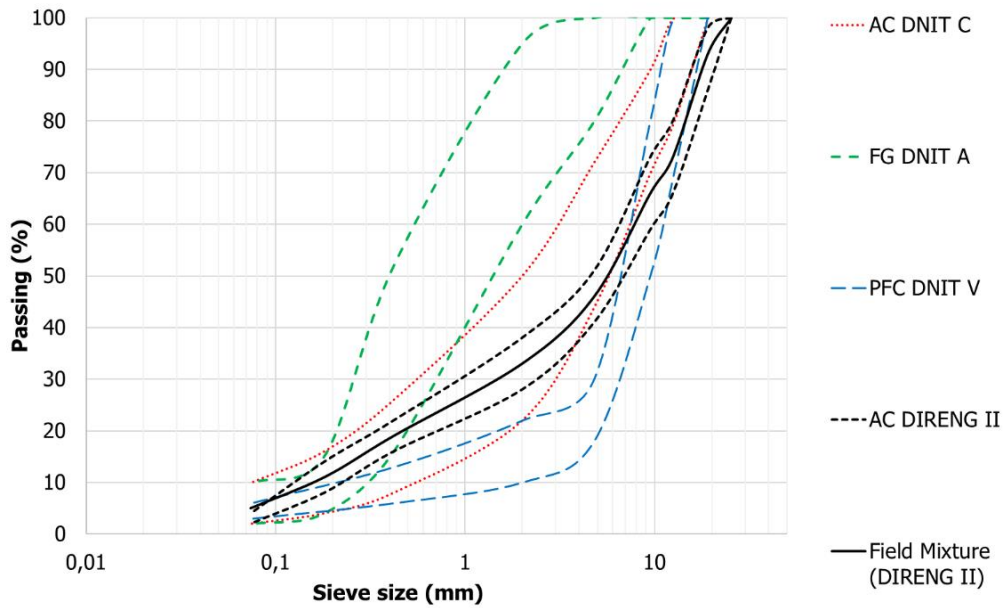
Figure 30 - Size distribution and design parameters of the asphalt mixture



Source: adapted from Araujo (2017).

The mixture in study was compared, in terms of particle size distribution, to other traditional standardized asphalt mixtures produced in Brazil. The analyzed mixtures were: (i) AC (roadways' standard), (ii) AC (airports' standard), (iii) fine-graded asphalt mixture (FG) (roadways' standard), and (iv) PFC (roadways' standard). A similarity between AC gradations from roadways and airports' standards can be observed when compared to the other gradations (Figure 31). The airport mixture gradation used in this research is similar to the coarser limit of the range of dense AC roadway mixture.

Figure 31 - Comparison between gradations



Source: the author.

The asphalt mixture was produced in a continuous plant (drum-mixer) with a nominal production capacity of 80 tons per hour. The temperature at the end of the blending process reached 170°C, and the compaction temperature was 160°C. The compaction process was performed by an asphalt paver (Leeboy 8510 model), pneumatic rollers (Dynapac CP221 models), and tandem rollers (Hamm HD75 models). Figure 32 shows the construction of the test runways.

Figure 32 - Construction of the full-scale experimental runways



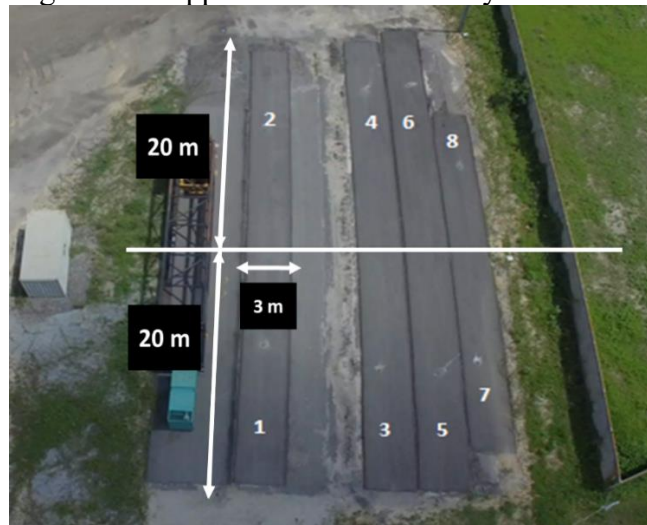
(a) asphalt paver and pneumatic roller

(b) tandem roller

Source: Araujo (2017).

Eight sections of approximately $20.00 \times 3.00 \times 0.05$ m (Figure 33) resulted from the compaction of the produced asphalt mixture. For each section, the drilling of core samples allowed the CD (%) verification. The use of different compaction protocols resulted in asphalt mixtures that presented variable CD, although the same aggregate gradation. Table 18 shows the compaction summary when it comes to the number of passes of rollers, compaction degree, and texture characterization from traditional tests (SP and BP). The texture classification refers to the Aps (2006) study. Observing the results of Mean Texture Depth (MTD), all evaluated sections presented macrotexture classified as "fine" or "intermediately fine". The exceptions concern to sections 2 and 4 (classified as "intermediately coarse"), in which the use of tandem rollers was not applied. The reduction in macrotexture with the tandem roller use occurs because the equipment applies a continuous and linearly uniform load throughout the pavement, reducing irregularities left by the pneumatic roller and accommodating particles.

Figure 33 - Upper view of the runways



Source: adapted from Araujo (2017).

Table 18 - Summary of compaction and texture results

Runway	Number of passes		CD (%)	MTD (mm)	Macrotexture Classification	BPN	Microtexture Classification
	Pneum. Roller	Tandem Roller					
1	8	4	97.3	0.35	Fine	68	Rough
2	8	-	96.1	0.84	Intermediately Coarse	73	Rough
3	4	2	95.1	0.38	Fine	76	Very Rough
4	4	-	96.0	0.90	Intermediately Coarse	79	Very Rough
5	-	4	95.0	0.35	Fine	85	Very Rough
6	-	2	92.4	0.48	Intermediately Fine	76	Very Rough
7	-	2*	90.0	0.45	Intermediately Fine	84	Very Rough
8	-	1*	87.7	0.47	Intermediately Fine	77	Very Rough

*Without vibration of tandem roller

Source: adapted from Araujo *et al* (2020).

3.4.2 Aggregate Imaging Measurement System (AIMS) analysis

The macrotexture profile obtained from AIMS must be processed for the obtention of standardized parameters. According to the ASTM-E 1845-15 (2015) standard, the SP test results in the MTD (Mean Texture Depth) parameter, represented by the average depth of the height of sand (Hs). From the processing performed for the AIMS profiles, the main computed parameter is the Mean Profile Depth (MPD). MPD is the average of the two maximum heights from each half-profile obtained from the two-dimensional profile analysis. Commonly, equations found in the literature can relate MPD to MTD (so-called MTD_{est}), thus converting a bidimensional to a volumetric parameter.

Other bidimensional parameters obtained from the analysis of a slope-suppressed AIMS macrotexture profile are (Equations 31 to 35) R_a (roughness average), R_q (root mean square), based on the deviations from a mean-line, and MPV (maximum peak value), from ISO 4287-97 (1997) standard. Figure 34 shows a general difference in results from the use of these equations from an AIMS macrotexture profile.

$$R_a = \frac{1}{N} \sum_{j=1}^N |r_j| \quad (31)$$

$$R_q = \sqrt{\frac{1}{N} \sum_{j=1}^N r_j^2} \quad (32)$$

$$MPV = \max(P1, P2) \quad (33)$$

$$MPD = \frac{P1+P2}{2} \quad (34)$$

$$MTD_{est} = 0.2 + 0.8 \times MPD \quad (35)$$

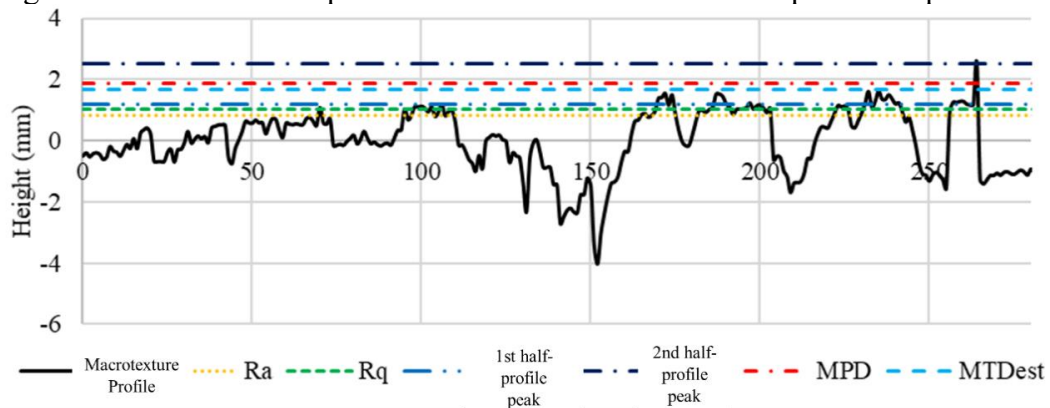
In which: N: number of captures;

j: capture index;

r: deviation from average slope-suppressed line where y(mm) = 0;

P1 and P2: half-profile peaks.

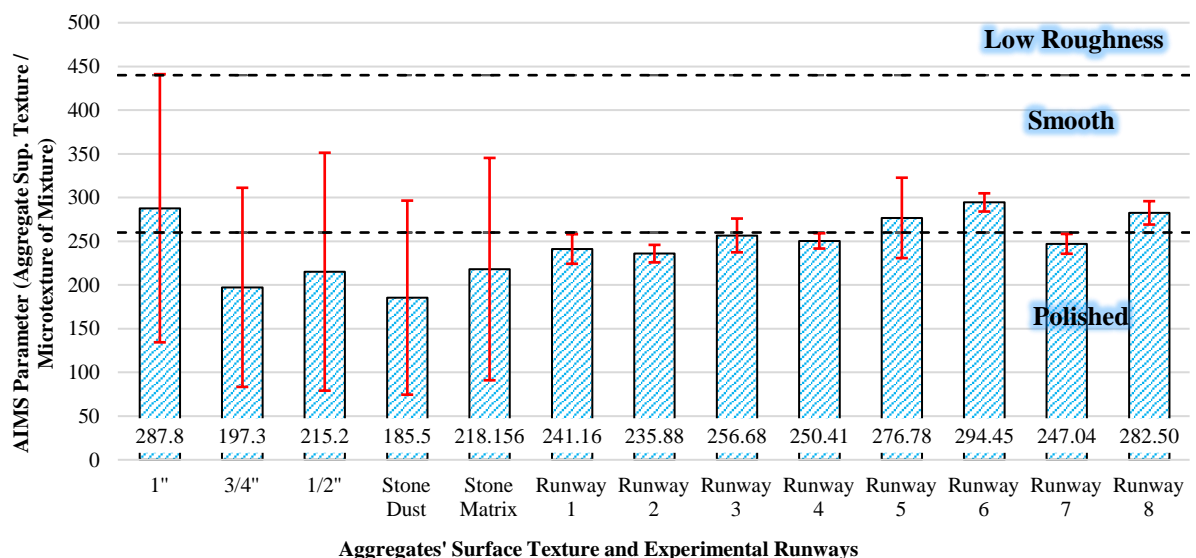
Figure 34 - Macrotexture parameters obtained from an AIMS-processed profile



Source: the author.

Each of the 8 sections analyzed in this study presented the AIMS microtexture parameter equivalent to the ones obtained for the aggregates' matrix surface texture. It is worth highlighting that the stone matrix surface texture is the weighted average of the surface textures of each aggregate fraction. The microtexture similarity was reflected not only in terms of average (between 200 and 300) but also in terms of qualitative classification (polished/smooth). Furthermore, the standard deviation of aggregates texture is higher than the one obtained from asphalt mixtures. The average microtexture values of each runway varied in the range of 1 standard deviation from the mean surface texture of the stone matrix, as shown in Figure 35. The difference in the error bars from aggregate and mixture is explained due to the variability of aggregates shape properties when it comes to different particle sizes.

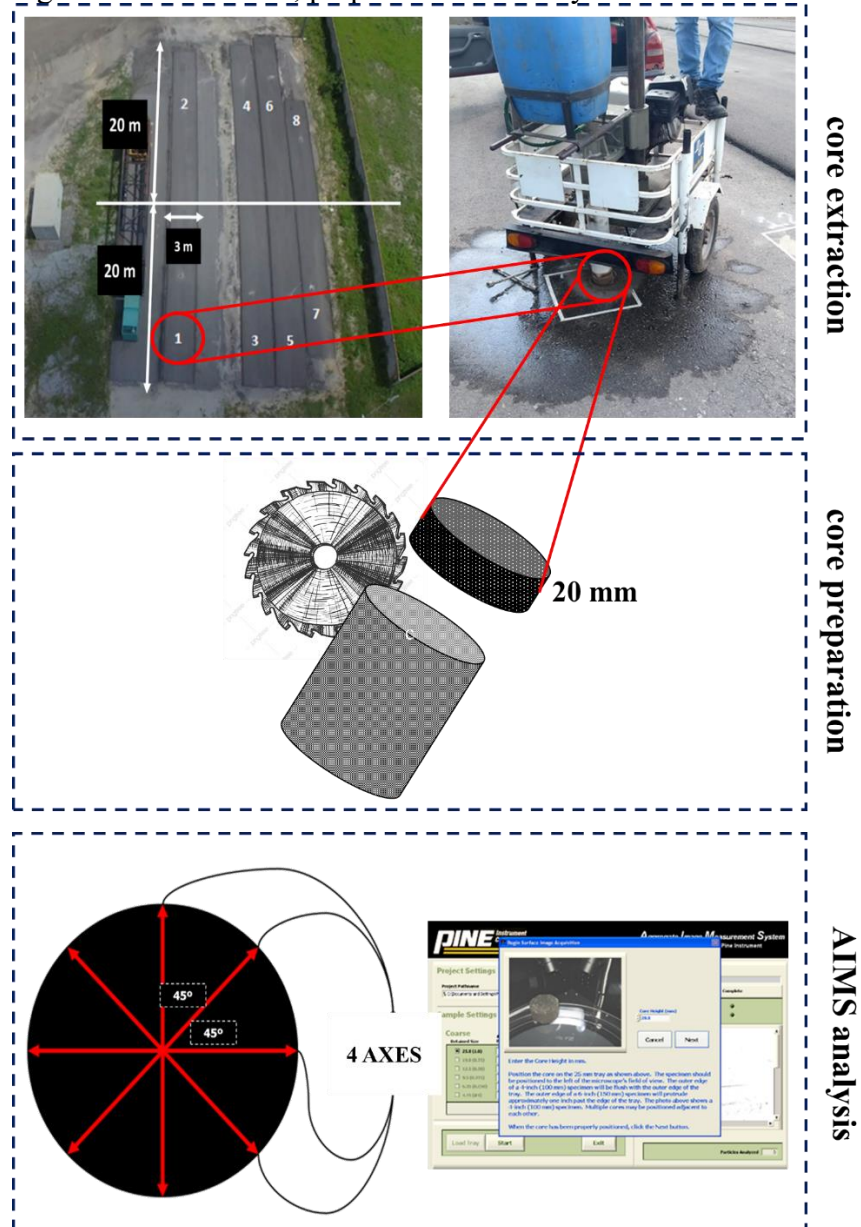
Figure 35 - AIMS stone matrix surface texture and asphalt mixture microtexture results (classification limits from IBIAPINA, 2018)



Source: adapted from Araujo *et al.* (2020).

The extraction of 3 specimens from each section described above preceded the AIMS texture evaluation. The analyses were carried out for 4 axes per core. Due to the low CD (%) and the susceptibility to the breaking, 2 cores were obtained from section 8. Traditional tests (SP and BP, harmonized in terms of IFI) were performed at each core-drilling point. Furthermore, for each extraction point, three-dimensional models were created using the CRP technique (see section 3.4.3). Figure 36 summarizes the extraction and preparation of samples to be analyzed in AIMS. The results were analyzed statistically for the introduction of a friction model as a function of AIMS-obtained parameters.

Figure 36 - Extraction, preparation and analysis of cores in AIMS

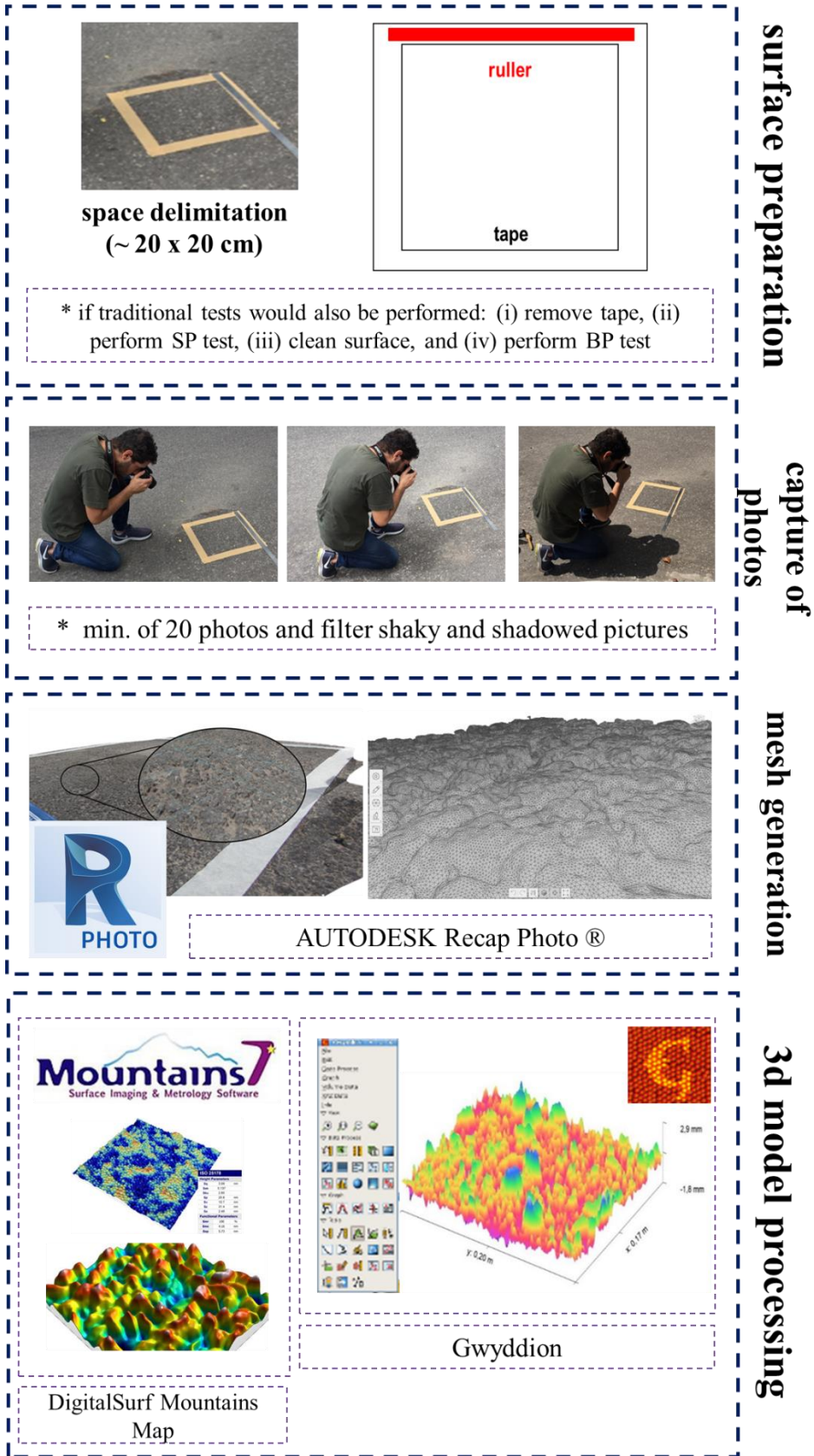


Source: the author.

3.4.3 Close-range photogrammetry (CRP) analysis

After the pavements' construction, the CRP technique can be applied to assess asphalt mixtures' surface characteristics without the use of heavy equipment or the drilling of cores. In this research, an ordinary camera was used to capture photographs of different spots from each test section (8 randomly selected points) in a circular pattern. For each point, at least 30 images were taken from the 8 delimited areas 30×30 (cm²). In each case, shaky and shadowed images were discarded, and a homogeneous lighting quality was assured. Several computational tools can contribute to the quick generation and analysis of topographic maps of surfaces (mesh). These tools include software such as Recap Photo (Autodesk), 3D Flow Zephyr Pro, Gwyddion, and Digital Surf MountainsMap (KOGBARA *et al.*, 2018). In this work, the 3D meshes were obtained using the use of Recap Photo software, exported as XYZ archives to post-processing with MeshLab, Gwyddion, and MountainsMap Premium computational tools. Also, a MATLAB code allowed the obtention of parameters such as MPD, MTD (ASTM-E 1845-15 2015), and ISO parameters (ISO 25178-2 2012). The estimation of the friction coefficient (μ) is quite relevant to the analysis of traffic safety (in terms of the DRAC and MADR indicators), which will be the focus of chapter 4 of this work. Figure 37 summarizes this analysis method. Table 19 details the main ISO 25178-2 (2012) parameters' meanings.

Figure 37 - CRP analysis method



Source: the author.

Table 19 - Texture parameters from ISO 25178-2 (2012)

Parameter	Meaning
Sq	Average height
Sp	Peak height
Sv	Maximum valley depth
Sz	Maximum height
Sa	Arithmetic mean height
Vm	Total material volume
Vv	Total voids volume
Vmp	Peak Volume (10% Threshold)
Vmc	Core material volume
Vvc	Core void volume
Vvv	Volume of voids in the valleys (80% Threshold)
Spd	Peaks density
Sdv	Average valleys volume
Shv	Average peaks volume

Source: adapted from ISO 25178-2 (2012).

Finally, the friction coefficients obtained through the application of the proposed methods (AIMS and CRP) were compared to the ones obtained through the application of the Kogbara *et al.* (2018) processing model. The same comparison was made in terms of the friction measured by the application of SP and BP tests. Considerations were also made concerning the compaction of asphalt mixtures.

3.5 Results and discussion

3.5.1 AIMS

Conventional tests were performed on the 8 sections to determine texture parameters (Hs from SP test and BP), as well as their harmonization in terms of friction by the IFI method (F60). The specimens processed in the AIMS resulted in the parameters MPD (MPD_AIMS), MTD (estimated) (MTD_AIMS), Microtexture (MIC_AIMS), roughness average (R_a), root mean square (R_q), and maximum peak value (MPV). Table 20 shows the correlation matrix between these values. It is relevant to mention that the most solid estimate of a regression model between the friction parameter and the AIMS parameters is obtained from the linear regression between F60 and MPD. The proposition of a multiple regression model with the presence of variables MPD and R_a or R_q is not recommended, given the multicollinearity between R_a , R_q , and MPD.

Table 20 - Correlation matrix between texture, friction and AIMS-obtained parameters

R²	Hs	BP	F60	CD	MPD_AIMS	MTD_AIMS	MIC_AIMS	Ra	Rq	MPV
Hs	-	0.11	0.80	0.04	0.59	0.59	0.00	0.20	0.21	0.63
BP		-	0.01	0.09	0.06	0.06	0.01	0.01	0.02	0.09
F60			-	0.01	0.57	0.57	0.00	0.27	0.27	0.56
CD				-	0.04	0.04	0.13	0.03	0.05	0.05
MPD_AIMS					-	1.00	0.02	0.68	0.62	0.97
MTD_AIMS						-	0.02	0.68	0.62	0.97
MIC_AIMS							-	0.00	0.03	0.02
Ra								-	0.97	0.62
Rq									-	0.58
MPV										-

Source: the author.

As expected, the aggregates' microtexture influence on F60 values was not captured within this analysis. This result reflects the use of the same aggregate source in the composition of the asphalt mixture of the 8 test sections. Furthermore, according to the findings presented in chapter 2 of this thesis, there is no statistically significant difference when it comes to different aggregates sources from the Fortaleza region in terms of post-construction predicted friction values. Equation 36 and Table 21 present the most reliable predictive model and its statistics. Equation 36 application is limited to polished and smooth aggregates (IBIAPINA, 2018). Figure 38 shows the 95% confidence interval of the predictive model. It is worth mentioning that the model, at this point, should have its use limited to aggregates from the Ceará state (Brazil) region. Further results must improve the robustness of data to allow the proposition of a predictive model considering the two texture scales captured in the AIMS analysis.

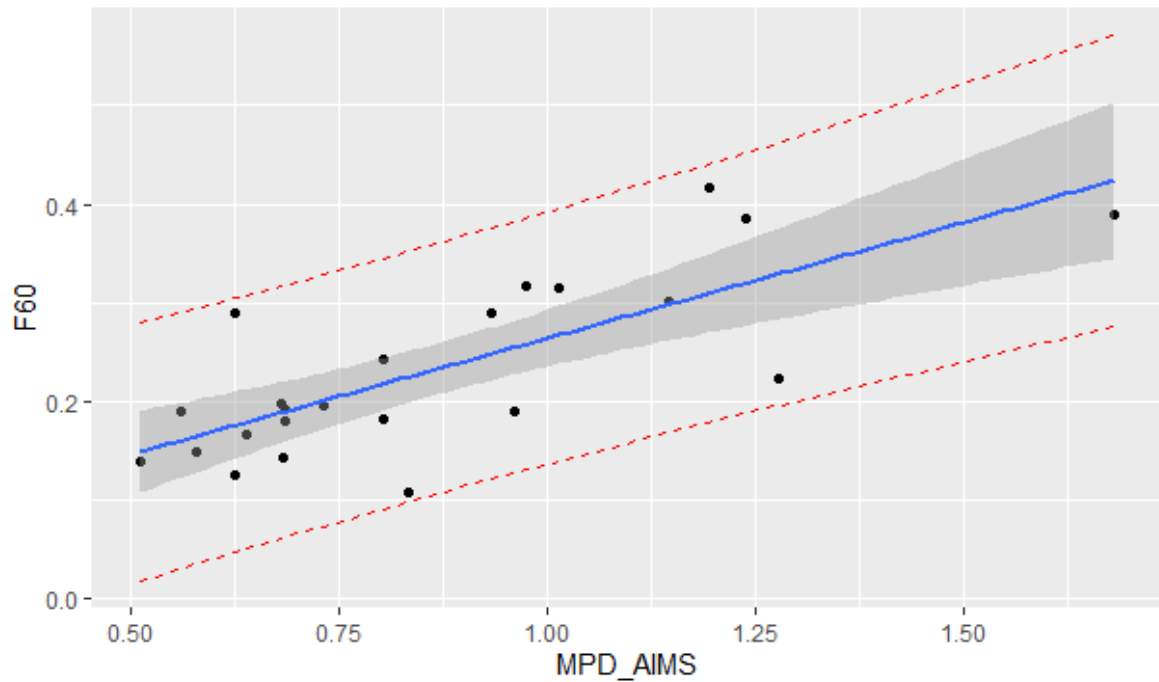
$$F60 = 0.028 + 0.236 \times MPD_{AIMS} \quad (36)$$

Table 21 - Friction ~ AIMS MPD parameter model statistics

Multiple R-squared	Adjusted R-squared	F-statistic	p-value
0.57	0.55	28.38	2.78E-05

Source: the author.

Figure 38 - Friction ~ AIMS MPD parameter model 95% confidence and prediction interval



Source: the author.

Equation 37 shows the relationship between the macrotexture parameter obtained through the SP test (MTD) and the MPD parameter obtained from the AIMS ($R^2 = 0.59$). Table 22 shows the statistical parameters of the model, and Figure 39 shows the 95% confidence interval for the proposed model. The lower R^2 value may reflect the empiricism of the SP test.

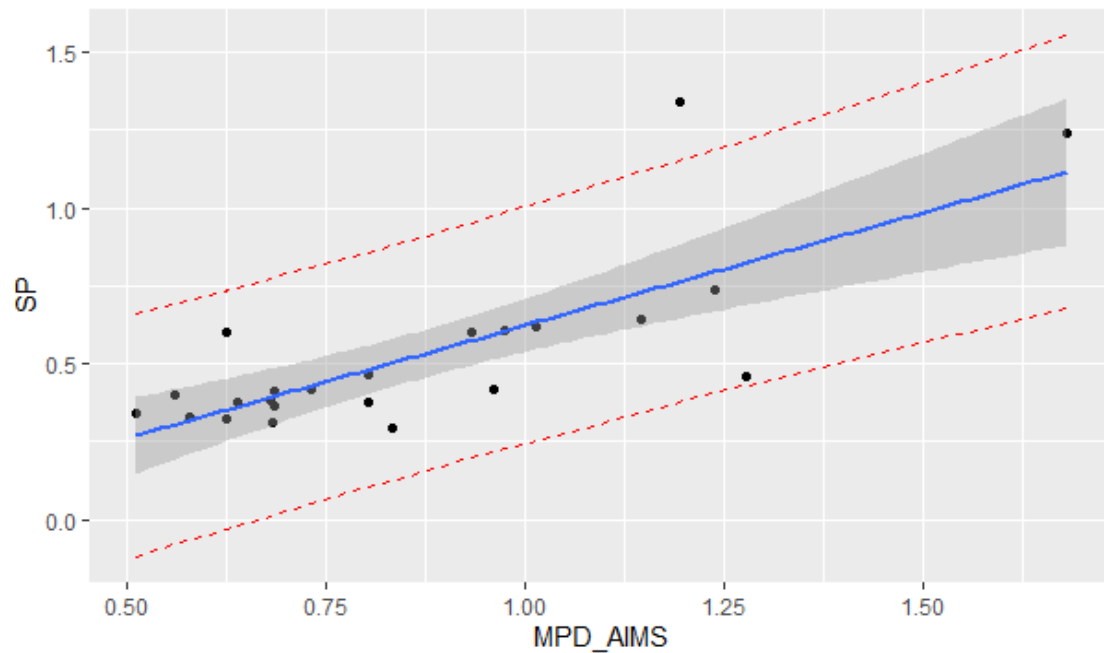
$$MTD_{SP\ test} = -0.103 + 0.726 \times MPD_{AIMS} \quad (37)$$

Table 22 - MTD (SP test) ~ MPD (AIMS) parameter model statistics

Multiple R-squared	Adjusted R-squared	F-statistic	p-value
0.59	0.57	30.39	1.81E-05

Source: the author.

Figure 39 - MTD (SP test) ~ MPD (AIMS) parameter model 95% confidence interval



Source: the author.

Statistical analysis confirmed the relative similarity between the 8 different test sections concerning AIMS microtexture (highly influenced by aggregates matrix surface texture), given the fact that this variable was found not to be significant for the friction results obtained using traditional tests (expected result given the use of the same aggregate source). No correlation ($R^2 = 0.00$) exists between AIMS microtexture and BP results (also expected result given the use of the same aggregate source). Moreover, the direct application of aggregates' texture classifications (AL ROUSAN, 2004; IBIAPINA, 2018) has led to contradictory results. This contradiction relies on comparing BP results (rough and very rough sections, as presented in Table 18) and AIMS (polished, smooth, and low roughness sections) results.

The average AIMS microtexture values were close to the aggregates matrix surface texture (average results between 200 and 300). Furthermore, both groups presented similar qualitative classification (polished, smooth, and low roughness). Table 23 presents the average and dispersion of the AIMS microtexture parameter, besides the matrix of Tukey test results for the similarity between different sections' microtexture. These results suggested that AIMS can capture minor differences of microtexture, even if those differences may not have a statistically significant impact on measured friction.

Table 23 - Microtexture results (AIMS) for the sections 1 to 8

Section	1	2	3	4	5	6	7	8	
Mean	241.16	235.88	256.68	250.41	276.78	294.45	247.04	282.50	
Standard Deviation	16.91	10.00	19.33	8.74	45.96	10.42	11.33	13.36	
Variation Coef. (%)	7	4	8	3	17	4	5	5	
AIMS Class.	Al Rousan (2004) Ibiapina (2018)	Smooth Polished	Smooth Polished	Smooth Polished	Smooth Polished	Low Rough. Smooth	Low Rough. Smooth	Smooth Polished	Low Rough. Smooth
	p-value	1	2	3	4	5	6	7	8
	1	-	0.46	0.11	0.20	0.07	0.00	0.43	0.00
	2		-	0.02	0.01	0.04	0.00	0.06	0.00
	3			-	0.42	0.28	0.00	0.25	0.01
	4				-	0.15	0.00	0.52	0.00
	5					-	0.32	0.11	0.74
	6						-	0.00	0.07
	7							-	0.00
	8								-
Green Labels	"Not different each other"								
Red Labels	"Different each other"								

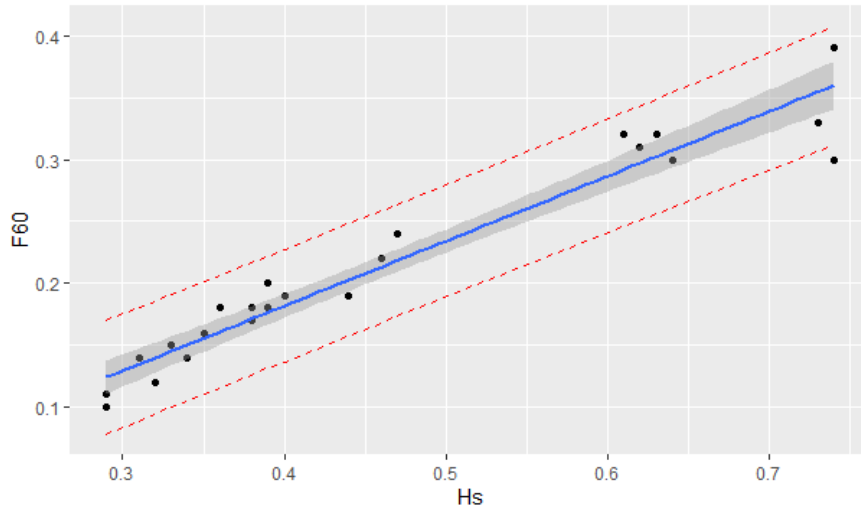
Source: the author.

3.5.2 3D computer vision

Data collected in this research was added to create a more comprehensive study, in which different surfaces in different locations were evaluated. In the mentioned study by Medeiros *et al.* (2020), co-authored by the author of this work, mathematical relationships between parameters obtained from the CRP technique and texture/friction measures obtained from traditional tests (SP and BP) have been proposed and validated after the comparison between CRP and laser-scanning results. Concerning the sections evaluated in this work, the mathematical models presented in Figure 40 were proposed, which includes the statistical analysis and the graphical representation of the confidence and prediction intervals (95%). More complete and reliable models will be found in the mentioned work (under peer-review). The variables' selection was based on the matrix of correlation between parameters found in Table 24 to avoid the proposition of models with multicollinearity issues.

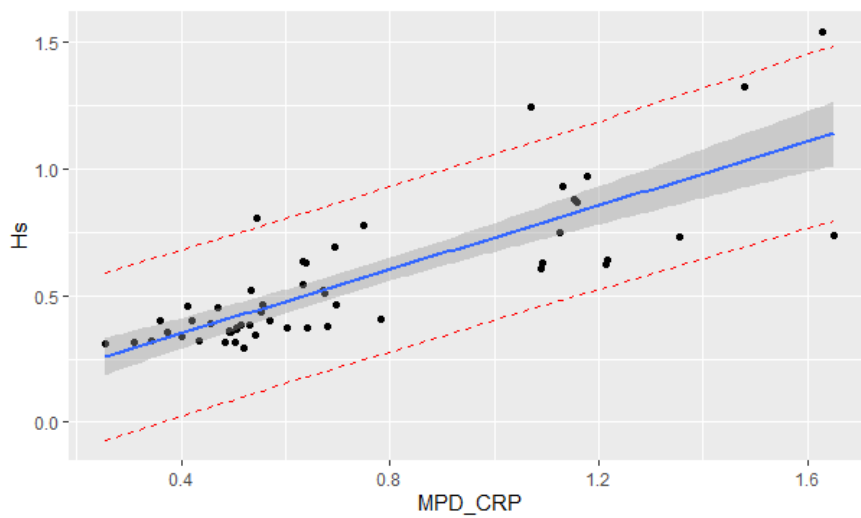
Figure 40 - Friction models obtained through the analysis of CRP parameters

Model	Mult. R ²	Adj. R ²	F-stat.	p-value
$F60 = -0.028 + 0.524 H_s$	0.94	0.93	326.9	1.086E-14



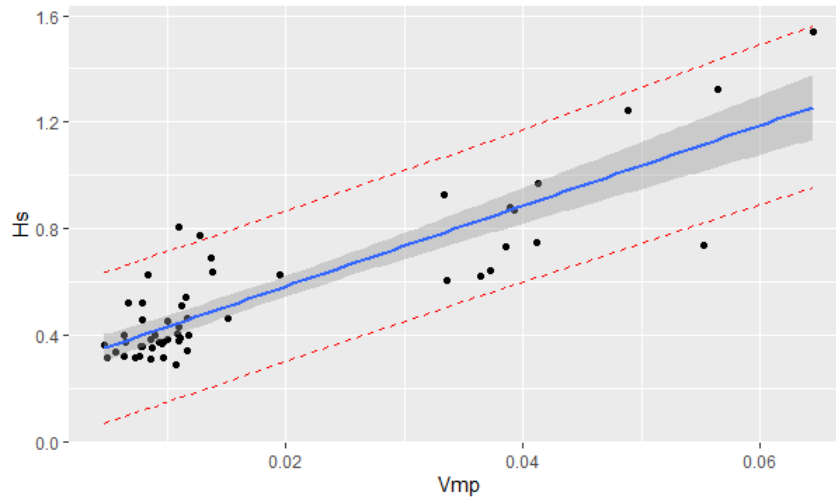
*Hs = height of sand (SP test) (mm)

Model	Mult. R ²	Adj. R ²	F-stat	p-value
$H_s = 0.099 + 0.630 MPD$	0.66	0.65	99.36	1.439E-13



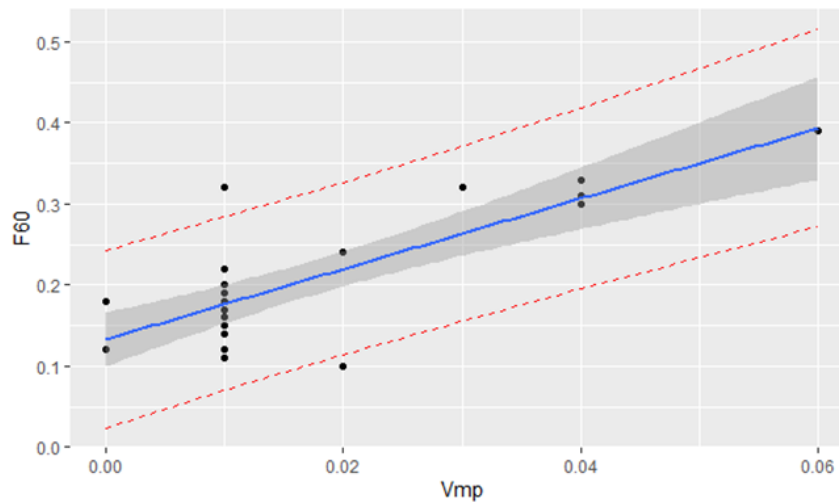
* MPD = mean profile depth (calculated from 3D model) (mm)

Model	Mult. R ²	Adj. R ²	F-stat	p-value
$H_s = 0.282 + 15.126 V_{mp}$	0.75	0.74	149.6	2.2E-16



* Vmp = volume of material (calculated from the 10% upper threshold of the 3D model) (mm³/mm²)

Model	Mult. R ²	Adj. R ²	F-stat	p-value
$F60 = 0.133 + 4.344 V_{mp}$	0.65	0.63	40.19	2.222E-06



* Vmp = volume of material (calculated from the 10% upper threshold of the 3D model) (mm³/mm²)

Source: the author.

Table 24 - Levelled 3D model parameters' correlation matrix

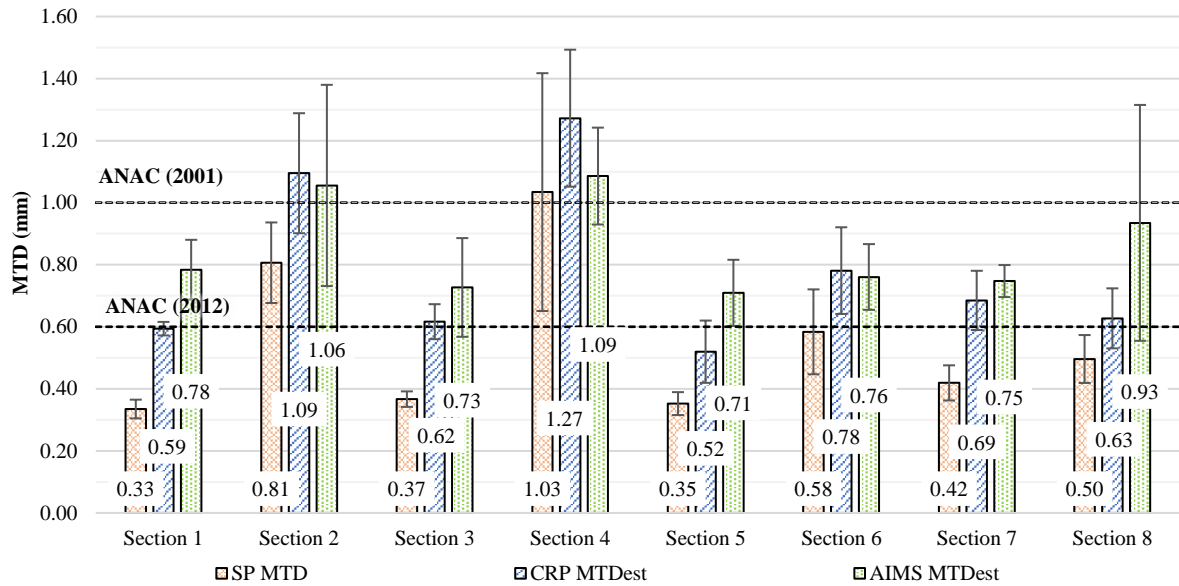
R ²	MTDest	Sq	Sp	Sv	Sz	Sa	Vm	Vv	Vmp	Vmc	Vvc	Vvv	Spd	Sdv	Shv
MTDest	1.00	0.69	0.74	0.07	0.47	0.73	0.89	0.87	0.89	0.71	0.90	0.04	0.01	0.41	0.32
Sq		1.00	0.64	0.40	0.74	0.99	0.62	0.90	0.62	0.97	0.83	0.45	0.11	0.49	0.52
Sp			1.00	0.16	0.72	0.66	0.73	0.74	0.73	0.65	0.75	0.07	0.10	0.71	0.60
Sv				1.00	0.68	0.34	0.07	0.21	0.07	0.31	0.16	0.53	0.31	0.41	0.57
Sz					1.00	0.71	0.46	0.64	0.46	0.67	0.58	0.34	0.27	0.79	0.83
Sa						1.00	0.64	0.92	0.64	0.99	0.86	0.40	0.10	0.49	0.49
Vm							1.00	0.84	1.00	0.60	0.89	0.01	0.03	0.39	0.34
Vv								1.00	0.84	0.91	0.99	0.16	0.06	0.49	0.48
Vmp									1.00	0.60	0.89	0.01	0.03	0.39	0.34
Vmc										1.00	0.85	0.39	0.09	0.49	0.47
Vvc											1.00	0.09	0.05	0.48	0.45
Vvv												1.00	0.13	0.12	0.21
Spd													1.00	0.26	0.23
Sdv														1.00	0.79
Shv															1.00

Source: the author.

3.5.3 Analysis of results from different techniques

For all sections, applying the volumetric SP test resulted in the lowest MTD values. Also, according to results obtained through DIP techniques, it is possible to note that sections of reduced CD (6, 7, and 8) achieved the minimum suggested value of MTD in Brazilian standards (0.60 mm), as shown in Figure 41. The macrotexture results (specifically MTD) obtained using DIP techniques (AIMS and CRP) were closer to each other. The higher MTD values obtained when employing the CRP technique indicates that the surface macrotexture peaks distribution is not captured by techniques such as AIMS and SP. In each of the 64 3D models, statistical analysis of macrotexture peaks distribution runs for multiple profiles, whose average results in the MTD parameter. Given this, CRP analysis tends to capture surface peaks more precisely. This means that: (i) CRP analysis correlates satisfactorily both to a traditional method (SP) and a DIP method (AIMS); (ii) despite fair R² values of correlation, the MTD values obtained using 3D models tend to be higher than the ones obtained by the other methods; (iii) the cause of these differences is the more precise capture of peaks provided by the CRP technique.

Figure 41 - MTD results obtained using different techniques



Source: the author.

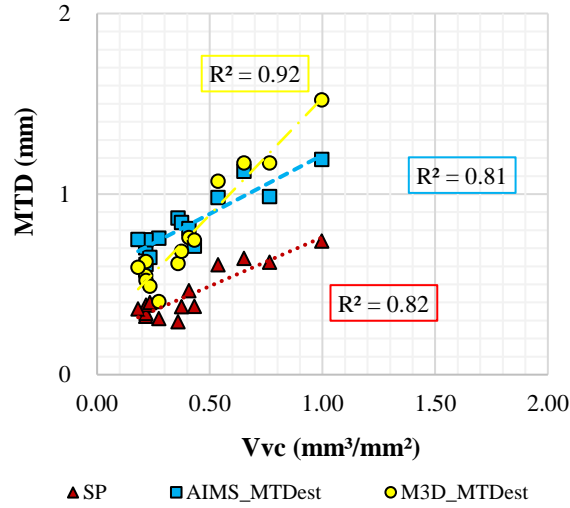
When analyzing the volumetric parameters of the Abbot-Firestone curve, 2 out of 5 parameters refer to the presence of material volume in direct contact with vehicles' tires. It should be expected that the higher the ISO parameters (V_{mp} and V_{mc}), the higher would be the hysteresis energy at the tire-pavement interface. This work confirms previous findings concerning the V_{mp} ISO parameter (KOGBARA *et al.*, 2018).

3 out of 5 parameters are related to the volume available to surface drainage (V_{vc} , V_{vv} , V_v). A satisfactory correlation between the MTD parameter was obtained from the three techniques applied with the volumetric parameters V_{mp} , V_{mc} , V_{vc} , and V_v (Figure 42). The correlations between the parameters MTD and V_{vv} are not significant. Although several limitations, it is worth mentioning that SP and AIMS techniques are useful for the estimation of volumetric (and consequently more practical applied) parameters. However, the results here presented do not suggest a correlation between MTD and S_{pd} , a significative parameter for friction estimation according to Kogbara *et al.* (2018).

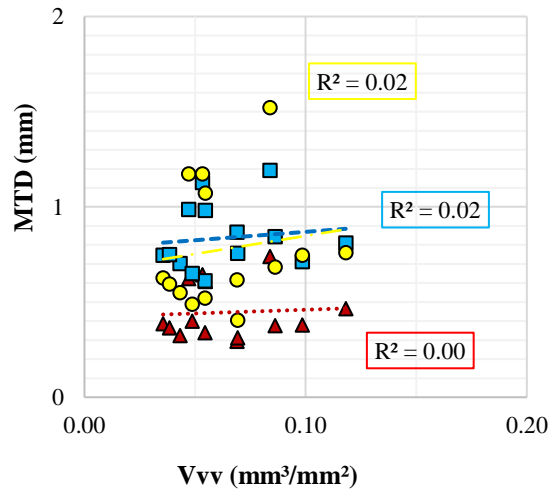
The obtention of fair correlation values concerning 4 out of 6 parameters (V_{vc} , V_{mp} , V_{mc} , and V_v) indicates a satisfactory capture of important volumetric parameters by the bidimensional parameter MTD. Also, these analyses captured similar trends between the methods for all the 6 parameters presented in this paper. Even so, 2 out of 6 parameters indicated no correlation between parameters and the MTD value obtained through different techniques and equipment. Also, in the case of the V_{mc} parameter, correlation values were lower than 0.8. This indicates that the application of the CRP technique may overcome limitations of SP

technique and AIMS equipment, which may not accurately capture the distribution of the peaks of a given spot.

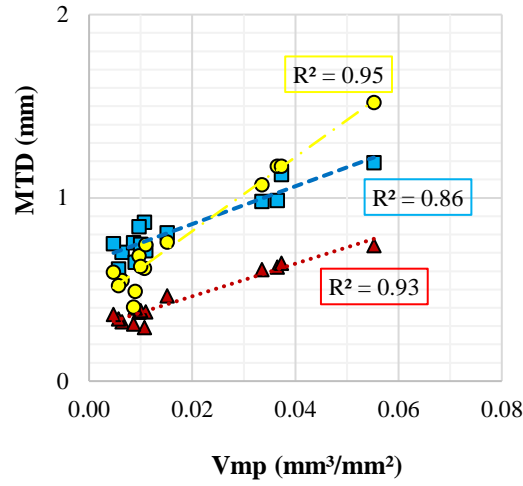
Figure 42 - Correlation between ISO and the unified MTD parameters from different techniques



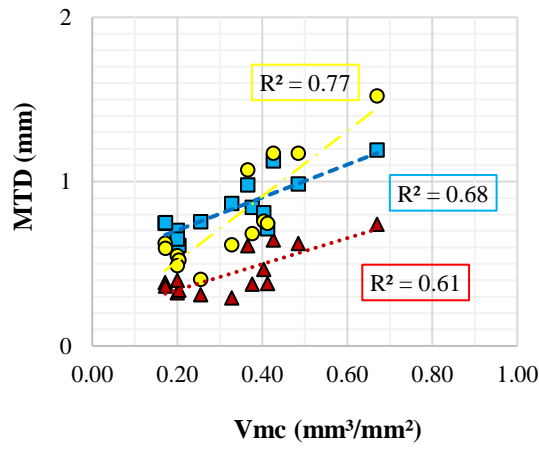
(a) Correlation MTD versus Vvc



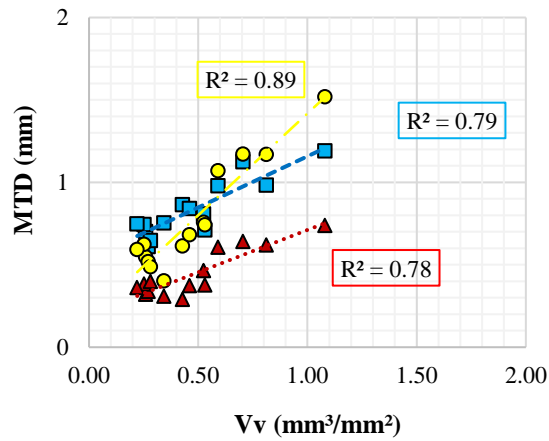
(b) Correlation MTD versus Vvv



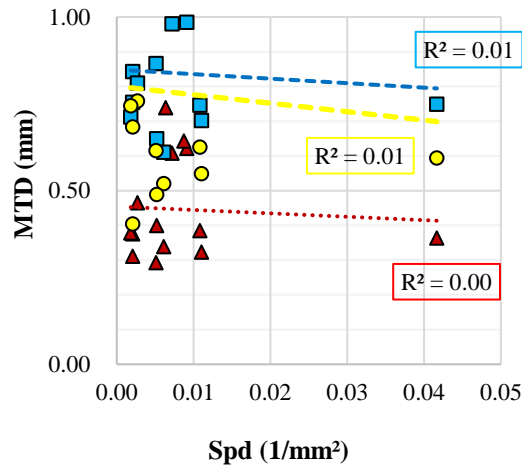
(c) Correlation MTD *versus* Vmp



(d) Correlation MTD *versus* Vmc



(e) Correlation MTD *versus* Vv

(f) Correlation MTD *versus* Spd

Source: the author.

When comparing the ISO 25178-2 (2012) parameters obtained from the analysis of the three-dimensional leveled and roughness-filtered model (obtained by applying the Gaussian filter with 0.8 mm threshold) to BP and AIMS microtexture (calculated from the wavelet method), no correlation was found to be minimally reasonable, as shown in Table 25. Such results may be an indicative that it is not proper to look for relations concerning microtexture in a set of test sections constructed using the same mineral aggregate source.

Table 25 - R^2 values between ISO parameters and microtexture results

R^2	Leveled Model		Roughness Model	
	BPN	AIMS Microtexture	BPN	AIMS Microtexture
SP MTD	0.03	0.02	0.03	0.02
AIMS MTDest	0.03	0.10	0.03	0.10
M3D MTDest	0.01	0.03	0.01	0.03
Sq	0.01	0.01	0.03	0.12
Sp	0.00	0.09	0.07	0.00
Sv	0.02	0.22	0.01	0.06
Sz	0.00	0.20	0.04	0.02
Sa	0.01	0.00	0.06	0.16
Vm	0.02	0.06	0.04	0.04
Vv	0.01	0.01	0.00	0.03
Vmp	0.02	0.06	0.04	0.04
Vmc	0.00	0.00	0.02	0.04
Vvc	0.01	0.03	0.01	0.00
Vvv	0.00	0.39	0.02	0.31
Spd	0.05	0.12	0.01	0.06
Sdv	0.01	0.10	0.09	0.14
Shv	0.02	0.21	0.05	0.06

Source: the author.

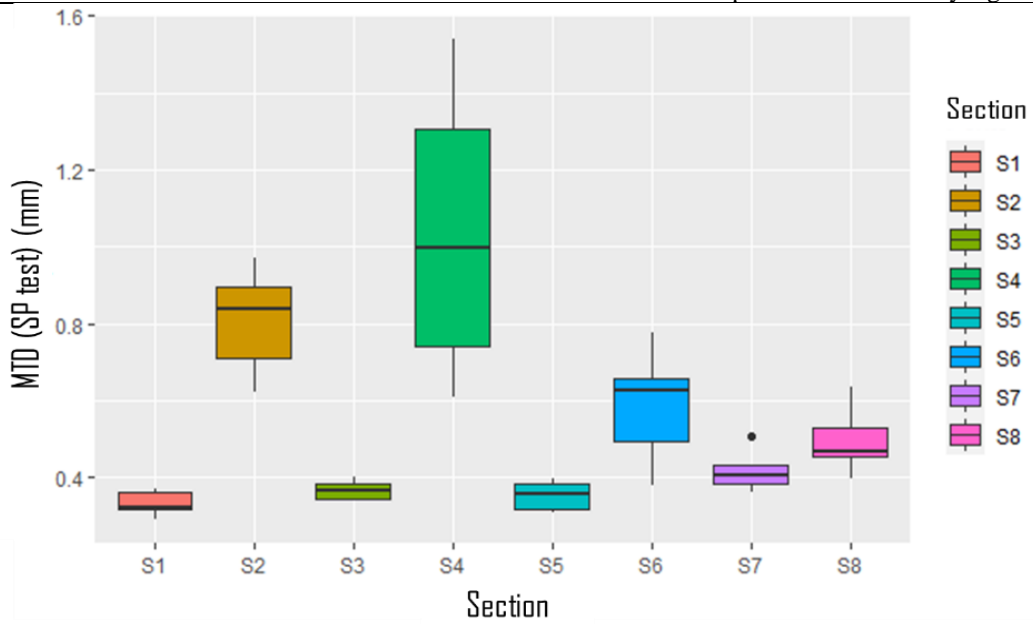
3.5.4 *Compaction assessment*

The analysis of variance (ANOVA) attested to the significance of the compaction protocols' variation on the macrotexture (MTD). Previous results support the conclusion that macrotexture was the main factor influencing the tire-pavement friction at the tire-pavement interface. As explained, the compaction variation occurs in terms of compaction degree and sequence of compactor rollers passes. The ANOVA analysis of compaction influence on SP results showed $R^2 = 0.73$, F-statistic = 17.75, and a p-value = 4.763E-11, thus compaction was proven significant. When it comes to the analysis of the CRP macrotexture results obtained using a MATLAB code, this paper found the same conclusion. The summary of statistics includes $R^2 = 0.81$, F-statistic = 26.98, and p-value = 4.127E-14. Figure 43 summarizes the mentioned statistical analyses.

However, as shown in Table 26, analyzing macrotexture pair-by-pair, some compaction solutions do not show statistically significant differences with each other. Also, the statistics matrix (paired Tukey test) in Table 26 suggests that macrotexture is the same in different pairs of solutions (such as 1-3, 1-5, 1-6, 1-7, 1-8). Also, a trend of higher macrotexture exists in sections where the tandem roller is the finishing compaction process (sections 2 and 4).

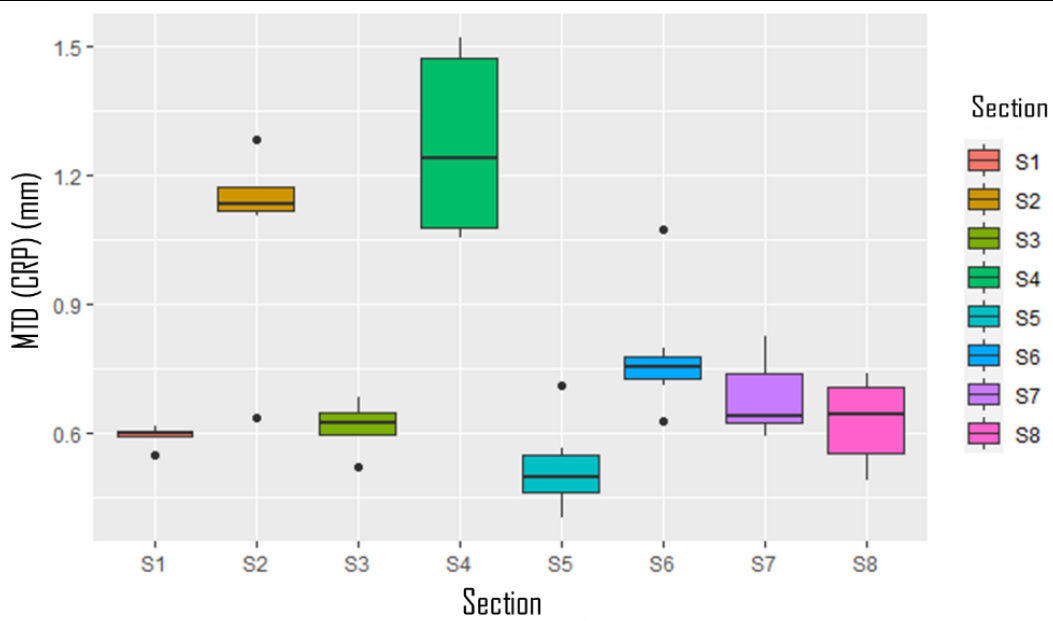
Figure 43 - Statistical analysis of compaction significance for macrotexture results

Method	R ²	F statistic	p-value	Conclusion
Sand Patch	0.73	17.75	4.763E-11	Compaction is statistically significant



(a) SP test

Method	R ²	F statistic	p-value	Conclusion
Close-range Photogrammetry	0.81	26.98	4.127E-14	Compaction is statistically significant



(b) CRP method

Source: the author.

Table 26 - Paired Tukey test for comparison between compaction solutions

p-value	S1	S2	S3	S4	S5	S6	S7	S8
S1	-							
S2	0.000	-						
S3	1.000	0.000	-					
S4	0.000	0.125	0.000	-				
S5	1.000	0.000	1.000	0.000	-			
S6	0.064	0.109	0.192	0.000	0.106	-		
S7	0.979	0.001	0.999	0.000	0.995	0.586	-	
S8	0.498	0.006	0.784	0.000	0.638	0.957	0.987	-

(a) MTD from SP test

p-value	S1	S2	S3	S4	S5	S6	S7	S8
S1	-							
S2	0.000	-						
S3	1.000	0.000	-					
S4	0.000	0.234	0.000	-				
S5	0.964	0.000	0.891	0.000	-			
S6	0.171	0.001	0.356	0.000	0.013	-		
S7	0.936	0.000	0.989	0.000	0.415	0.917	-	
S8	1.000	0.000	1.000	0.000	0.796	0.390	0.995	-

(b) MTD from CRP analysis

*Green labels: MTD values are statistically different each other

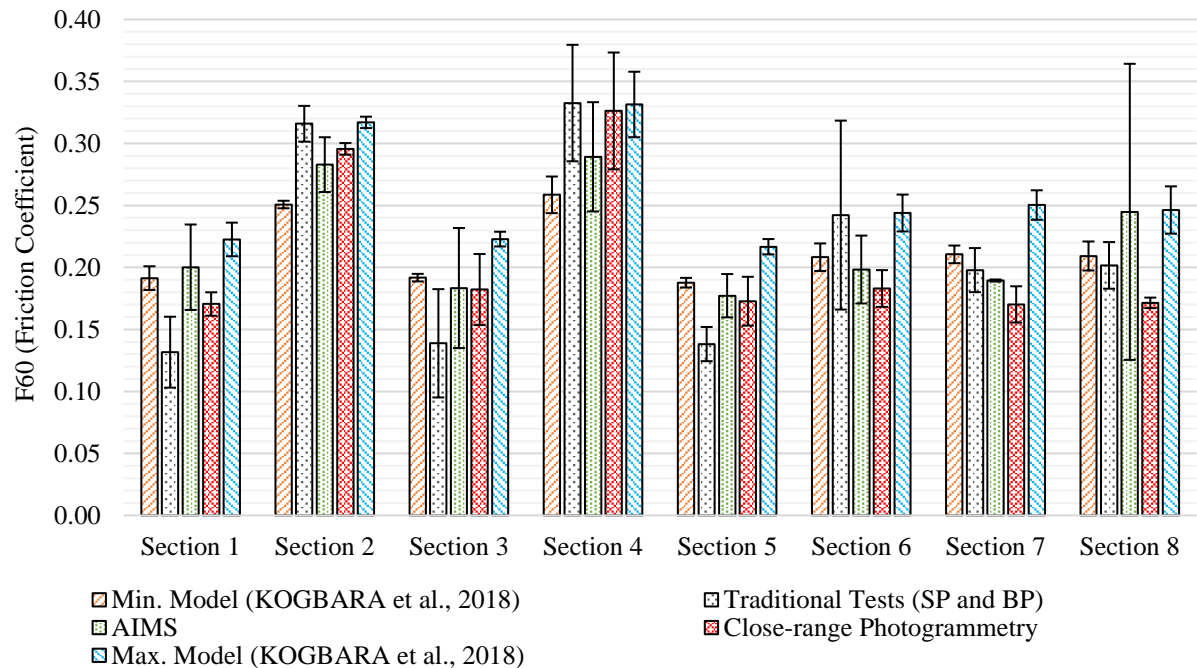
*Red labels: MTD values are not statistically different each other

Source: the author.

3.5.5 Tire-pavement friction analysis

The test sections with higher macrotexture values (2 and 4) presented the highest predicted F60 values. This is an expected finding because the main inputs for the friction estimation models are macrotexture parameters. Figure 44 summarizes the predicted values of μ at 60 km/h (F60) and standard deviation obtained through different methods and harmonized according to the IFI theory (WAMBOLD *et al.*, 1995).

Figure 44 - Friction coefficient obtained through different techniques



Source: the author.

The advanced Tukey test evaluated the paired statistical similarity between the different friction models. Only the results from sections 1, 3, 5, 6, 7, and 8 were selected, because previous analyses suggested no statistically significant differences in macrotexture. According to the p-values obtained from the Tukey formal statistical test (Table 27), the methods evaluated in this work do not have statistically significant differences between each other.

Table 27 - Tukey test matrix for verification of statistical differences between methods

p-value	SP and BP	AIMS	CRP	Kogbara et al. (2018) (Min)	Kogbara et al. (2018) (Max)
SP and BP	-				
AIMS	1.00	-			
CRP	1.00	0.99	-		
Kogbara et al. (2018) (Min)	1.00	1.00	1.00	-	
Kogbara et al. (2018) (Max)	0.52	0.69	0.44	0.55	-

*Green labels: no statistically significant difference.

Source: the author.

3.6 Partial conclusions

The analysis of asphalt pavement surfaces in terms of texture and friction is often thought to be unfeasible due to the need to use contact equipment. For developing countries, especially, the use of this type of equipment faces some challenges such as the economic cost

and even the lack of specialized operators. Therefore, DIP techniques such as AIMS and 3D computer vision (through CRP) appear as potential methods to allow a low-cost, practical, simplified, precise, and real-time analysis of pavement surface conditions when it comes to texture and friction.

An important asset for the proactive approach to traffic safety is the consideration of aspects such as the surface friction coefficient before construction, specifically. Even so, advances achieved for the assessment of pavements during and after construction are also relevant. In this perspective, the content exposed in Chapter 2 of this work would support the prediction of μ before construction and the content exposed in Chapter 3 contributes to the advancement of the real-time assessment of asphalt pavement surfaces during service life.

The evaluation of the macrotexture of mixtures subjected to different field compaction methods (in terms of CD and types of used rollers) indicated that different mixtures may have similar macrotexture when compaction is finished using the same type of roller. On the other hand, the type of compaction roller does not cause significant changes in the microtexture evaluated according to the BP test. This characteristic is determined by the aggregate surface texture (HALL *et al.*, 2009). Even so, the AIMS analysis of microtexture was proven capable of capturing minor microtexture variations between the different test sections.

For the surfaces evaluated in this work, a coefficient of correlation (R^2) of 0.93 was obtained for the relation friction-macrotexture (SP test). Thus, models for estimating the friction coefficient in the post-construction phase were proposed from parameters obtained from the texture analysis in AIMS (MPD), as well as from the processing of three-dimensional models (MPD and V_{mp}). Further results of this research were incorporated into a larger scale study, under development, which seeks to expand the range of covered materials for the proposition of friction models based on CRP. As the main partial conclusion of this work, the contributions presented in this chapter may support the consolidation of real-time low-cost methods for the assessment of texture and friction.

4 USING MICROSCOPIC SIMULATION TO ASSESS ASPHALT PAVEMENTS' TIRE-PAVEMENT FRICTION REQUIREMENTS

4.1 Initial considerations

Studying Road Safety Performance (RSP) (or Traffic Safety Performance, TSP) is essential given the multifactorial nature of traffic collisions. Such events derive from human, vehicular, environmental, and pavement-related factors. Therefore, it is quite complex to analyze isolated causes of crashes. Some crashes' governing factors are deeply associated with transport engineering. When it comes to transport infrastructures engineering (pavements) specifically, TSP is most directly associated with the friction developed at the tire-pavement interface, as well as factors like the geometric design and the presence of pavement distresses.

Studies have attempted to quantify the positive effects of pavements' friction on reducing crash rates on rainy days (IVEY *et al.*, 1981; MAYORA and PIÑA, 2009; NAJAFI, FLINTSCH and MEDINA, 2015). However, such relation is complex as the effects of combining tire-pavement friction and drivers' behavior are not fully understood. Also, investigating TSP through crash records is a reactive approach, and researchers need to deal with imprecise data, which includes incomplete, inconsistent, and even inexistent records. Additionally, it is needed the acquisition of historical series to provide minimal consistency to the analysis of crashes to reduce misinterpretations and misleading conclusions (HAUER and HAKKERT, 1989; CHIN and QUEK, 1997; FARMER, 2003).

Examining vehicular conflicts instead of the record of real crashes for the identification of potential risk situations to assess TSP dates from the '60s (PERKINS and HARRIS, 1968). Microscopic traffic simulators (such as VISSIM) can provide a greater amount of data, and records of the dynamics of simulated vehicles in reduced time-steps, including vehicle trajectories with their respective positions, speeds, and accelerations. Associating microscopic simulation to TSP studies is one way to develop the proactive approach to safety (BARCELÓ *et al.*, 2003; HUGUENIN *et al.*, 2005; CUNTO, 2008).

4.2 Specific objective

The specific objective addressed in this section is to develop a method to set acceptable conditions of asphalt pavement tire-pavement friction based on the traffic safety performance. To do so, the assessment of vehicular conflicts in different scenarios can be performed using microscopic traffic simulation and Surrogate Measures of Safety (SMoS). Afterward, multiple possibilities for materials' selection might be assessed in terms of the suitability of use for the urban environment.

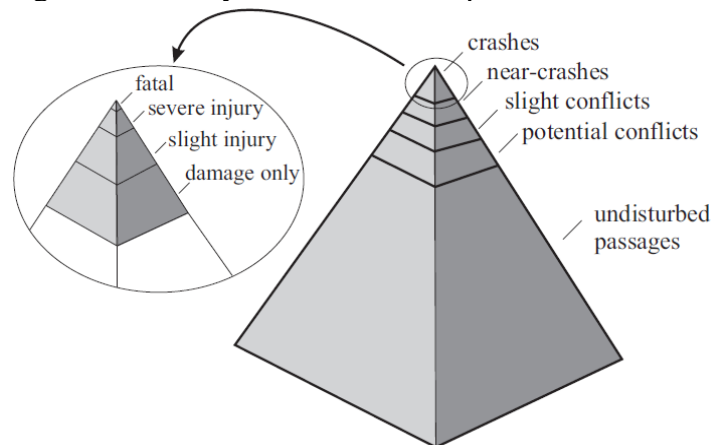
4.3 Literature review

4.3.1 *Proactive approach to Traffic Safety*

The concept of vehicular conflict as a way to study TSP was proposed in the '60s and defined in the '70s to overcome the necessity of historical crash databases, as well as to proactively contribute to TSP studies (PERKINS and HARRIS, 1968; AMUNDSEN and HYDÉN, 1977). Based on temporal analysis of the events before an accident, the safety continuum concept was introduced, understanding that the probability of a collision increases as the interaction severity rises.

The premise of the continuum concept is that a traffic crash is a result of a complex series of factors that interact with the occurrence of conflicts between vehicles, so that it may lead or not to the crash occurrence. Precisely, a vehicular conflict occurs when two or more vehicles approach each other in time and space, so that there is a high risk of collision if their movements remain unchanged (HYDÉN, 1987). Figure 45 presents the Hydén pyramid, which hierarchizes the series of events that may lead to the occurrence of traffic crashes.




Figure 45 - Safety continuum concept



Source: Hydén (1987).

The feasibility of evaluating TSP through conflicts observations, using the proactive approach, is defended since studies reported the existence of a proportional relationship between vehicular conflicts' occurrence and real traffic-related crashes data (EL-BASYOUNY and SAYED, 2013). However, it is worth to mention that vehicular conflicts can be classified according to widely different parameters, so the nature of these interactions is not always the same. For example, **Table 28** presents the classification of conflicts according to interaction angle and trajectory of vehicles and the images exemplify what kind of crashes can result from each type of conflict.

Table 28 - Conflicts' classification according to angle and trajectory

Conflict	Interaction angle (°)	Example
Longitudinal (rear-end)	< 30	 (https://www.adamjoneslaw.com)
Transversal (crossing)	> 85	 (http://www.engeplus.com.br)
Lateral (lane change)	> 30 and < 85	 (https://cooperhurley.com)

Source: adapted from Gettman and Head (2003).

Conflicts may result in crashes which can be evaluated according to different severity levels, from material damages only, passing through minor or incapacitating injuries, culminating in deaths. It is important to measure not only the frequency but also the severity associated to the captured conflicts and potential crashes. The SMOs were proposed to resolve such a gap by combining and quantifying conflicts frequency and collision risks. In this way, researchers have been introducing indicators based on the spatiotemporal proximity between vehicles in risky situations, known as Proxy Indicators of Road Safety. Table 29 presents a summary of some of the most relevant proxy indicators. In addition to these concepts, some can also be mentioned: Time to Accident (TA), Encroachment Time (ET), and Gap Time (GT) (CUNTO and LOUREIRO, 2011).

Table 29 - Summary of proxy indicators' meanings

Proxy Indicator	Source	Meaning
TTC – Time to Collision	Hayward (1972)	Time in which a conflict could lead to a collision if vehicles' trajectories and speeds remained unchanged. Conflicts are usually defined as events which occur at 1.0 to 1.5 s of TTC.
PET – Post-Encroachment Time	Cooper (1983)	Time difference between the instant that a conflicting vehicle was at a potential collision point and the instant that another vehicle reaches this same point (appropriate for crossings).
DRAC – Deceleration Rate to Avoid the Crash	Cooper and Ferguson (1976)	Quantification of the kinetic energy involved in the interaction by means of the deceleration rate necessary so that there would not happen a collision (relates to pavements' friction condition).
CPI – Crash Potential Index	Cunto (2008)	Sum of interactions over time, calculated based on DRAC and MADR (Maximum Available Deceleration Rate) statistical distributions.

Source: adapted from Cunto and Loureiro (2011).

Guido *et al.* (2011) conducted a study to evaluate TSP from vehicle interactions captured by videotaping traffic at a roundabout. The vehicle trajectories were obtained over one hour, and sequential frames were set to 30 per second. The sensitivity of the phenomenon analysis to 5 proxy indicators was evaluated in terms of TTC, DRAC, and CPI, among others. In roundabouts, different SMOs highlight different locations or geometric features when it comes to potential safety issues (CPI, for example, highlights more confined risky areas, is therefore seen as a “more specific” measurement when compared to the others). The authors identified higher-risk areas in locations with more disturbed traffic, with more vehicle interactions, more frequent braking, and different speeds, for example. It is important to

mention the simplified consideration of MADR by the authors, which considered two options of MADR calculation, one expressed in Equation 38, and the other a truncated normal distribution, ranging from minimum 4.2 m/s² and maximum 12.7 m/s². Canale (1989) exposes more complex formulations of MADR.

$$\text{MADR} = g (f_a \pm i) \quad (38)$$

In which: g: 9.81 m/s² (gravity);
 f_a: 0.40 (constant friction coefficient);
 i: 0% (cross grade).

4.3.2 Tire-pavement friction influence on TSP

One of the first published studies relating crash records to surface friction conditions was conducted by evaluating 770 miles of highways (all two-lane and limited access), grouped into 110 test sections. The authors proposed an exponential model in which the proportion of wet-track accidents was the dependent variable, indicating that the higher the measured friction, the lower the frequency of crashes. The authors observed considerable dispersion evidenced by graphical analysis as a limitation of the obtained results, which suggested the existence of other factors that could also affect the occurrence of crashes, such as geometric design and traffic volume. The discussion was limited to the operational and geometric aspects of highways, not raising hypotheses about the effects of behavioral adjustment of drivers due to precipitation (RIZENBERGS *et al.*, 1976).

Lindenmann (2006) evaluated 790 points considered critical concerning crash occurrence. Only 2.4% presented the so-called “low friction” surface condition. The author did not find any trend of the superficial condition effect on the occurrence of accidents in wet roads, evidencing that the evaluation of this relationship is not a trivial task and demanded more studies. On the other hand, Najafi *et al.* (2015) related skid resistance to urban traffic-related crash rates, being the surface conditions statistically significant in both dry and wet pavement for different types of roads (main roads, highways in urban environments and secondary roads). However, despite the sound results, the analysis was limited to high-severity crashes (occurrences with injuries and deaths).

Lyon and Persaud (2008) investigated the impacts of improving tire-pavement friction on TSP by analyzing data from New York state (USA). In this study, points with high frequency of wet-surface skid-related crashes were identified, leading to the adoption of a road maintenance program aiming to recovering the tire-pavement friction quality. Based on before-after studies, the authors established a Crash Modification Factor (CMF) of 0.799 (standard error 0.028) for all selected road and accident types. This number represents an expectation of a reduction of approximately 20% in accidents predicted at the points under analysis, highlighting the importance of the surface condition in terms of friction to the TSP.

In the literature, the relationship between surface conditions of pavements and occurrence of traffic-related crashes is not fully understood. This is due to, among other factors, the fact that studies conducted by different authors in different locations have, in many cases, relatively divergent conclusions. In the study conducted by Lyon, Persaud and Merritt (2017), different pavement surface rehabilitation strategies were evaluated, including thin hot mix asphalt (HMA) overlay, open graded friction course (OGFC), ultra-thin bonded wearing course (UTBWC), microsurfacing, chip seal, slurry seal, and diamond grinding and grooving (for concrete pavements). The Empirical Bayes methodology for observational before–after studies was applied for estimating the Crash Modification Factors (CMF) of the different maintenance strategies at different conditions (including factors such as crash type, dry/wet condition, and traffic volume). Crash information was collected from 4 American states (California, Minnesota, North Carolina, and Pennsylvania). The results suggested that the treatments may provide benefits in reducing wet-road crashes (exception of thin HMA for two lane roads, and for OGFC for two-lane and multilane roads). Also, CMF values higher than 1 were observed, explained because of speed adaptation after a pavement recovery. The importance of this observation concerns to the fact that not always performing a pavement maintenance will reflect in a reduction of skid-related crashes. Depending on the selected strategy, the increase in the “driving comfort” may lead drivers to adjust behaviors to a more aggressive driving, with higher speeds and reduced headways between leading and follower vehicles.

4.3.3 Microscopic traffic simulation and safety analysis

Although objectively defined, proxy indicators of safety may present some complexities for calculation, requiring technological tools to minimize such limitations. The field data collection for quantifying these indicators can lead to inconsistent records, and even

with the support of trained technicians there is a subjective bias of evaluation (CHIN and QUEK, 1997). The use of tools that allow the controlled analysis of vehicular interactions, precisely providing speed and position information in small time intervals, such as traffic microscopic simulators and DIP (computer vision) applied to traffic conflicts analysis, can contribute to the accuracy of determination of the proxy indicators.

In the 1980s and 1990s, computer-based traffic microscopic simulation tools emerged as ways to overcome some practical limitations for the consolidation of the proactive approach to traffic safety. Although not originally conceived for the modeling of traffic crash occurrence, simulators allow the application of vehicle conflict detection tools. Microscopic simulation incorporates the possibility of obtaining a greater quantity of data to be analyzed. Microscopic models are more advantageous because these packages can provide outputs of the trajectories of all simulated vehicles with their respective positions, speeds, and accelerations. Therefore, facilitating the calculation of proxy indicators is a direct benefit of the acquisition of data from traffic microscopic simulators (BARCELÓ *et al.*, 2003; HUGUENIN *et al.*, 2005; CUNTO, 2008).

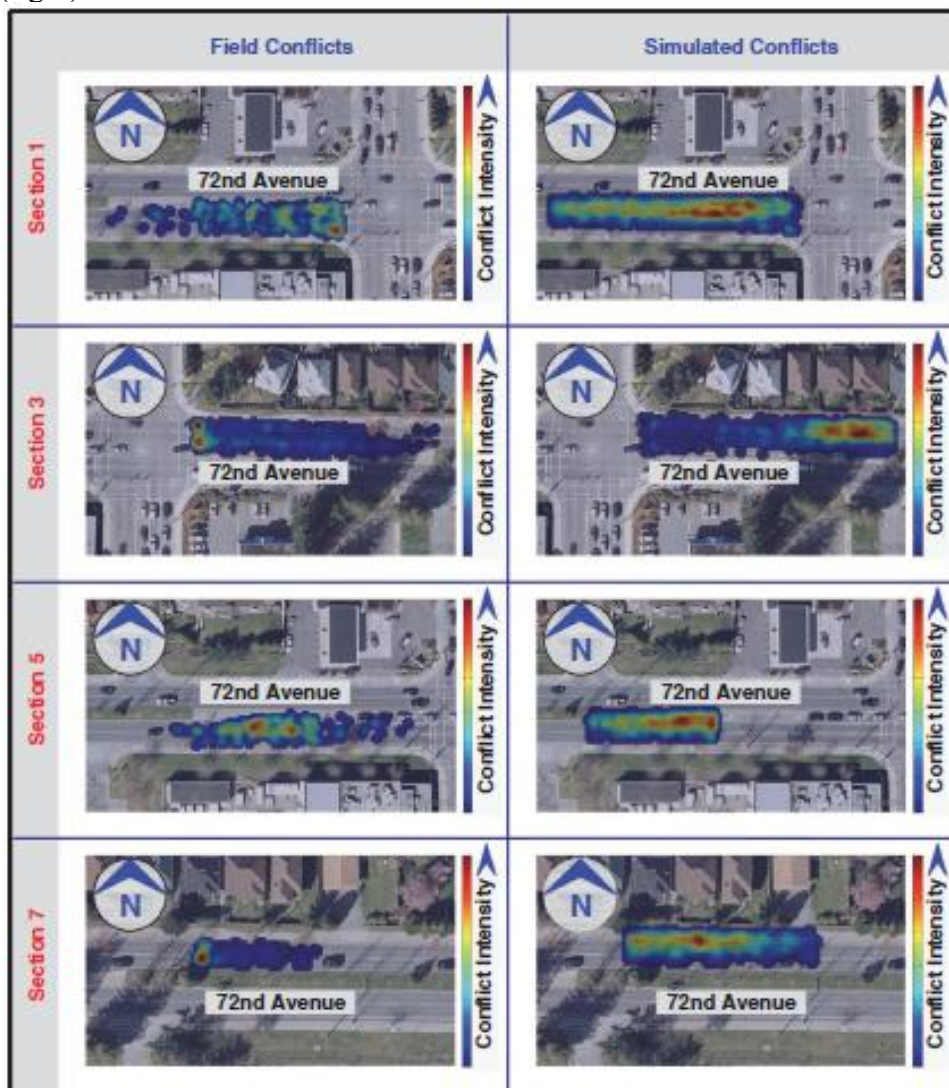
When it comes to the acquisition of data for TSP analysis, the following traffic microsimulation tools stand out: CORSIM, SIMTRAFFIC, VISSIM, HUTSIM, Paramics, TEXAS, AIMSUN, WATSIM, and Integration, evaluated concerning the measurement of traffic safety proxy indicators by FHWA (2003). An important microscopic traffic simulator is VISSIM (PTV Group), which incorporates five models: i) car-following, which represents the longitudinal movements; ii) lane-changing, which characterizes the willingness to drivers' changing of the lane; iii) lateral movement, which represents the driver insertion in a traffic band; iv) gap acceptance; and v) route choice (PTV, 2018). To correctly apply microscopic simulation tools, it is necessary that the simulated conditions precisely represent the reality observed in the field. Therefore, simulation calibration is fundamental.

4.3.4 Practical application of microscopic traffic simulation for TSP analysis

Essa and Sayed (2015) conducted a study justified by the fact that, despite numerous advantages, the traffic microscopic simulation process requires high accuracy in its calibration. The authors used 60 hours of automatic video processing, in which vehicle trajectories were observed, as well as vehicle conflict indicators (such as TTC) that occurred at a signalized intersection of Surrey (British Columbia, Canada). Actual data from the footage was used to

calibrate and validate traffic microsimulation in VISSIM software (PTV Group), and vehicle conflict data analysis was obtained using a Surrogate Safety Assessment Model (SSAM). The performance of the calibration procedures of the vehicle platoon modeling parameters was observed and the average delay was responsible for increasing the correlation between the results obtained from the simulation and the processing of footage. Inconsistencies were observed in the spatial correspondence of the conflicts, as shown in the heat maps in Figure 46.

Figure 46 - Heat maps for footage-observed (left) and simulator-predicted (right) vehicular conflicts



Source: Essa and Sayed (2015).

Huang *et al.* (2013) conducted a study aiming to identify if vehicular conflicts simulated in VISSIM and captured by the SSAM software would satisfactorily represent the conflicts observed in field at intersections. For this purpose, the authors obtained 80 hours of

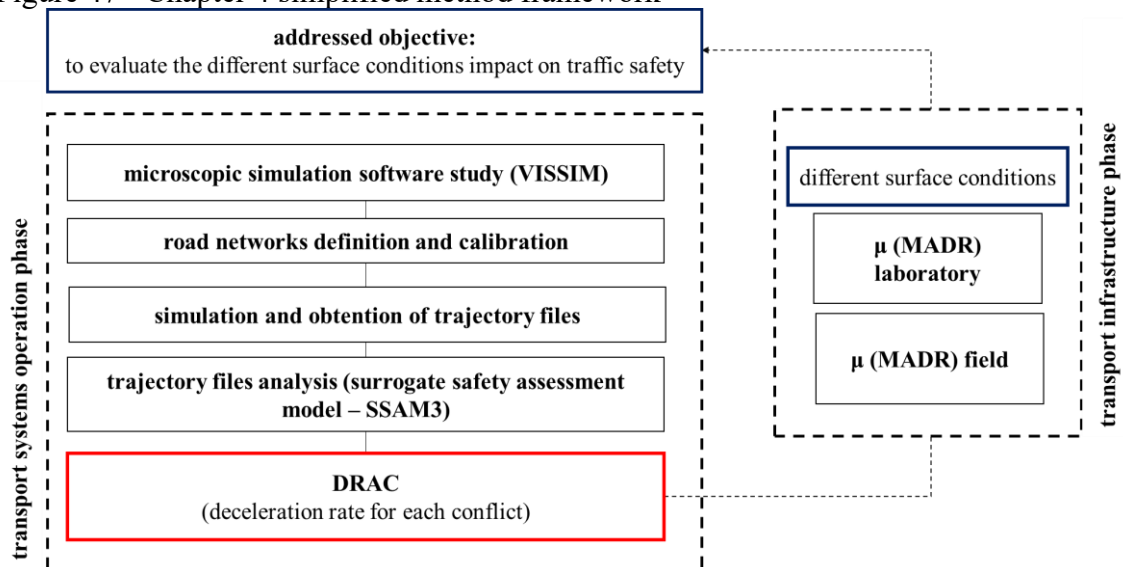
footage from 10 different intersections. Concerning the network calibration and validation focused on VISSIM Wiedemann 74 car-following model, the ax , bx_add , and bx_mult parameters were identified as the most significant for validating the relation between computational and real conflicts. In the results' analysis, an average absolute percentage error of 24% was observed concerning the total number of conflicts in relation to those observed in field. For longitudinal conflicts, the observed error was 16%. In the regression analysis, the regression coefficients (R^2) of 0.78 were obtained for all conflicts and 0.57 for the longitudinal conflicts, which allowed the authors to conclude about the suitability of VISSIM and SSAM in the representation of vehicle conflicts in the field.

In the study conducted by Costa (2017), an evaluation of the impact of tire-pavement friction on the TSP in an urban environment was carried out using the VISSIM software and the Surrogate Safety Assessment Model (by the SSAM3 software), which captures and registers vehicular conflicts through the analysis of the trajectories of the vehicles in microsimulation. For an arterial road in the city of Fortaleza (Brazil), simulation parameters were calibrated and macro and microtexture measurements were performed, statistically analyzed, and converted to friction coefficient (μ) values - at different speeds. These values were incorporated into a maximum available deceleration model by means of the Maximum Available Deceleration Rate (MADR) indicator, which can be compared to the DRAC proxy indicator. MADR values were found to be dependent on the vehicular demand and the drivers' behavior.

4.4 Materials and methods

This chapter aims to evaluate the influences of different tire-pavement friction conditions on Traffic Safety Performance (TSP). In summary, it intends to compare, by road safety indicators, the necessary deceleration rates for vehicles to avoid a crash (DRAC) and the maximum available deceleration rates (MADR) limited by the road surface conditions. To obtain DRAC, microscopic traffic simulation and vehicle trajectory analysis tools were used to capture vehicle conflicts' occurrence and information related to these interactions. MADR is a function, among other variables, of friction coefficient (μ), vehicle speeds and aerodynamics, and characteristics of the road. The simplified framework of the method to be applied in this chapter is presented in Figure 47.

Figure 47 - Chapter 4 simplified method framework

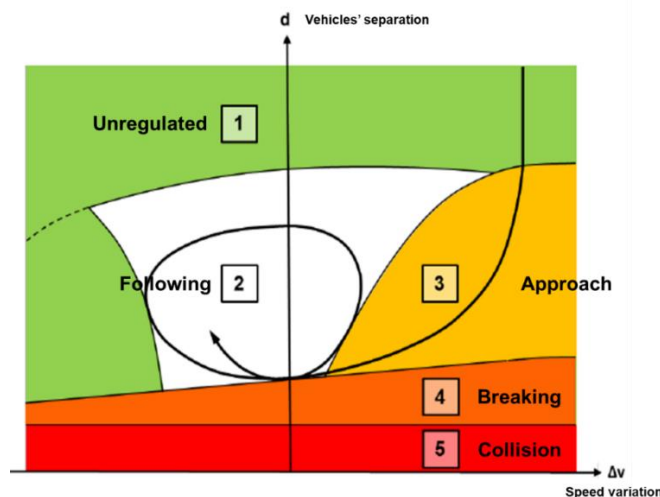


Source: the author.

4.4.1 Simulation framework

The microscopic simulations in this work were performed using the software VISSIM (PTV Group, Germany). The algorithm of this simulation platform incorporates a microscopic psychophysical model based on the assumption of action limits triggered by the following vehicles drivers' perception of the position and speed of the leading vehicle, as shown in Figure 48 (WIEDEMANN, 1974). The simulator VISSIM is based on 5 models: (i) car-following, for longitudinal movements; (ii) lane-changing; (iii) lateral movements; (iv) gap acceptance; and (v) route choice.

Figure 48 - Wiedemann (1974) model



Source: adapted from PTV (2020).

The simulated conditions need to precisely represent the traffic reality observed in the field. Thus, calibrating the simulation models is fundamental, because this factor directly impacts on the quality of the obtained results. In addition to the more general traffic conditions (road geometry, traffic hourly volume, traffic composition, proportion of movements, among others), it is necessary to calibrate the drivers' behavioral pattern, which is variable, and tends to be unique for each evaluated environment.

Costa (2017) selected saturation flow (SF) and free flow speed (FFS) as target parameters for VISSIM driving behavior calibration. SF is the maximum traffic flow rate, obtained from the observation of the saturation headway (SH), according to the Highway Capacity Manual (HCM) (TRB, 2010). FFS is the mean vehicle speed in a section, measured in the low-traffic condition (TRB, 2010), to be considered in occasions when there is no impedance to speeds' development.

SF and FFS can be directly measured in field or obtained through the analysis of data collected by speed cameras. The main VISSIM driving behavior parameters are: (i) standstill distance in front of static obstacles (ax), (ii) additive factor of security distance (bx_add), and (iii) multiplicative factor of security distance (bx_mult). These parameters impact the dispersion and queue formation simulated by the car-following model. Lacerda (2016) suggested default values for behavioral parameters' calibration when it comes to the representation of Fortaleza city, Brazil. Costa (2017) estimated such values for three different conditions (variable weather conditions and drivers' cautiousness), as summarized in Table 30. However, the calibration of the wet weather/cautious driver scenario was found to severely differ from "normal" behavior estimated by Lacerda (2016), which led to an unexpected behavioral heterogeneity and increase in conflicts account. Therefore, in terms of the methodological application presented in this work, driving behaviors in simulations were limited to the wet/aggressive scenario, specifically because friction models and measurement tools refer to the contact of vehicle tires with the wet pavement.

Table 30 - Typical values for driving behavior parameters

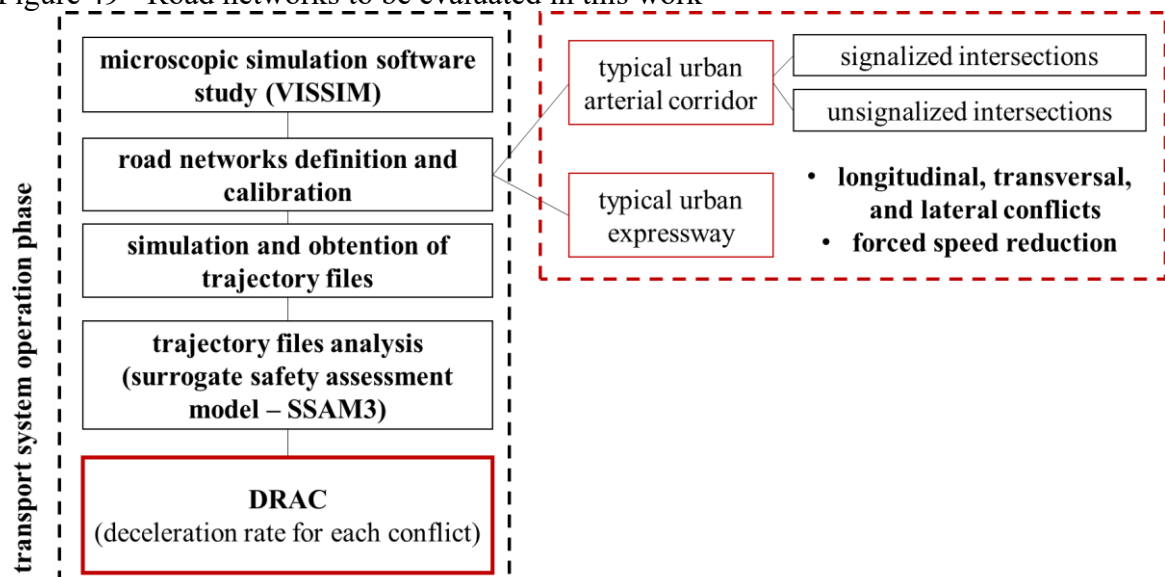
Scenario	Source	ax (m)	bx_add	bx_mult
Default	PTV (2018)	2.00	2.00	3.00
Fortaleza	Lacerda (2016)	2.20	5.00	5.00
Fortaleza - Dry weather	Costa (2017)	2.20	4.70	4.70
Fortaleza - Wet / Aggressive	Costa (2017)	2.20	5.00	5.00
Fortaleza - Wet / Cautious	Costa (2017)	2.20	6.50	6.50

Source: the author.

Typical corridors of Fortaleza (Brazil) were represented in this work: (a) a typical urban expressway, and (b) a typical urban arterial corridor, including signalized and unsignalized crossings. For each selected section, the following inputs were calibrated: (i) links (corridors) geometry, (ii) vehicle inputs (volume and composition), (iii) turning movements and proportions, (iv) desired speed behavior, (v) behavioral parameters, and (vi) traffic lighting times, if applicable. SF and FFS consistency of values was then analyzed to allow the obtention of trajectory files. Such values are aimed to refer to peak hours, typical days, and good weather conditions. Even so, the driving behavior in rainy conditions may also be represented with the use of parameters' values suggested by Costa (2017). As the aim of this work is to consolidate a method in simplified networks' structures, the representation of further complexities in terms of traffic system may be enhanced in the scope of future works.

The selection of the mentioned typical corridors was proposed because of the sensible differences between the expected nature of conflicts between the both conditions, partially shown in Figure 49. In the case study of urban expressways, higher speeds are developed and it is possible to compare normal conditions of flow and questions such as forced speed reduction, which may be a function of traffic speed cameras' monitoring, pavements' defects, and unexpected presence of animals and pedestrians. When it comes to urban arterial corridors, the simulation process can capture what happens in crossings (transversal conflicts), in forced speed reductions (traffic lights and stop signals), and in vehicles' turnings. As it will be furtherly discussed, there is also a difference between the expected traffic composition in terms of proportion of heavy vehicles.

Figure 49 - Road networks to be evaluated in this work



Source: the author.

4.4.2 Case study one: default network – expressway

The first set of simulations was proposed for a typical expressway located in the city of Fortaleza, Brazil. These corridors are characterized by their high traffic capacity and the absence of interruptions (such as crossings). Also, the access of vehicles from the secondary roads occurs smoothly. In this first moment, one seeks to capture the occurrence of conflicts from the drivers' own behavioral pattern. For this set of simulations, a straight section (500 m) of the BR-116 highway was selected. The traffic assumptions are summarized in Table 31. It is worth mentioning that the traffic volume estimation was based on a simplified analysis of the capacity of the road by the Greenshields model (high demand scenario), and also the assumptions of the low traffic volume, and the driving behaviors were set to be the same as the assumed in previous works of this research group, such as Costa (2017) and Maia *et al.* (2020). For each case study, a total of 500 minutes of simulation (divided into 60 simulations of 500 seconds of flow and 100 seconds of network warm-up).

Table 31 - Expressway calibration parameters

	Lanes	3
Links	Lanes' width (m)	3.5
	Lanes' extension (m)	500
Vehicle	Low demand scenario (vph/lane)	300
	High demand scenario (vph/lane)	2500
	Cars proportion (%)	80
	Trucks proportion (%)	20
	Desired speed (cars) (km/h) *	60
	Desired speed (trucks) (km/h) *	60
	<i>ax</i>	2.2
Driving behavior	<i>bx_add</i>	5.0
	<i>bx_mult</i>	5.0

*Regulated and monitored road

Source: the author

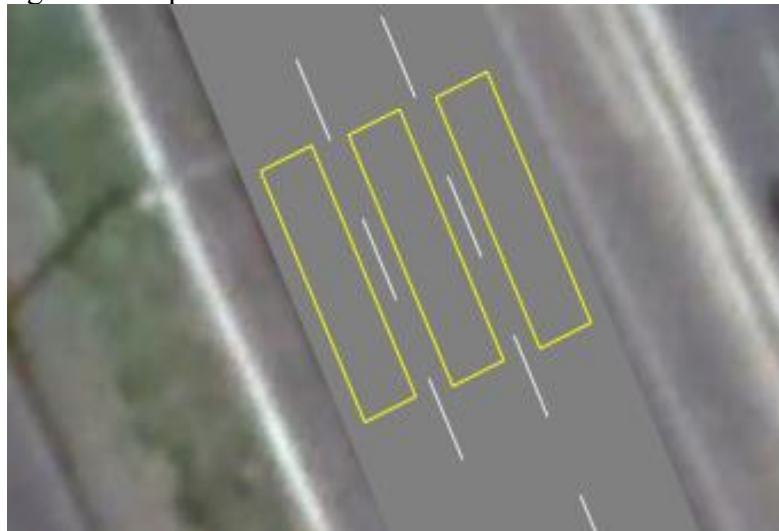
4.4.3 Case study two: forced speed reduction in an expressway

In VISSIM, the programming of reduced speed areas is applied to model short temporary speed reductions, such as the deceleration performed by drivers in turning movements. In this work, the second case study was performed to analyze the impact of a deceleration wave triggered by a sudden deceleration of a random leading vehicle. When vehicles enter the network in high speeds and this network is relatively stable (such as a limited speed monitored expressway), the disruptions of the network are rarer, and may be developed

by the invasion of a pedestrian, an animal, or even by the presence of a pavement distress. These events can lead to a sudden stop (quick deceleration).

The “forced speed reduction” function is continuous and fixed throughout the simulation (applied to all vehicles entering the area highlighted in Figure 50 (a). After a certain moment, the effect of the braking wave ceases. At this point, vehicles already enter the system at lower speeds due to a speed adjustment in function of the saturation caused by the queue formed (Figure 50, b). For this purpose, 60 simulations were performed, limited to 200 seconds and the maximum possible deceleration input (-10 m/s^2).

Figure 50 - Speed reduction simulation in VISSIM



(a) Adding speed reduction area to a link

Reduced Speed Area

No.: Name:

Link - lane:

Length: Time From:

At: until

Show label

Count	VehClass	DesSpeedDistr	Decel
1	10: Car	15: 15 km/h	10.00
2	20: HGV	15: 15 km/h	10.00

(b) Speed reduction programming

Source: the author

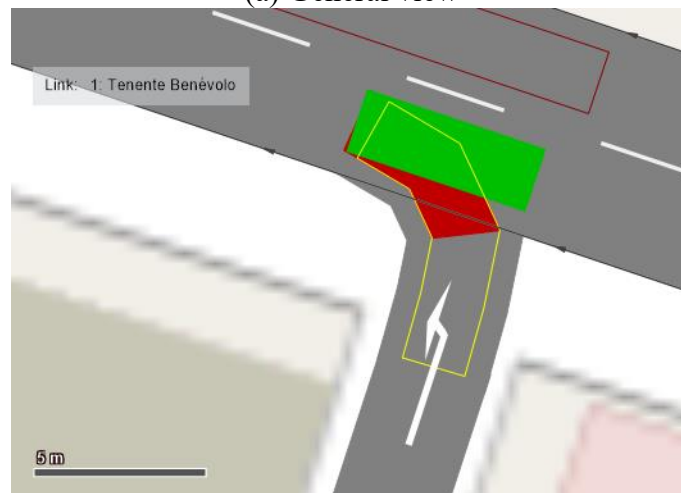
4.4.4 Case study three: typical urban arterial corridor

A typical arterial corridor of the city of Fortaleza was selected to be evaluated in terms of TSP indicators (Figure 51). According to assumptions taken by Costa (2017) and Maia *et al.* (2020), the following traffic volumes would satisfactorily represent the reality in this city: (i) high - 1200 vph, (ii) intermediate - 900 vph, (iii) low - 600 vph and (iv) very low - 300 vph. Field measurements performed in a peak hour of a typical day in 2018 resulted in the estimation of 904 vph to the main road and 764 vph to the secondary road, being such corridor estimated to present intermediate traffic. It is important to mention the following characteristics of the corridor: traffic entering the represented link coming from a signalized intersection (half from each corridor), 3 unsignalized intersections and 1 signalized intersection. The vehicular composition of traffic includes cars, trucks (VUC standard, given the restrictions on the circulation of larger cargo vehicles), public transportation buses, and motorcycles.

Figure 51 - Fortaleza city selected typical arterial corridor



(a) General view



(b) Advance rule

Source: the author.

4.4.5 Traffic safety analysis considering tire-pavement friction

Data (trajectory files) from vehicle interactions obtained from simulations in VISSIM were analyzed by the Surrogate Safety Assessment Model (SSAM) through the SSAM3 software. This tool registers conflict situations at default values of 1.5 s for TTC and 5.0 s for PET (GETTMAN and HEAD, 2003, PU and JOSHI, 2008). Once temporal indicators of vehicular conflicts are deeply limited to the characterization of vehicles' conflicts severity, due to the exclusion of kinetic energy effects (CUNTO, 2008), the proxy indicator deceleration rate to avoid the crash (DRAC) is used in this research to characterize the severity of traffic conflicts. The mathematical formulation of the DRAC is shown in Equation 39. According to Hydén (1996), situations in which $DRAC > 6.0 \text{ m/s}^2$ require emergency reactions by drivers.

$$DRAC = \frac{(V_{i,t} - V_{i-1,t})^2}{2[(S_{i-1,t} - S_{i,t}) - L_{i-1,t}]} \quad (39)$$

In which: $V_{i,t}$ e $V_{i-1,t}$: the initial speeds of the following and leading vehicles, respectively;

$S_{i-1,t}$ e $S_{i,t}$: positions of vehicles at the time the conflict is captured;

$L_{i-1,t}$: leading vehicle length.

In addition to the minimum required braking rate to avoid a crash (DRAC), each distinct traffic interaction can be referred to a maximum available deceleration rate (MADR). For the MADR calculation, the presence of the variable μ (friction coefficient) is the main link between surfaces' texture/friction and traffic safety SMOs. In summary, MADR is a function of: (i) friction coefficient, (ii) surface slope, and (iii) aerodynamic drag. This method (CANALE, 1989) is applicable to 4-wheel vehicles. The mathematical formulation of the MADR is shown in Equation 40 and the parameters adopted in this work are shown in Table 32.

$$MADR = \frac{g}{\gamma_b} \times \left\{ \mu + \left[0,01 + 0,0162 \times \left(\frac{v}{160} \right)^{2,5} \right] - \text{sen } \theta + \frac{C_a \times \rho \times A \times v^2}{2g \times W} \right\} \quad (40)$$

Simplifying:

$$\text{MADR} = g \times \mu \quad (41)$$

In which:

- g : acceleration of gravity (m/s^2);
- γ_b : influence factor of vehicle rotating parts;
- μ : friction coefficient;
- θ : surface slope ($^\circ$);
- ρ : air density (kg/m^3);
- C_a : drag coefficient;
- A : vehicle front area (m^2);
- v : vehicle speed (m/s);
- W : vehicle weight (N).

Table 32 - MADR inputs

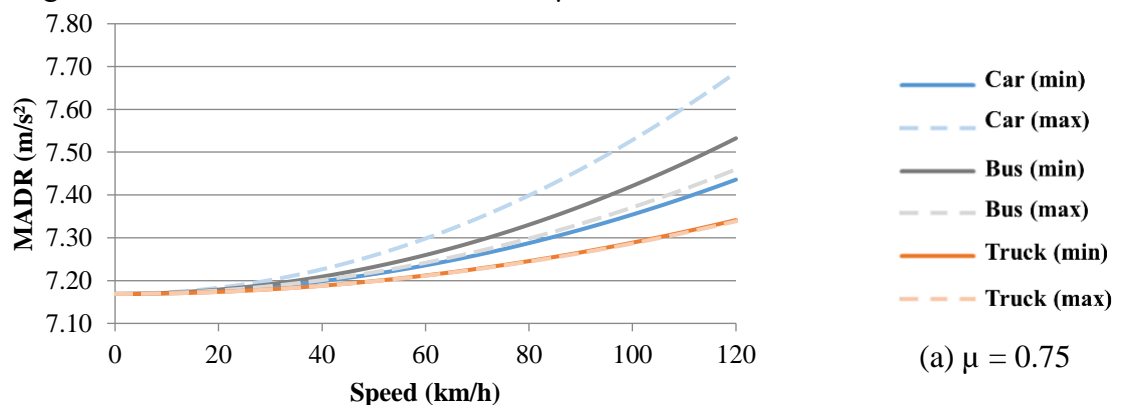
Vehicle	g (m/s^2)	γ_b	θ ($^\circ$)	ρ (kg/m^3)	Mass (kg)	C_a	A (m^2)
Car	9.81	1.04	0	1.1644	1000 - 2000	0.25 - 0.45	1.30 - 2.80
Truck (UCV*)	9.81	1.04	0	1.1644	8000 - 16000	0.60 - 0.70	5.90 - 8.10
Bus	9.81	1.04	0	1.1644	16000 - 33000	0.80 - 1.00	4.20 - 6.20

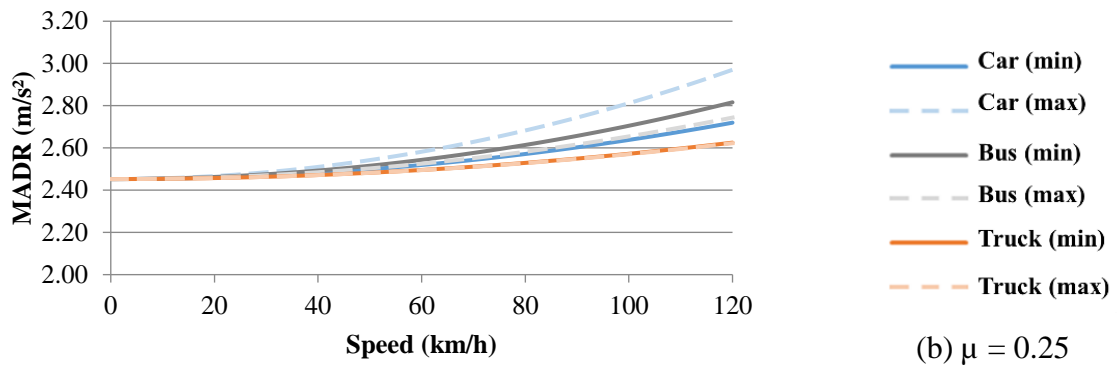
*UCV: Urban cargo vehicle (standardized vehicle with size and weight limitations)

Source: adapted from Costa (2017).

An observation exists regarding the sensitivity of the MADR parameter to Canale (1989) equation inputs variation. One may observe that only the μ parameter is significant to the MADR result for speeds below 60 km/h (COSTA, 2017). Maia *et al.* (2019a) highlighted that vehicular conflicts tend to occur at speeds below 60 km/h in urban environments such as Fortaleza (Figure 52). This phenomenon is a function of the growing vehicular demand, the existence of intersections, as well as the speed limits.

Figure 52 - MADR variation for different μ values





Source: adapted from Costa (2017).

The vehicle interactions in which $DRAC \leq MADR$ were interpreted as situations that the following driver can develop the necessary deceleration, avoiding evasive maneuvers (for example, lane changing). The $DRAC > MADR$ situations were considered as forcing drivers to perform any action to avoid collision. For each performed microsimulation, the trajectory files (.trj) were obtained and imported into the SSAM3 software, which identifies vehicular conflicts for the 1.5 s TTC and 5.0 s PET thresholds. It is important to mention that part of the captured conflicts in SSAM3 is related to a $TTC=0$, which, according to Giuffrè *et al.* (2018), tend to represent mere processing errors. The assessment of TSP in this study was conducted by the statistical analysis of DRAC and MADR results for the three case studies, and the sensitivity of TSP to the different tire-pavement friction conditions, predicted by the method proposed by Aldagari *et al.* (2020) was discussed. Table 33 and Table 34 recover the materials evaluated in chapter 2.

Table 33 - Gradations of different Brazilian traditional mixtures

Code	Type of gradation	Type of use	Brazilian standard	Range/Limit
A	Dense-graded	Roadway	DNIT 031/2006 - ES	C - Lower
B	Dense-graded	Roadway	DNIT 031/2006 - ES	C - Upper
C	Fine-graded	Roadway	DNIT 032/2005 - ES	A - Lower
D	Fine-graded	Roadway	DNIT 032/2005 - ES	A - Upper
E	Porous Friction Course	Roadway/Airport	DNER 386/1999 - ES	II - Lower
F	Porous Friction Course	Roadway/Airport	DNER 386/1999 - ES	II - Upper
G	Porous Friction Course	Roadway/Airport	DNER 386/1999 - ES	V - Lower
H	Porous Friction Course	Roadway/Airport	DNER 386/1999 - ES	V - Upper
I	Dense-graded	Airport	DIRENG 04.05.610 (2002)	II - Lower
J	Dense-graded	Airport	DIRENG 04.05.610 (2002)	II - Upper
K	Dense-graded	Airport	DIRENG 04.05.610 (2002)	III - Lower
L	Dense-graded	Airport	DIRENG 04.05.610 (2002)	III - Upper

Source: the author.

Table 34 - Aggregates' database

	Origin	Code	Mineralogy
Northeast Brazil	Ceará	DAC	Gneiss*
	Ceará	DBI	Phonolite**
	Ceará	DBJ	Phonolite**
	Ceará	DCC	Gneiss*
	Ceará	DDC	Gneiss*
Southeast Brazil	São Paulo	TBA	Basalt
	Minas Gerais	TMC	Meta-limestone
	Rio de Janeiro	TGN	Migmatic gneiss***
	Rio de Janeiro	TPA	Paleosome
	Rio de Janeiro	TML	Melanosome
	Rio de Janeiro	TLE	Leucosome
	Rio de Janeiro	TPE	Pegmatite
	Rio de Janeiro	TGR	Granitoid

* Aggregates DAC, DCC, and DDC were obtained from different quarries, but all from conic crushers.

** Aggregate DBI was obtained from impact crusher and DBJ from jaw crusher.

*** Aggregate TGN is the mixture of the 5 lithotypes that originated aggregates TPA, TML, TLE, TPE, and TGR.

Source: adapted from Diógenes (2018) and Trotta (2020)

The described steps detailed the method to obtain the deceleration values that vehicles would need to apply to avoid crashes (DRAC). Many factors influence vehicles to achieve safe deceleration performance. However, the focus of this work, the friction in the tire-pavement interface, is the main variable (μ) for determining MADR. This parameter represents the deceleration potential offered by the surface on which the vehicle travels.

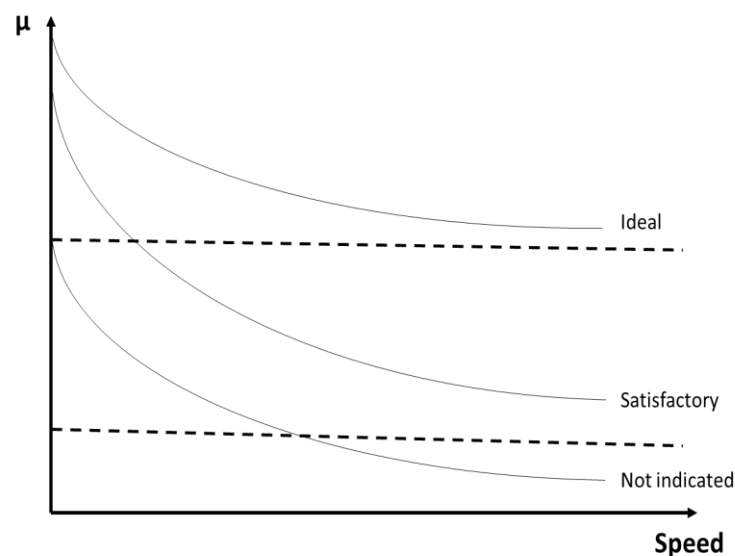
This work adopted the premise that satisfactory performance in terms of friction could be represented by a μ value that would result in a mean MADR = mean DRAC. This condition (MADR equal to the calculated average of DRAC) represents that in 50% of the simulated conflicts, the vehicle deceleration would occur adequately. In this case, there would be no need for a more efficient braking system by the vehicle or even the application of an emergency maneuver.

The ideal condition, however, would represent that all conflicts occur within a range where MADR > DRAC. This definition can come from the decision-makers themselves. Some thresholds can be suggested. First, they could pursue a pavement μ that results in a MADR higher than the highest DRAC value obtained. In other cases, the definition of a μ value higher than the DRAC+1Sd or DRAC+2Sd values would be more proper. It is worth to mention that the value of μ admitted as the ideal one in this work was assumed to result in a situation in which only 1% of conflicts would occur in a DRAC > MADR condition. Furthermore, according to the exceptionality of SMOs results from the simulation, there would be impeding factors for the existence of corridors with high μ . This can include the availability of materials with

satisfactory surface texture characteristics, as well as the availability of financial resources for the adequation of roads in operation to comply with very high μ values.

It is noteworthy that this definition must be a reason for discussion between the analysts of the problem to be investigated, given the specificity of the traffic safety goals and local conditions. Figure 53 shows a graphic in which the bold lines represent asphalt mixture friction curves (IFI), and the dashed lines represent the μ values defined as the goals to be achieved by the pavement surface. In the ideal situation, the predicted (or measured) friction tends to provide sufficiently safe conditions for the vast majority of conflicts captured in the simulation. On the other hand, in the not indicated situation, above some speeds, vehicles would be in a scenario with an unsafe tendency. This condition would represent that the DRAC value would be higher than the maximum deceleration possible to be achieved in more than 50% of conflicts. This would increase the risk of crashes and compromise traffic safety performance in this environment.

Figure 53 - Assessment of materials' suitability to urban environments in terms of friction and traffic safety



Source: the author.

4.5 Results and discussion

4.5.1 Case study one: default network – expressway

The "low vehicular demand" scenario has led to a lower number of observed conflicts. Such perception is a consequence of more freedom of maneuvering, despite the

possibility of drivers to perform higher speeds. Indeed, in such a situation, the number of conflicts is irrelevant in comparison to the "higher vehicular demand" scenario, as shown in Table 35. In both cases, lane changing conflicts are predominant (above 80%). As a function of the high CV values obtained to the entire SMoS extent, there is no statistical significance of differences between the scenarios, only punctual trends. The scenario of higher vehicular demand represents higher DRAC average, implying in greater severity of conflicts, unlike the analysis of TTC and PET results.

Table 35 - Conflicts and proxy indicators results for an expressway

Summary of conflicts		Low demand (300 vph/lane)	High demand (2500 vph/lane)
Conflicts	Total	6	466
	Rear-end (%)	17	11
	Lane change (%)	83	89
	Crossing (%)	0	0
Proxy indicators		Low demand (300 vph/lane)	High demand (2500 vph/lane)
TTC	Mean (s)	0.5	0.8
	Sd (s)	0.4	0.3
	CV (%)	82	45
PET	Mean (s)	0.5	1.0
	Sd (s)	0.3	0.6
	CV (%)	54	60
DRAC	Mean (m/s ²)	1.4	2.2
	Sd (m/s ²)	1.6	1.7
	CV (%)	112	77
	Number of DRAC > 6 m/s ²	0	8
	DRAC > 6 m/s ² (%)	0	2

Source: the author.

Speeds at which conflicts happen are lower in the "higher vehicle demand" scenario (average), as Table 36 shows. The maximum captured following vehicle speed increases with vehicle demand. This trend is an implication of the development of higher desired speeds and greater maneuverability allowed by lower traffic volumes. An issue that one must account is the fact that the friction coefficient varies according to the vehicle's travel speed.

Table 36 - Summary of speed results for conflicts in an expressway

Following vehicle speed (Km/h)	Low demand (300 vph/lane)	High demand (2500 vph/lane)
Maximum (Km/h)	63.0	53.0
Minimum (Km/h)	39.4	16.2
Mean (Km/h)	55.2	35.9
Sd (Km/h)	5.8	5.9
CV (%)	11	16

Source: the author.

The necessary friction coefficient has been predicted based on Equation 41 (see the section "Materials and Methods" of this work). 3 "minimum required MADR" scenarios were set based on the average DRAC values (1.4 to 2.2 m/s²), up to the limit of 2 standard deviations above the DRAC average value (4.6 to 5.6 m/s²) (Table 37). It is important to mention that the minimum value of μ referring to a MADR > 6.0 m/s² (value referring to DRAC in which urgent maneuvers are required by the drivers) is 0.64.

Table 37 - Minimum μ requirements for an expressway

Scenario	Low demand (300 vph/lane)		High demand (2500 vph/lane)	
	MADR (m/s ²)	μ	MADR (m/s ²)	μ
MADR = Mean DRAC	1.4	0.15	2.2	0.23
MADR = DRAC + 1 Sd	3.0	0.32	3.9	0.41
MADR = DRAC + 2 Sd	4.6	0.48	5.6	0.59

Source: the author.

4.5.2 Case study two: forced speed reduction in an expressway

In summary, the proportion of rear-end conflicts increases in comparison to case study 1 (30%, against 11 to 17%). However, the severity of conflicts (SMoS) did not change and maintained the trend of high CV, as well as the following vehicle speeds. Finally, there are no major changes in terms of friction coefficient requirements. It is important to remember that the simulation period was shorter, as the intention was to capture the effect of the deceleration wave. A longer simulation period would capture the traffic adjustment because of the loss of traffic capacity (which may trigger jams and reduced speeds). In the case of a normalized phenomenon, the probability of conflicts higher than the average + 2 Sd is remote. Table 38, Table 39, and Table 40 retrieve such results.

Table 38 - Conflicts and proxy indicators results for deceleration waves in an expressway

Summary		
	Total	44
Conflicts	Rear-end (%)	30
	Lane change (%)	70
	Crossing (%)	0
Proxy Indicators		
TTC	Mean (s)	0.7
	Sd (s)	0.5
	CV (%)	71
PET	Mean (s)	0.7
	Sd (s)	0.5
	CV (%)	81
DRAC	Mean (m/s ²)	1.5
	Sd (m/s ²)	1.8
	CV (%)	122
	Number of DRAC > 6 m/s ²	2
	DRAC > 6 m/s ² (%)	5

Source: the author.

Table 39 - Summary of speed results for conflicts in deceleration waves in an expressway

Following vehicle speed	
Maximum (Km/h)	69.4
Minimum (Km/h)	5.1
Mean (Km/h)	34.1
Sd (Km/h)	17.0
CV (%)	50%

Source: the author.

Table 40 - Minimum μ requirements for deceleration waves in an expressway

Scenario	MADR (m/s²)	μ
MADR = Mean DRAC	1.5	0.16
MADR = DRAC + 1 Sd	3.3	0.35
MADR = DRAC + 2 Sd	5.2	0.55
MADR = Maximum indicated DRAC	6.0	0.64

Source: the author.

4.5.3 Typical urban arterial corridor

1438 vehicular conflicts were recorded in the corridor, which represents an average of 2.5 conflicts per simulation minute. This was obtained by applying the limits of 1.5 s of TTC (minimum) and 5.0 s of PET (maximum). 66% of the conflicts were classified as rear-end

conflicts. Such behavior may be a function of the presence of signalized intersections, as well as the existence of non-signalized intersections (and perhaps the entry of vehicles in the main link). These conditions may generate a wave of deceleration right after the moment that a leading vehicle slows down. The existence of intermediate traffic (900 vph) on the main link (measured at a peak time on a typical day), directly impacts the proportion of lane-change conflicts. On one side, this represents fewer acceptable gaps for changing lanes, but on the other hand, there is a tendency for these gaps to be shorter, which can lead to more severe conflicts.

In terms of SMOs, the simulation resulted in averages of 1.2 s of TTC and 1.8 s of PET. The PET parameter presented greater dispersion in terms of CV (68%, compared to 30% of the TTC indicator). The analysis of DRAC has indicated a 1.6 m/s² average deceleration. However, this indicator has shown the highest CV (119%). This value suggests the presence of “extremely high” values. 1% of these "extreme" values were greater than 6 m/s². DRAC values above 6 m/s² suggest the need for urgent driver reactions (Hydén, 1996). Table 41 presents a summary of conflicts and proxy indicators results.

Table 41 - Typical urban arterial corridor conflicts and proxy indicators results

Summary of conflicts		
	Total	1438
Conflicts	Rear-end (%)	65.0
	Lane change (%)	34.2
	Crossing (%)	0.8
Proxy indicators		
TTC	Mean (s)	1.2
	Sd (s)	0.4
	CV (%)	30
PET	Mean (s)	1.8
	Sd (s)	1.2
	CV (%)	68
DRAC	Mean (m/s ²)	1.6
	Sd (m/s ²)	1.9
	CV (%)	119
	Number of DRAC > 6 m/s ²	11
	DRAC > 6 m/s ² (%)	1

Source: the author.

The necessary friction coefficient has been predicted based on Equation 41 (see the section "Materials and Methods" of this work). 3 "minimum required MADR" scenarios were set based on the average DRAC value (1.6 m/s²), up to the limit of 2 standard deviations above the DRAC average value (5.3 m/s²) (Table 42). It is important to mention that the minimum

value of μ referring to a MADR $> 6.0 \text{ m/s}^2$ (value referring to DRAC in which urgent maneuvers are required by the drivers) is 0.64.

Table 42 - Minimum μ requirements

Scenario	DRAC (m/s ²)	μ
MADR = Mean DRAC	1.6	0.17
MADR = DRAC + 1 Sd	3.5	0.37
MADR = DRAC + 2 Sd	5.3	0.57
MADR = Maximum indicated DRAC	6.0	0.64

Source: the author

An issue that one must account is the fact that the friction coefficient varies according to the vehicle's travel speed. This phenomenon is the basis for the harmonization described by Wambold *et al.* (1995) in proposing the IFI method. Table 43 presents a summary of the captured speeds of the simulation procedure. The maximum speed captured in the simulation process is 54.4 Km/h. The average speed is 27.7 km/h, with Sd of 10.2 km/h (CV = 37%).

Table 43 - Summary of speed results for conflicts in a typical urban corridor

Following vehicle speed results	Speed (Km/h)
Maximum	53.4
Mean	27.7
Standard deviation	10.2

Source: the author.

On expressways, vehicular conflicts may happen in lower quantity than in typical urban arterial corridors. Such perception may be a function of the greater network organization, which leads to fewer disturbing vehicular interactions. According to its own formulation, the higher the traffic speed, the higher tends to be DRAC values. Even so, the results presented in this work suggest that specific situations (the urban arterial corridor) may result in more severe conflicts. In urban corridors, the enforcement of maximum speed limits and the greater road saturation indexes (peak times) may lead to lower speeds, but the traffic characteristics of the urban environment (such as the presence of transversal crossings) may increase DRAC values and its variability. Table 44 confirms this trend of higher variability of DRAC values for different scenarios. The mentioned variability may difficult finding statistically significant differences between different scenarios, even so, specifically due to the higher number of more severe vehicular conflicts on arterial roads, frictional properties in urban environments like a typical arterial corridor cannot be neglected.

Table 44 - ANOVA analysis for DRAC comparison in different scenarios

p-value	DRAC (Expressway – High demand)	DRAC (Expressway – Low demand)	DRAC (Expressway – Deceleration wave)	DRAC (Signalized Intersection)
DRAC (Expressway – High demand)	-			
DRAC (Expressway – Low demand)	0.733	-		
DRAC (Expressway – Deceleration wave)	0.091	0.999	-	
DRAC (Signalized Intersection)	0.000	0.996	0.993	-

*Green labels: not statistically different each other

*Red labels: statistically different each other.

Source: the author

4.5.4 Selecting asphalt materials for urban environments

Previous results confirm that one can define minimum friction coefficient requirements. This way, one can trace the most suitable strategies for the construction and the maintenance of asphalt courses. The methods presented in chapters 2 and 3 can support this analysis. Aps (2006) suggests $\mu > 0.15$ as "good" and $\mu > 0.34$ as "excellent" friction coefficient values. From the presented results, this work defines higher values for "minimum" (0.20) and "ideal" (0.65) limits for the Fortaleza urban environment (Table 45).

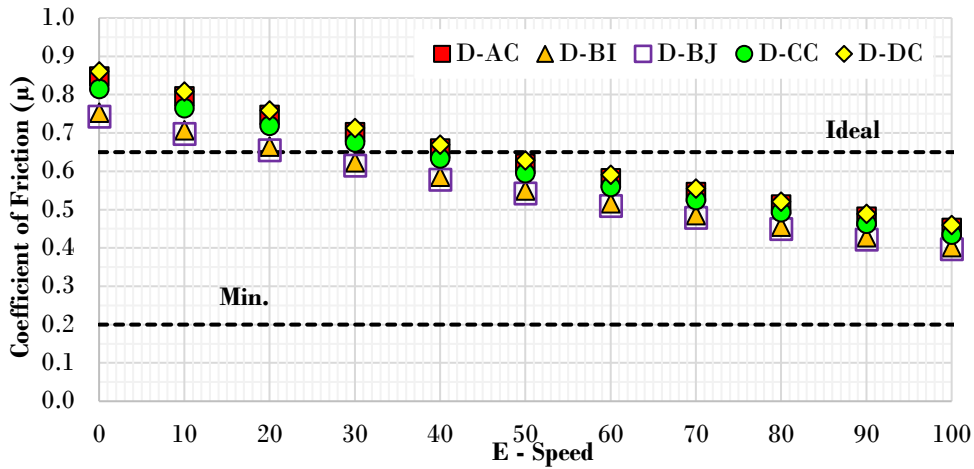
Table 45 - Proposed μ limits to inform materials' selection

Limit	μ	Justification
Minimum	0.20	Minimum requirement for MADR to be higher than the mean DRAC values.
Ideal	0.65	Ideal requirement, given that drivers would take urgent actions to avoid a crash in only approximately 1% of conflicts.

Source: the author.

When it comes to the northeastern aggregates, all gradations were satisfactory in terms of the use in the urban environment of the city of Fortaleza. A more drastic reduction in μ values would occur only for higher speeds. Speeds above 60 Km/h are not common in the urban environment, given speed limits and higher traffic volumes. Even so, the aggregates DAC and DDC (rougher), and the gradations E, F, G, and H (PFC) presented FC values closer to the one considered "ideal" (0.65). Figure 54 shows a positive example of aggregate-gradation combination.

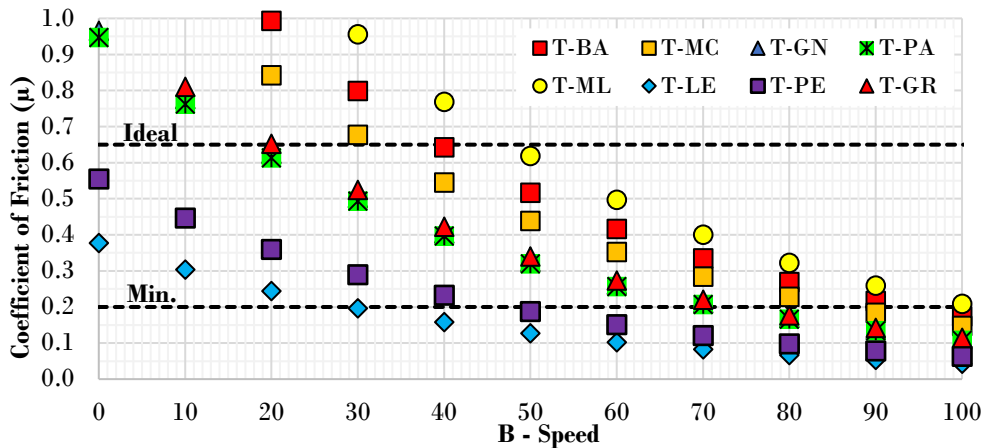
Figure 54 - Analysis of μ limits for PFC (DNER 386/1999 – ES, Range II – Lower) and NE aggregates



Source: the author.

The southeastern aggregates showed greater variability. Some combinations of aggregate gradations do not favor safety, providing $\mu < 0.2$ at the typical maximum speed of urban roads (60 Km/h). According to the example shown in Figure 55, the combinations of the TPE and TLE aggregates with the B, C, D, J, L gradations are not indicated when selecting materials.

Figure 55 - Analysis of μ limits for DG (DNIT 031/2006 – ES, Range C - Upper) and South-east Brazil aggregates



Source: the author.

It is important to mention that the IFI method is limited when it comes to lower speeds, of which friction values may be inflated. This collides with the theory of hysteresis, which is higher the higher is the macrotexture. Thus, the conflicts that are captured between

average and maximum speeds must be prioritized (in the urban area of the city of Fortaleza, the limits of 30 and 60 Km/h were found to be satisfactory).

4.6 Partial conclusions

The objective of this chapter was to set rational requirements for μ based on TSP. Microscopic traffic simulation (VISSIM software) and surrogate measures of safety (SMOS) supported the assessment of vehicular conflicts in different scenarios. Multiple possibilities of materials' selection were assessed to determine their suitability of use in the urban environment.

In summary, road safety indicators can be used to compare two main conditions: the necessary deceleration rates for vehicles to avoid a crash (DRAC), and the maximum available deceleration rates (MADR). DRAC was obtained using microscopic traffic simulation and vehicle trajectory analysis tools (SSAM3 software). MADR is a function of μ , as well as vehicles' speeds and aerodynamics, and road characteristics. Typical corridors of Fortaleza (Brazil) were represented in this work: (a) a typical urban expressway, and (b) a typical urban arterial corridor. In the vehicle interactions which $DRAC \leq MADR$, the following driver can develop the necessary deceleration, avoiding evasive maneuvers. The $DRAC > MADR$ interactions force drivers to perform immediate actions to avoid a collision. The analysis of DRAC and MADR values resulted in the proposition of minimum and ideal requirements of μ for the assessment of the materials' suitability.

On expressways, fewer vehicular conflicts were recorded when compared to typical urban arterial corridors. Such perception was found to be a function of a greater network organization, which leads to fewer disturbing vehicular interactions. In general, the higher the traffic speed, the higher tend to be DRAC values. Despite this theory, in urban corridors, the enforcement of maximum speed limits and the greater roads' saturation indexes may lead to statistical equality of mean DRAC for different scenarios. This work defined the following μ limits: minimum (0.20) and ideal (0.65) (for Fortaleza). Also, all the northeastern aggregates (despite gradations) were found to be suitable for use.

5 CONCLUSIONS AND RECOMMENDATIONS FOR FUTURE WORKS

5.1 Practical application of this work

The practical application of some of the contributions presented in this work are exemplified by the analysis of the urban environment studied in the works conducted by Costa (2017) and Maia *et al.* (2020). In the first study, the authors evaluated the surface conditions of an arterial corridor in Fortaleza (*Senador Virgílio Távora* avenue). By the time of the data collection, two main surface conditions were identified: worn and resurfaced areas, highlighting the heterogeneity of the conservation state of the 1.5 Km section. Extensive data was collected for each conservation state in terms of texture and friction (by the application of the traditional SP and BP tests). Note that, in Fortaleza, it is standard to use fine-graded asphalt mixtures (FG AC) as the main type of maintenance treatment for resurfacing worn sections (stop-gaps, for example).

Given the fact that the mentioned avenue concerns an aged pavement surface, the contributions presented in Chapter 3 support the contactless assessment of tire-pavement friction. In this case, if available, the drilling of cores would allow the assessment using AIMS equipment, and the application of the CRP technique also represents an alternative to friction assessment. However, even if the friction coefficient is obtained through a contactless method, the impact of this value on traffic safety performance is not fully understood. The friction coefficient values classification contained in the Asphalt Pavements Restoration Manual (DNIT, 2006) reflects indications for roadways, in which the traffic conditions are considerably different from urban environments.

Chapter 4 represents an innovative asset for the consideration of surface conditions in urban environments. Municipal authorities and transportation departments have more extensively used simulation tools to support solutions for traffic in the cities. To some extent, any modification that increases the quality of mobility in the cities may contribute to their economy, environment, and social conditions. Therefore, infrastructure studies, which usually neglect information that can be obtained through operational tools such as microscopic simulations, can also benefit from these technological advances.

The traffic simulation of an arterial avenue from Fortaleza city performed in chapter 4, analyzed in terms of DRAC and MADR, resulted in the definition of tire-pavement friction requirements that city pavements must meet. For the conditions simulated in this work, the following μ limits were defined: minimum (0.20) and ideal (0.65). $\mu = 0.20$ represents the

friction coefficient that represents the situations in which MADR would be higher than the mean DRAC values. $\mu = 0.65$ represents the "ideal" requirement, given that in only approximately 1% of the conflicts, the drivers would take urgent actions to avoid a crash ($\text{DRAC} > \text{MADR}$).

When the decision to construct a new pavement or wearing course is made, it is not required that particular attention be paid to texture and friction requirements. This is true especially for urban environments. Therefore, simple actions can be useful to support the selection of material to achieve the "ideal" specifications found in the application of the method presented in Chapter 4. In the case of this work, a model is presented in Chapter 2, first introduced in Texas (USA), which allows the estimation of tire pavement friction from laboratory materials characterization. Therefore, if a massive database of aggregates' shape properties and resistance to polishing is gathered, the pavement technician would easily know if the materials are suitable for the future pavement constructions in the cities (considering also factors such as gradation and traffic).

Based on Figure 56, we can see that, according to the results from Costa (2017), the resurfacing protocol (continuous black line) is not suitable in terms of safety for Fortaleza. Above 30 km/h speed, μ did not meet the minimum indicated for the city of Fortaleza (0.20). From 2018, the use of PFC mixtures as wearing courses became frequent in Fortaleza. This strategy was well received by public managers and the population in general. Maia *et al.* (2019b) state comfort and safety as the justification of this perception. In such circumstances, the predictive method discussed in chapter 2 supports the assessment of the fulfillment of minimum and ideal friction requirements (chapter 4) using different aggregate sources. This example shows the integration of the methods proposed in the three Chapters of this thesis:

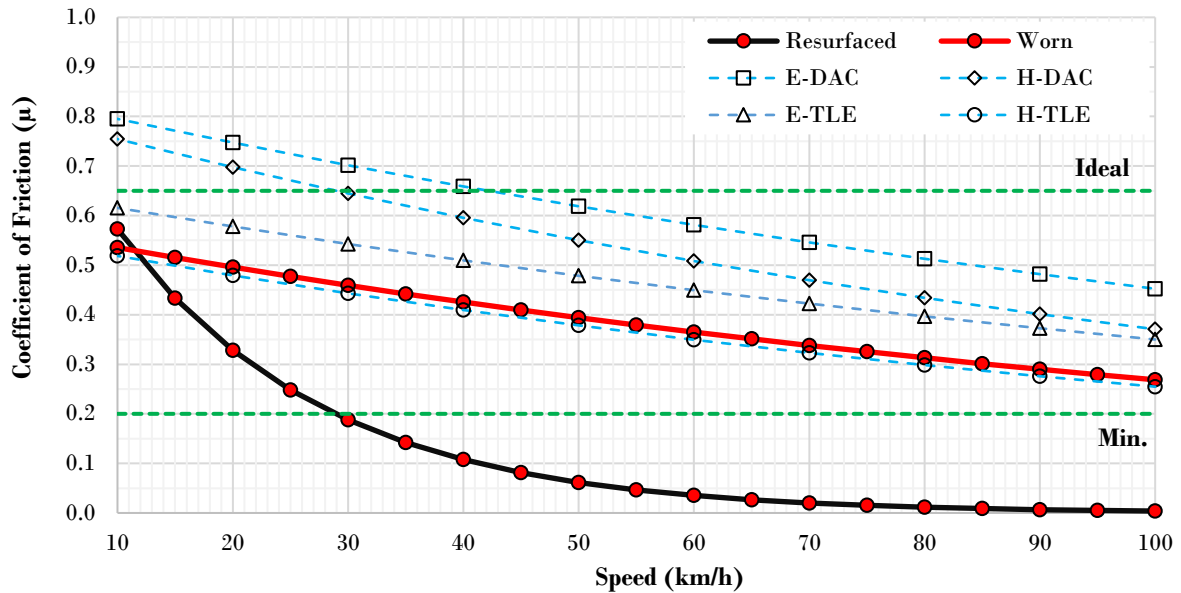
(i) Chapter 4: Once a traffic simulation is performed in the VISSIM or similar software, the TSP analysis using the SSAM tool and applying SMOs allows the estimation of minimum and ideal friction limits (dashed green lines in Figure 56).

(ii) Chapter 3: If there is an aged asphalt pavement, DIP tools presented in chapter 3 (AIMS and 3D Modeling using CRP) can support the assessment of friction conditions (continuous red and black lines) through contactless protocols. It is important to remember that the design and construction quality will determine how texture and friction evolve with time, and the possibility of an aged pavement to need for more or less frequent maintenance.

(iii) Chapter 2: The FC prediction based on material characteristics integrated into a database can give indications of the suitability of the construction or maintenance strategies to be used. In the example shown in this section, the use of the proposed gradation-aggregate combinations (PFC and two aggregates from different sources) would not compromise the

traffic safety performance.

Figure 56 - Assessment of the maintenance strategy of replacement of aged asphalt wearing course with PFC



Source: the author.

5.2 Final considerations

One way to contribute to the proactive approach of traffic safety is to assess whether it is possible to predict and improve the characteristics of the pavements before traffic crashes happen (so before the road construction and opening to traffic). I detected that the DIP and the efforts to develop a national database with references to the use of AIMS in Brazil would be an asset for the application of friction prediction models. Systematic research in the literature showed that studies conducted in Texas relied on the application of equipment already used in this research group (AIMS and MD).

Therefore, a database was organized in a way that could be as wide as possible (assuming some premises, such as the similarity between behaviors in terms of surface texture for #9.5 and #6.3 mm, and that little surface texture transformation happens on aggregates after approximately 100 minutes of polishing in MD). 12 gradations and 13 aggregates sources from recent works developed in Brazil were selected to analyze. One observed limitation was the variation range of the aggregates' characteristics that gave rise to the original Texas model, which differs from the extreme behaviors of Brazilian aggregates. Even so, most of the sources analyzed proved suitable for the prediction not only of $IFI_{initial}$ but also of IFI_{final} . The model

application presents some limitations, so future works may introduce a new friction prediction model, entirely based on Brazilian materials and field tests carried out using state-of-art friction-measurement equipment.

The statistical analysis attested to the significance of the selected variables (gradations/aggregate sources). Coarser gradations lead to better IFI performance in the initial years of the service life, but different gradations tend to be equivalent at the end of the pavement service life. The origin of the aggregate, expressed by its shape properties, is critical both at the beginning and at the end of the pavement service life. Furthermore, the aggregates of the Fortaleza metropolitan area tend to generate asphalt mixtures with similar characteristics in terms of tire-pavement friction, if used in the same gradation. Also, field studies carried out could validate the application of the final IFI prediction for the worn and resurfaced sections of an avenue in the city of Fortaleza.

Even proven the relevance of proactively evaluating the possibilities of materials selection from the safety perspective before the construction of the roads, the evaluation of the present conditions must always be considered with attention. These conditions define whether there is a need to construct a new pavement or carrying out maintenance. Thus, this work studied real-scale test sections to propose models for estimating the friction coefficient in the post-construction phase from parameters obtained from the texture analysis in AIMS (MPD), as well as from the processing of three-dimensional models (MPD and V_{mp}). Further results of this research were incorporated into a larger-scale study, under development, which seeks to expand the range of covered materials for the proposition of friction models based on CRP.

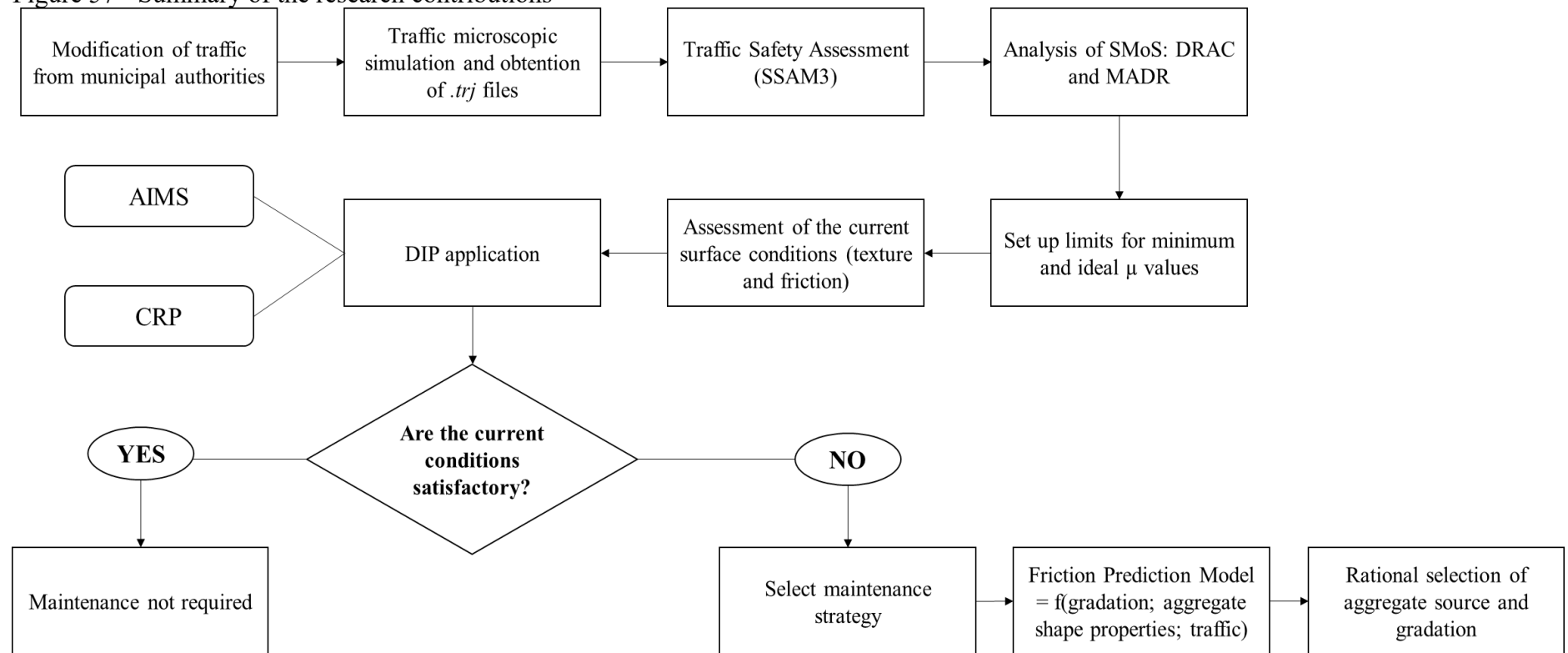
The use of microscopic simulation for the assessment of traffic safety is recurrent. Municipal authorities have been using these tools for analysis and proposition of scenarios aimed at improving traffic conditions in cities. However, infrastructure studies do not usually use the inputs that can be generated from these simulations. From Costa (2017), I verified that the analysis of traffic safety based on SMOs (DRAC and MADR) can provide information that may be valuable for the characterization and consequent selection of materials for paving.

This research group had previously gathered knowledge in terms of micro-simulation using the VISSIM software. Therefore, I represented different urban scenarios in this simulator: an urban expressway, speed sudden reduction in an urban expressway, and a typical arterial avenue. Based on the DRAC analysis obtained from the application of the SSAM3 software and the MADR estimation from literature equations, each proposed scenario showed particularities. On expressways, the increase in traffic increases the number of vehicular

conflicts, however, these conflicts tend to occur at slightly lower speeds due to the reduction in speed with increased saturation. Even so, in arterial avenues, despite a greater restriction on the development of higher speeds, the number of conflicts increases considerably.

For the city of Fortaleza, Brazil's 5th largest city, with enforced traffic rules, the obtained minimum requirements of μ were close to what was previously considered "good" for Brazilian highways ($\mu > 0.15$). The DRAC limit of 6 m/s^2 is rarely reached in the traffic conditions of the city (such as limiting the development of speeds above 60 Km/h). Thus, we consider that limiting an ideal μ to one that generates a DRAC above 6 m/s^2 (Hydén, 1996) would be a way to ensure that, in less than 1% of vehicular conflicts, emergency maneuvers would be required. Figure 57 presents the summary, in the form of a mental map, of the contribution of the present work to the characterization of the phenomenon of tire-pavement friction from the perspective of a proactive approach to traffic safety.

Figure 57 - Summary of the research contributions



Source: the author.

5.3 Recommendations for future works

The following recommendations are presented for future research in this area:

(a) Infrastructure studies:

- Propose a national friction prediction model for Brazil, by extending the national aggregates' database, standardizing procedures for use of AIMS, and looking forward to the utilization of state-of-art friction tests for field data collection.
- Develop a technical standard of the use of AIMS for the analysis of the texture of core samples, as Ibiapina (2018) proposed for the aggregates' shape properties analysis.
- Broaden the scale of the analyses of the 3D modeling, covering a wider range of aggregate sources, mixture types, and regions to propose a more general and reliable model for the relation between 3D parameters and friction.
- Investigate the microtexture scale in 3D models and use computational tools for gathering 3D-friction related information such as the tire properties and the environmental conditions.
- Investigate the influence of air pollution on the surface conditions of asphalt pavements.
- Search for partnerships and projects to incorporate knowledge from programming and automation to potentialize the use of CRP and provide to the public in the meantime an open-access mobile app to real-time measurement of texture and friction estimation.

(b) Operation and Traffic Safety studies:

- Create partnerships between municipal authorities and planning/operation research groups to obtain a database of trajectory files from official and better calibrated and validated microscopic simulations to be incorporated into infrastructure studies and therefore potentialize the functionalities of the simulation tools.

- Incorporate to the simulation efforts the presence of pedestrians, motorcycles, and bikes to the simulated scenarios, and increase the simulation running-time to acquire more reliable data.
- Propose the application of the friction requirements assessment method from the analysis of the DRAC and MADR SMOs also to real conflicts (not simulated conflicts). Research groups dedicated to traffic safety studies have been applying DIP tools to capture real conflicts, which therefore may be translated into trajectory files with the full information necessary to the replication of the method presented in the chapter 4 of this work.

BIBLIOGRAPHICAL REFERENCES

Chapter 1

ALDAGARI, S.; AL-ASSI, M.; KASSEM, E.; CHOWDHURY, A.; MASAD, E. Development of predictive models for skid resistance of asphalt pavements and seal coat. **International Journal of Pavement Engineering**. 2020. DOI: <https://doi.org/10.1080/10298436.2020.1766685>.

ARAUJO, V. M.; BESSA, I. S.; CASTELO BRANCO, V. T. F. Measuring skid resistance of hot mix asphalt using the aggregate image measurement system (AIMS). *Construction and Building Materials*, n. 98, pp. 476–481, 2015. DOI: <https://doi.org/10.1016/j.conbuildmat.2015.08.117>.

ARAUJO, V. M.C; MAIA, R.S.; CASTELO BRANCO, V.T.F; MAIA, A.O.; RODRIGUES, C.B. Avaliação das Relações entre Propriedades de Forma de Agregados, Compactação, Parâmetros do Esqueleto Mineral e Textura de Revestimentos Asfálticos Aeroportuários a partir do Processamento Digital de Imagens (PDI). **Revista Transportes (Rio de Janeiro)**. Accepted for publication in March 2019. In Portuguese.

BUSINESS INSIDER. China could beat the US in a race to get solar power from highways. Available on <<https://www.businessinsider.com/solar-power-roads-china-compared-to-us-2018-6>>. Access in 16 September 2019.

CATRACA LIVRE. Coletivos organizam Paulista aberta aos pedestres e ciclistas neste domingo. Available on <<https://catracalivre.com.br/arquivo/coletivos-organizam-paulista-aberta-aos-pedestres-e-ciclistas-neste-domingo/>>. In Portuguese. Access in 16 September 2019.

CHOUDHARY, J.; KUMAR, B.; GUPTA, A. Utilization of solid waste materials as alternative fillers in asphalt mixes: A review. **Construction and Building Materials**, Vol. 234(2020), pp. 1-19. 2020. DOI: <https://doi.org/10.1016/j.conbuildmat.2019.117271>

CHOWDHURY, A.; KASSEM, E., ALDAGARI, S.; MASAD, E. Validation of Asphalt Mixture Pavement Skid Prediction Model and Development of Skid Prediction Model for Surface Treatments. Report 0-6746-01-1, Project 0-6746, Texas Department of Transportation, Austin, Texas, USA. 2017.

COLONY, D. C. Influence of Traffic, Surface Age and Environment on Skid Number. Final Report Project Number 14460(0). Ohio Department of Transportation. 1992.

CONFEDERAÇÃO NACIONAL DO TRANSPORTE (2019). Painel de Acidentes 2019. Available on: <<https://www.cnt.org.br/painel-acidente>>. In Portuguese. Access in 8 June 2020.

DAN, H. C.; HE, L. H.; XU, B. 2017. Experimental Investigation on Skid Resistance of Asphalt Pavement Under Various Slippery Conditions. **International Journal of Pavement Engineering**. Vol.18, N.6, pp.1-15. DOI: <https://doi.org/10.1080/10298436.2015.1095901>.

DO, M. T.; CERREZO, V.; ZAHOUANI, H. Laboratory Test to Evaluate the Effect of Contaminants on Road Skid Resistance. **Institution of Mechanical Engineers, Part J: Journ. of Engineering Tribology**. N.228(11), pp.1276-1284. 2014. <https://doi.org/10.1177%2F1350650114530109>.

DUARTE, F.; FERREIRA, A. Energy harvesting on road pavements: state of the art. **Proceedings of the Institution of Civil Engineers – Energy**. Vol. 169 (2), pp. 79-90. 2016. DOI: <https://doi.org/10.1680/jener.15.00005>

DEPARTAMENTO NACIONAL DE INFRAESTRUTURA DE TRANSPORTES (DNIT). Manual de Restauração de Pavimentos Asfálticos. 2nd. Ed., Rio de Janeiro-RJ, Brazil, 2006. In Portuguese.

EMPRESA BRASILEIRA DE COMUNICAÇÃO (EBC). Mais de 193 mil pessoas morreram em acidentes de trânsito em 3 meses. Available on <http://agenciabrasil.ebc.com.br/geral/noticia/2018-09/mais-de-193-mil-pessoas-morreram-em-acidentes-de-transito-em-3-meses>>. In Portuguese. Access in 13 September 2018.

FWA, T. F.; ONG, G. P. Wet-Pavement Hydroplaning Risk and Skid Resistance: Analysis. **Journal of Transportation Engineering**. Vol.134(5), pp.182-190. 2008. [https://doi.org/10.1061/\(ASCE\)0733-947X\(2008\)134:5\(182\)](https://doi.org/10.1061/(ASCE)0733-947X(2008)134:5(182)).

GOMES, G. A.; REIS, R. S.; PARRA, D. C.; RIBEIRO, I.; HINO, A. A. F.; HALLAL, P. C.; MALTA, D. C.; BROWNSON, R. Walking for leisure among adults from three Brazilian cities and its association with perceived environment attributes and personal factors. **International Journal of Behavioral Nutrition and Physical Activity**, Vol. 8(111), pp. 1-8. 2011. DOI: <https://doi.org/10.1186/1479-5868-8-111>

HALL, J. W.; SMITH, K. L.; TITUS-GLOVER, L.; WAMBOLD, J. C.; TAGER, T.J.; RADO, Z. NCHRP Project 01-43: Guide for Pavement Friction, National Cooperative Highway Research Program (NCHRP), Transportation Research Board, Washington-DC, USA. 2009.

HENRY, J. Evaluation of pavement friction characteristics: a synthesis of highway practice. NCHRP Synthesis No. 291. National Cooperative Highway Research Program (NCHRP), Transportation Research Board. Washington-DC, USA. 2000.

JIANG, W.; YUAN, D.; XU, S.; HU, H.; XIAO, J.; SHA, A.; HUANG, Y. Energy harvesting from asphalt pavement using thermoelectric technology. **Applied Energy**. Vol. 205 (1), pp. 941-950. 2017. DOI: <https://doi.org/10.1016/j.apenergy.2017.08.091>

LOPES, M.; GABET, T.; BERNUCCI, L.; MOUILLET, V. Durability of hot and warm asphalt mixtures containing high rates of reclaimed asphalt at laboratory scale. **Materials and Structures**, 2015(48), pp.3937–3948. DOI: <https://doi.org/10.1617/s11527-014-0454-9>

KOGBARA, R. B.; MASAD, E. A.; KASSEM, E.; SCARPAS, A.; ANUPAM, K. A State-of-the-Art Review of Parameters Influencing Measurement and Modeling of Skid Resistance of Asphalt Pavements. **Construction and Building Materials**, Vol.114, p.602-617, 2016. DOI: 10.1016/j.conbuildmat.2016.04.002.

KOGBARA, R. B.; MASAD, E. A.; WOODWARD D.; MILLAR, P. Relating surface texture parameters from close range photogrammetry to Grip-Tester pavement friction measurements. **Construction and Building Materials**, Vol.166, p.227-240, 2018. DOI: [10.1016/j.conbuildmat.2018.01.102](https://doi.org/10.1016/j.conbuildmat.2018.01.102).

KOKKALIS, A. G.; PANAGOULI, O. K. Fractal Evaluation of Pavement Skid Resistance Variations – I: Surface Wetting. **Chaos, Solitons & Fractals**. Vol.9, N.11, pp.1875-1890. 1998. DOI: [https://doi.org/10.1016/S0960-0779\(98\)00185-4](https://doi.org/10.1016/S0960-0779(98)00185-4)

KOUCHAKI, S., ROSHANI, H., PROZZI, J. A., GARCIA, N. Z., & HERNANDEZ, J. B. Field Investigation of Relationship between Pavement Surface Texture and Friction. **Transportation Research Record: Journal of the Transportation Research Board**. Vol. 2672, Issue 40, 2018. DOI: <https://doi.org/10.1177/0361198118777384>

LYON, C.; PERSAUD, B. Safety Effects of Targeted Program to Improve Skid Resistance. **Transportation Research Record: Journal of the Transportation Research Board**, No. 2068, p. 135–140, 2008. DOI: <https://doi.org/10.3141/2068-15>

MASAD, E. A. Aggregate Imaging Measurement System (AIMS): Basics and Applications. Texas Transportation Institute. The Texas A&M University System. Project Performed in Cooperation with the Texas Department of Transportation and the Federal Highway Administration. Report n° FHWA/TX-05/5-1707-01-1. College Station-TX, USA, 2005.

REZAEI, A., HOYT, D., MARTIN, A. E. Simple Laboratory Method for Measuring Pavement Macrotecture. **Transportation Research Record: Journal of the Transportation Research Board**, Vol. 2227, pp. 146-152, 2011. DOI: <https://doi.org/10.3141/2227-16>.

ROAD TRAFFIC TECHNOLOGY. Feature the world’s biggest road networks. Available on <<https://www.roadtraffic-technology.com/features/featurethe-worlds-biggest-road-networks-4159235/>>. Access in 16 September 2019.

ROCHA SEGUNDO, I. R.; DIAS, E. A. L.; FERNANDES, F. D. P.; FREITAS, E. F.; COSTA, M. F.; CARNEIRO, J. O. Photocatalytic asphalt pavement: the physicochemical and rheological impact of TiO₂ nano/microparticles and ZnO microparticles onto the bitumen, **Road Materials and Pavement Design**, Vol. 20:6, pp. 1452-1467. DOI: <https://doi.org/10.1080/14680629.2018.1453371>

SÃO PAULO CITY HALL. **Seminário 2017 – Comissão de Normas**. São Paulo, Brazil. 2017. In Portuguese.

SEGURADORA LÍDER. Relatório Anual de 2019. 2019. Available on: <[https://www.seguradoralider.com.br/Documents/Relatorio-Anual-2019.pdf?#zoom=65%](https://www.seguradoralider.com.br/Documents/Relatorio-Anual-2019.pdf?#zoom=65%>)>. In Portuguese. Access in 8 June 2020.

VEITH, A. G. 1983. Tires – Roads – Rainfall – Vehicles: The Traction Connection. Frictional Interaction of Tire and Pavement, ASTM STP 793, pp.3-40. DOI: <https://doi.org/10.1520/STP28516S>.

WAMBOLD, J.C.; ANTLE, C.E.; HENRY, J.J.; RADO, Z. International PIARC Experiment to Compare and Harmonize Texture and Skid Resistance Measurements. Paris, France. 1995.

WANG, D.; CHEN, X.; OESER, M.; STANJEK, H.; STEINAUER, B. Study of microtexture and skid resistance change of granite slabs during the polishing with the Aachen Polishing Machine. **Wear**, Vol.318, p.1–11. 2014. DOI: <http://doi.org/10.1016/j.wear.2014.06.005>

WANG D.; ZHANG Z.; KOLLMANN J.; OESER M. Development of aggregate microtexture during polishing and correlation with skid resistance. **International Journal of Pavement Engineering**, 2018. DOI: <http://doi.org/10.1080/10298436.2018.1502436>

WILSON, D. J. The Effect of Rainfall and Contaminants on Road Pavement Skid Resistance. Report 515, New Zealand Transport Agency. Wellington, New Zealand, 2013.

WORLD HEALTH ORGANIZATION (WHO). Global Status Report on Road Safety 2018. Geneva, Switzerland. 2018.

Chapter 2

ALDAGARI, S., AL-ASSI, M., KASSEM, E., CHOWDHURY, A., MASAD, E. Development of predictive models for skid resistance of asphalt pavements and seal coat. **International Journal of Pavement Engineering**. DOI: 10.1080/10298436.2020.1766685.

AL ROUSAN, T. M. **Characterization of Aggregate Shape Properties Using a Computer Automated System**. PhD Dissertation. Department of Civil Engineering, Texas A&M University, College Station, TX, USA, 2004.

ARAUJO, V.M.; BESSA, I.S.; CASTELO BRANCO, V.T.F. Measuring skid resistance of hot mix asphalt using the aggregate image measurement system (AIMS). **Construction and Building Materials**, n.98, p.476–481, 2015. DOI: 10.1016/j.conbuildmat.2015.08.117.

ARAUJO, V.M.C; MAIA, R.S.; CASTELO BRANCO, V.T.F; MAIA, A.O.; RODRIGUES, C.B. (2019) Avaliação das Relações entre Propriedades de Forma de Agregados, Compactação, Parâmetros do Esqueleto Mineral e Textura de Revestimentos Asfálticos Aeroportuários a partir do Processamento Digital de Imagens (PDI). **Revista Transportes (Rio de Janeiro)**. Accepted for publication in March 2019. In Portuguese.

APS, M. **Classificação da Aderência Pneu-Pavimento pelo Índice Combinado IFI – International Friction Index para Revestimentos Asfálticos**. PhD Dissertation, Universidade de São Paulo, São Paulo, Brazil, 2006. In Portuguese.

BESSA, I. S., CASTELO BRANCO, V. T. F., SOARES, J. B. Avaliação do Processo de Produção de Agregados por Meio da Utilização Processamento Digital de Imagens. Anais do XXV Congresso de Pesquisa e Ensino em Transportes - ANPET, Belo Horizonte-MG, Brazil, 2011. In Portuguese.

BESSA, I. S. **Avaliação do Processamento Digital de Imagens como Ferramenta para Caracterização de Agregados e Misturas Asfálticas**. Masters' Thesis. Programa de Pós-graduação em Engenharia de Transportes, Universidade Federal do Ceará. Fortaleza, CE, Brazil, 2012. In Portuguese.

CHEN, D.; SEFIDMAZGI, N. R.; BAHIA, H. Exploring the feasibility of evaluating asphalt pavement surface macro-texture using image-based texture analysis method. **Road Materials and Pavement Design**, 16 (2), 405–420. 2015. DOI: <https://doi.org/10.1080/14680629.2015.1016547>

CHEN, B.; ZHANG, X.; YU, J.; WANG, Y. Impact of contact stress distribution on skid resistance of asphalt pavements. **Construction and Building Materials**, Vol.133, pp.330–339, 2017. DOI: <http://dx.doi.org/10.1016/j.conbuildmat.2016.12.078>.

CHEN, J.; HUANG X.; ZHENG, B.; ZHAO, R.; LIU, X.; CAO, Q.; ZHU, S. Real-time identification system of asphalt pavement texture based on the close-range photogrammetry. **Construction and Building Materials**, Vol. 26, P. 910-919, 2019. DOI: <https://doi.org/10.1016/j.conbuildmat.2019.07.321>.

CHOWDHURY, A.; KASSEM, E., ALDAGARI, S.; MASAD, E. Validation of Asphalt Mixture Pavement Skid Prediction Model and Development of Skid Prediction Model for Surface Treatments. Report 0-6746-01-1, Project 0-6746, Texas Department of Transportation, Austin, Texas, USA, 2017.

DEPARTAMENTO NACIONAL DE INFRAESTRUTURA DE TRANSPORTES (DNIT). **Manual de Restauração de Pavimentos Asfálticos**. 2nd. Ed., Rio de Janeiro-RJ, Brazil, 2006. In Portuguese.

DIÓGENES, L. M. **Avaliação das Relações entre Propriedades de Agregados Minerais com base nas Características do Processo de Britagem e da Rocha de Origem**. Masters' Thesis. Programa de Pós-graduação em Engenharia de Transportes, Universidade Federal do Ceará. Fortaleza, CE, Brazil, 2018. In Portuguese.

G1. Reforma da pista central do Aeroporto de Congonhas é concluída em São Paulo. Available on: <<https://g1.globo.com/sp/sao-paulo/noticia/2020/09/03/reforma-da-pista-central-do-aeroporto-de-congonhas-e-concluida-em-sao-paulo.ghtml>> Access in 30 September 2020.

HALL, J. W.; SMITH, K. L.; TITUS-GLOVER, L.; WAMBOLD, J. C.; TAGER, T.J.; RADO, Z. Guide for Pavement Friction, NCHRP Web-Only Document 108. National Cooperative Highway Research Program (NCHRP), Washington-DC, USA, 2009.

IBIAPINA, D. S. **Proposição de um Sistema de Classificação das Propriedades de Forma de agregados caracterizados com o uso do Processamento Digital de Imagens para a seleção de materiais brasileiros**. PhD Dissertation. Universidade Federal do Ceará, Fortaleza, CE, Brazil, 2018. In Portuguese.

KASSEM, E.; AWD, A.; MASAD, E.; LITTLE, D. Development of Predictive Model for Skid Loss of Asphalt Pavements. **Transportation Research Record: Journal of the Transportation Research Board**, No. 2372, Transportation Research Board of the National Academies, Washington, D.C., 2013. DOI: 10.3141/2372-10.

KOKKALIS, A. G.; PANAGOULI, O. K. Fractal Evaluation of Pavement Skid Resistance Variations – I: Surface Wetting. **Chaos, Solitons & Fractals**, Vol. 9, No. 11, pp. 1875-1890, 1998. DOI: [https://doi.org/10.1016/S0960-0779\(97\)00138-0](https://doi.org/10.1016/S0960-0779(97)00138-0)

MASAD, E. A. Aggregate Imaging Measurement System (AIMS): Basics and Applications. Texas Transportation Institute. The Texas A&M University System. Project Performed in Cooperation with the Texas Department of Transportation and the Federal Highway Administration. Report n° FHWA/TX-05/5-1707-01-1. College Station-TX, USA, 2005.

MASAD, E.; LUCE, A.; MAHMOUD, E.; CHOWDHURY, A. Relationship of Aggregate Texture to Asphalt Pavement Skid Resistance Using Image Analysis of Aggregate Shape. Final Report for Highway IDEA Project 114. Washington, DC, 2007.

MASAD, E.; REZAEI, A.; CHOWDHURY, A.; HARRIS, P. Predicting Asphalt Mixture Skid Resistance Based on Aggregate Characteristics. Report No. FHWA/TX-09/0-5627-1. Texas Transportation Institute, The Texas A&M University System, College Station, Texas, 2009.

MASAD, E.; REZAEI, A.; CHOWDHURY, A. Field Evaluation of Asphalt Mixture Skid Resistance and its Relationship to Aggregate Characteristics. Report No. FHWA/TX-11/0-5627-3. Texas Transportation Institute, The Texas A&M University System, College Station, Texas, 2010.

O GLOBO. Santos Dumont reabre no sábado com mais voos. Available on: <<https://oglobo.globo.com/economia/santos-dumont-reabre-no-sabado-com-mais-voos-23953518>> Access in 30 September 2020.

REZAEI, A., HOYT, D., MARTIN, A. E. Simple Laboratory Method for Measuring Pavement Macrottexture. **Transportation Research Record: Journal of the Transportation Research Board**, Vol. 2227, pp.146-152, 2011. DOI: <https://doi.org/10.3141/2227-16>.

SIRIPHUN, S.; CHOTISAKUL, S.; HORPIBULSUK, S. Skid resistance of asphalt concrete at the construction stage based on Thai aggregates. **Journal of Materials in Civil Engineering**, 2016. DOI:10.1061/(ASCE)MT.1943-5533.0001662

SIRIPHUN, S.; HORPIBULSUK, S.; CHOTISAKUL, S.; SUDDEEPPONG, A.; CHINKULKIJNIWAT, A.; ARULRAJAH, A. Effect of cumulative traffic and statistical predictive modelling of field skid resistance. **Road Materials and Pavement Design**, Vol.20 (Issue 2), 2017. DOI:10.1080/14680629.2017.1385511

WAMBOLD, J. C.; ANTLE, C. E.; HENRY, J. J.; RADO, Z. International PIARC Experiment to Compare and Harmonize Texture and Skid Resistance Measurements. Paris, France, 1995.

Chapter 3

AL ROUSAN, T. M. **Characterization of Aggregate Shape Properties Using a Computer Automated System.** PhD Dissertation. Department of Civil Engineering, Texas A&M University, College Station, TX, USA, 2004.

ARAUJO, V.M.; BESSA, I.S.; CASTELO BRANCO, V.T.F. Measuring skid resistance of hot

mix asphalt using the aggregate image measurement system (AIMS). **Construction and Building Materials**, n.98, p.476–481, 2015. DOI: 10.1016/j.conbuildmat.2015.08.117.

ARAUJO, V. M. C. (2017) **Avaliação da Textura de Misturas Asfálticas em face à Compactação para uso em Revestimentos Aeroportuários a partir do uso do Processamento Digital de Imagens**. Masters' Thesis. Programa de Pós-graduação em Engenharia de Transportes, Universidade Federal do Ceará. Fortaleza, CE, Brazil, 2017. In Portuguese.

ARAUJO, V.M.C; MAIA, R.S.; CASTELO BRANCO, V.T.F; MAIA, A.O.; RODRIGUES, C.B. (2019) Avaliação das Relações entre Propriedades de Forma de Agregados, Compactação, Parâmetros do Esqueleto Mineral e Textura de Revestimentos Asfálticos Aeroportuários a partir do Processamento Digital de Imagens (PDI). **Revista Transportes (Rio de Janeiro)**. Accepted for publication in March 2019. In Portuguese.

APS, M. **Classificação da Aderência Pneu-Pavimento pelo Índice Combinado IFI – International Friction Index para Revestimentos Asfálticos**. PhD Dissertation, Universidade de São Paulo, São Paulo, Brazil, 2006. In Portuguese.

BESSA, I. S., CASTELO BRANCO, V. T. F., SOARES, J. B. Avaliação do Processo de Produção de Agregados por Meio da Utilização Processamento Digital de Imagens. Anais do XXV Congresso de Pesquisa e Ensino em Transportes - ANPET, Belo Horizonte-MG, Brazil, 2011. In Portuguese.

BESSA, I. S. **Avaliação do Processamento Digital de Imagens como Ferramenta para Caracterização de Agregados e Misturas Asfálticas**. Masters' Thesis. Programa de Pós-graduação em Engenharia de Transportes, Universidade Federal do Ceará. Fortaleza, CE, Brazil, 2012. In Portuguese.

CASEY, T.; MCGOWAN, R.; MILLAR, P.; WOODWARD, D. Enveloping of Hot Rolled Asphalt Macrotecture Using 3-D Modeling. Transportation Research Board 97th Annual Meeting, Washington-DC, United States, 2018.

DEPARTAMENTO NACIONAL DE INFRAESTRUTURA DE TRANSPORTES (DNIT). **Manual de Restauração de Pavimentos Asfálticos**. 2nd. Ed., Rio de Janeiro-RJ, Brazil, 2006. In Portuguese.

DIÓGENES, L. M. **Avaliação das Relações entre Propriedades de Agregados Minerais com base nas Características do Processo de Britagem e da Rocha de Origem**. Masters' Thesis. Programa de Pós-graduação em Engenharia de Transportes, Universidade Federal do Ceará. Fortaleza, CE, Brazil, 2018. In Portuguese.

CHEN, B.; ZHANG, X.; YU, J.; WANG, Y. Impact of contact stress distribution on skid resistance of asphalt pavements. **Construction and Building Materials**, Vol.133, pp.330–339, 2017. DOI: <http://dx.doi.org/10.1016/j.conbuildmat.2016.12.078>.

CHEN, J.; HUANG X.; ZHENG, B.; ZHAO, R.; LIU, X.; CAO, Q.; ZHU, S. Real-time identification system of asphalt pavement texture based on the close-range photogrammetry. **Construction and Building Materials**, Vol. 26, P. 910-919, 2019. DOI: <https://doi.org/10.1016/j.conbuildmat.2019.07.321>.

CHOWDHURY, A.; KASSEM, E., ALDAGARI, S.; MASAD, E. Validation of Asphalt Mixture Pavement Skid Prediction Model and Development of Skid Prediction Model for Surface Treatments. Report 0-6746-01-1, Project 0-6746, Texas Department of Transportation, Austin, Texas, USA, 2017.

COLONY, D. C. Influence of Traffic, Surface Age and Environment on Skid Number. Final Report Project Number 14460(0). Ohio Department of Transportation. Ohio, 1992.

COSTA, S. L. **Influência da Aderência Pneu-Pavimento nos Conflitos Veiculares Microssimulados**. Masters' Thesis. Programa de Pós-graduação em Engenharia de Transportes, Universidade Federal do Ceará. Fortaleza, CE, Brazil, 2017. In Portuguese.

DO, M. T.; CERESO, V.; ZAHOUANI, H. Laboratory Test to Evaluate the Effect of Contaminants on Road Skid Resistance. **Proceedings of the Institution of Mechanical Engineers, Part J: Journal of Engineering Tribology**, n.228(11), pp.1276-1284, 2014. DOI: <https://doi.org/10.1177%2F1350650114530109>.

DAN, H. C.; HE, L. H.; XU, B. Experimental Investigation on Skid Resistance of Asphalt Pavement Under Various Slippery Conditions. **International Journal of Pavement Engineering**, Vol.18, N.6, pp.1-15, 2017. <https://doi.org/10.1080/10298436.2015.1095901>.

FWA, T. F.; ONG, G. P. Wet-Pavement Hydroplaning Risk and Skid Resistance: Analysis. **Journal of Transportation Engineering**, 2008. Vol.134, N.5, pp.182-190. [https://doi.org/10.1061/\(ASCE\)0733-947X\(2008\)134:5\(182\)](https://doi.org/10.1061/(ASCE)0733-947X(2008)134:5(182)).

HALL, J. W.; SMITH, K. L.; TITUS-GLOVER, L.; WAMBOLD, J. C.; TAGER, T.J.; RADO, Z. Guide for Pavement Friction, NCHRP Web-Only Document 108. National Cooperative Highway Research Program (NCHRP), Washington-DC, USA, 2009.

HARTLEY, R. I.; STURM, P. Triangulation. **Computer Vision and Image Understanding**, Vol. 68, n.2, pp.146–157, 1997. DOI: <https://doi.org/10.1006/cviu.1997.0547>.

HENRY, J. J. Evaluation of Pavement Friction Characteristics – A Synthesis of Highway Practice. NCHRP Synthesis 291. National Cooperative Highway Research Program, Washington D. C., 2000.

IBIAPINA, D. S. **Proposição de um Sistema de Classificação das Propriedades de Forma de agregados caracterizados com o uso do Processamento Digital de Imagens para a seleção de materiais brasileiros**. PhD Dissertation. Universidade Federal do Ceará, Fortaleza, CE, Brazil, 2018. In Portuguese.

KOGBARA, R. B.; MASAD, E. A.; KASSEM, E.; SCARPAS, A.; ANUPAM, K. A State-of-the-Art Review of Parameters Influencing Measurement and Modeling of Skid Resistance of Asphalt Pavements. **Construction and Building Materials**, v.114, p.602-617, 2016. DOI: 10.1016/j.conbuildmat.2016.04.002.

KOGBARA, R. B.; MASAD, E. A.; ANUPAM, K.; SCARPAS, A. GIPTester measurements and texture-friction relationship. In: *Advances in Materials and Pavement Performance Prediction*. Taylor&Francis Group. Doha, Qatar, 2018

KOGBARA, R. B.; MASAD, E. A.; WOODWARD D.; MILLAR, P. Relating surface texture parameters from close range photogrammetry to Grip-Tester pavement friction measurements. **Construction and Building Materials**, v.166, p.227-240, 2018. DOI: 10.1016/j.conbuildmat.2018.01.102.

KOKKALIS, A. G.; PANAGOULI, O. K. Fractal Evaluation of Pavement Skid Resistance Variations – I: Surface Wetting. **Chaos, Solitons & Fractals**, Vol. 9, No. 11, pp. 1875-1890, 1998. DOI: [https://doi.org/10.1016/S0960-0779\(97\)00138-0](https://doi.org/10.1016/S0960-0779(97)00138-0)

KOUCHAKI, S., ROSHANI, H., PROZZI, J. A., GARCIA, N. Z., & HERNANDEZ, J. B. Field Investigation of Relationship between Pavement Surface Texture and Friction. **Transportation Research Record: Journal of the Transportation Research Board**. Vol 2672, Issue 40, 2018. DOI: 10.1177/0361198118777384

MCQUAID, G.; MILLAR, P; WOODWARD, D. A Comparison of Techniques to Determine Surface Texture Data. In Civil Engineering Research in Ireland Conference, Belfast, Ireland, 2014.

MASAD, E. A. Aggregate Imaging Measurement System (AIMS): Basics and Applications. Texas Transportation Institute. The Texas A&M University System. Project Performed in Cooperation with the Texas Department of Transportation and the Federal Highway Administration. Report n° FHWA/TX-05/5-1707-01-1. College Station-TX, USA, 2015.

MEDEIROS, M. S.; UNDERWOOD, B. S.; CASTORENA, C.; RUPNOW, T.; RAWLS, M. 3D Measurement of Pavement Macrotecture Using Digital Stereoscopic Vision. Transportation Research Board 95th Annual Meeting, Washington-DC, United States, 2016.

REZAEI, A., HOYT, D., MARTIN, A. E. Simple Laboratory Method for Measuring Pavement Macrotecture. **Transportation Research Record: Journal of the Transportation Research Board**, Vol. 2227, pp.146-152, 2011. DOI: <https://doi.org/10.3141/2227-16>.

SADEK, H.; MASAD, E.; SIRIN, O.; AL-KHALID, H.; HASSAN K. Performance evaluation of full-scale sections of asphalt pavements in the State of Qatar. **Journal of Performance of Constructed Facilities**, Vol. 29 (5), 2015. DOI: [https://doi.org/10.1061/\(ASCE\)CF.1943-5509.0000627](https://doi.org/10.1061/(ASCE)CF.1943-5509.0000627).

SCHONFELD, R. Pavement surface texture classification and skid resistance photo-interpretation. In The physics of tire traction: Theory and experiment. Boston,-MA, United States, 1974.

SIRIPHUN, S.; CHOTISAKUL, S.; HORPIBULSUK, S. Skid resistance of asphalt concrete at the construction stage based on Thai aggregates. **Journal of Materials in Civil Engineering**, 2016. doi:10.1061/(ASCE)MT.1943-5533.0001662

SIRIPHUN, S.; HORPIBULSUK, S.; CHOTISAKUL, S.; SUDDEEPPONG, A.; CHINKULKIJNIWAT, A.; ARULRAJAH, A. Effect of cumulative traffic and statistical predictive modelling of field skid resistance. **Road Materials and Pavement Design**, Vol.20 (2018) (Issue 2), 2017. DOI:10.1080/14680629.2017.1385511

TIGGS, B.; MCLAUCHLAN, P.; HARTLEY R.; FITZGIBBON, A. Bundle Adjustment - A Modern Synthesis. In: International Workshop on Vision Algorithms, Corfu, Greece, 2000. Springer-Verlag.

UECKERMANN, A.; WANG, D.; OESER, M., STEINAUER, B. A contribution to non-contact skid resistance measurement. *International Journal of Pavement Engineering*, Vol.16, n.7, pp.646–659, 2015. DOI: <http://dx.doi.org/10.1080/10298436.2014.943216>.

VEITH, A. G. Tires – Roads – Rainfall – Vehicles: The Traction Connection. *Frictional Interaction of Tire and Pavement*, ASTM STP 793, p.3-40, 1983. DOI: <https://doi.org/10.1520/STP28516S>.

WAMBOLD, J. C.; ANTLE, C. E.; HENRY, J. J.; RADO, Z. International PIARC Experiment to Compare and Harmonize Texture and Skid Resistance Measurements. Paris, France, 1995.

WANG D.; CHEN, X.; OESER M.; STANJEK, H.; STEINAUER, B. Study of micro-texture and skid resistance change of granite slabs during the polishing with the Aachen Polishing Machine. *Wear*, Vol. 318, p. 1–11, 2014. DOI: <http://dx.doi.org/10.1016/j.wear.2014.06.005>.

WANG D.; ZHANG Z.; KOLLMANN J.; OESER M. Development of aggregate micro-texture during polishing and correlation with skid resistance. **International Journal of Pavement Engineering**, 2018. DOI: 10.1080/10298436.2018.1502436

WILSON, D. J. The Effect of Rainfall and Contaminants on Road Pavement Skid Resistance. Report 515, New Zealand Transport Agency. Wellington, New Zealand, 2013.

Chapter 4

ALDAGARI, S., AL-ASSI, M., KASSEM, E., CHOWDHURY, A., MASAD, E. Development of predictive models for skid resistance of asphalt pavements and seal coat. **International Journal of Pavement Engineering**. DOI: 10.1080/10298436.2020.1766685.

AMUNDSEN, F.; HYDÉN, C. Proceedings: First Workshop on Traffic Conflicts. Institute of Transport Economics. Oslo, Norway, 1977.

APS, M. **Classificação da Aderência Pneu-Pavimento pelo Índice Combinado IFI – International Friction Index para Revestimentos Asfálticos**. PhD Dissertation, Universidade de São Paulo, São Paulo, Brazil, 2006. In Portuguese.

BARCELÓ, J.; DUMONT, A.; MONTERO, L.; PERARNAU, J.; TORDAY, A. Safety Indicators for Microsimulation-Based Assessments. 82nd Annual Meeting of the Transportation Research Board. Washington, D.C., 2003.

CANALE, A. C. **Automobilística: Dinâmica, Desempenho**. Livros Érica, São Paulo, 1989. In portuguese.

CHIN, H. C.; QUEK, S. T. Measurement of Traffic Conflicts. **Safety Science**, Vol. 26(3), p. 169-185, 1997. DOI: [https://doi.org/10.1016/S0925-7535\(97\)00041-6](https://doi.org/10.1016/S0925-7535(97)00041-6).

COOPER, D.; FERGUSON, N. A Conflict Simulation Model. **Traffic Engineering and Control**. Vol.17, pp.306-309. 1976.

COOPER, P. J. Experience with Traffic Conflicts in Canada with Emphasis on “Post Encroachment Time” Techniques. Proceedings of the NATO Advanced Research Workshop on International Calibration Study of Traffic Conflict Technique, 1983.

COSTA, S. L. **Influência da Aderência Pneu-Pavimento nos Conflitos Veiculares Microssimulados**. Masters’ Thesis. Programa de Pós-graduação em Engenharia de Transportes, Universidade Federal do Ceará. Fortaleza, CE, Brazil, 2017. In Portuguese.

CUNTO, F. J. C. **Assessing Safety Performance of Transportation Systems Using Microscopic Simulation**. PhD Dissertation, University of Waterloo, Waterloo, Canada, 2008.

CUNTO, F. J. C.; LOUREIRO, C. F. G. O Uso da Microssimulação na Avaliação do Desempenho da Segurança Viária. **Revista Transportes (Rio de Janeiro)**, v.19, n.3, p.5–1, 2011. DOI: 10.14295/transportes.v19i3.527. In Portuguese.

DIÓGENES, L. M. **Avaliação das Relações entre Propriedades de Agregados Minerais com base nas Características do Processo de Britagem e da Rocha de Origem**. Masters’ Thesis. Programa de Pós-graduação em Engenharia de Transportes, Universidade Federal do Ceará. Fortaleza, CE, Brazil, 2018. In Portuguese.

EL-BASYOUNY, K.; SAYED, T. Safety Performance Functions Using Traffic Conflicts. **Safety Science**, n. 51, p. 160-164, 2013. DOI: <https://doi.org/10.1016/j.ssci.2012.04.015.7>.

ESSA, M.; SAYED, T. Transferability of calibrated microsimulation model parameters for safety assessment using simulated conflicts. **Accident Analysis & Prevention**, vol. 84, pp. 41–53, 2015.

ESSA, M.; SAYED, T. Simulated Traffic Conflicts: Do They Accurately Represent Field-Measured Conflicts? **Transportation Research Record**, n. 2514, p.48–57, 2015. DOI: 10.3141/2514-06.

FARMER, C. M. Reliability of Police-Reported Information for Determining Crash and Injury Severity. **Traffic Injury Prevention**, 2003, n.4, p.38-44, 2003. DOI: <https://doi.org/10.1080/15389580309855>.

FEDERAL HIGHWAY ADMINISTRATION – FHWA. Surrogate Safety Measures from Traffic Simulation Models – Final Report Report No. FHWA-RD-03-050, 2003.

GETTMAN, D.; HEAD, L. **Surrogate Safety Measures from Traffic Simulation Models**. Federal Highway Administration Final Report No. FHWA-RD-03-050. Virginia, United States of America, 2003.

GIUFFRÈ, O., GRANÀ, A., TUMMINELLO, M. L., GIUFFRÈ, T., TRUBIA, S., SFERLAZZA, A., RENCCELJ, M. Evaluation of Roundabout Safety Performance through

Surrogate Safety Measures from Microsimulation. **Journal of Advanced Transportation**, Vol. 2018. DOI: <https://doi.org/10.1155/2018/4915970>.

GUIDO, G.; SACCOMANNO F.; VITALE, A.; ASTARITA, V.; FESTA, D. Comparing Safety Performance Measures Obtained from Video Capture Data. **Journal of Transportation Engineering**. Vol. 137(7). 2011. DOI: 10.1061/(ASCE)TE.1943-5436.0000230.

HAUER, E.; HAKKERT, A. S. The Extent and Implications of Incomplete Accident Reporting. **Transportation Research Record: Journal of the Transportation Research Board**, n.1185, p.1-10, 1989.

HAYWARD, J. C. Near-miss Determination through Use of Scale of Danger. Report No. TTSC-7115, Pennsylvania Transportation and Traffic Safety Center, The Pennsylvania State University. Pennsylvania, 1972.

HUGUENIN, F.; TORDAY, A.; DUMONT, A. G. Evaluation of Traffic Safety Using Microsimulation. 5th Swiss Transport Research Conference (STRC), Ascona, Switzerland, 2005.

HYDÉN, C. The Development of a Method for Traffic Safety Evaluation: The Swedish Traffic Conflicts Technique. Bulletin 70, Department of Traffic Planning and Engineering, Lund University. Lund, Sweden, 1987.

HYDÉN, C. Traffic Safety Work with Video-Processing. Technical Report, Transportation Department, University Kaiserlautern, Kaiserlautern, Germany, 1996.

HUANG, F.; LIU, P.; YU, H.; WANG, W. Identifying if VISSIM Simulation Model and SSAM Provide Reasonable Estimates for Field Measured Traffic Conflicts at Signalized Intersections. **Accident Analysis and Prevention**. N.50, pp.1014-1024. 2013. <https://doi.org/10.1016/j.aap.2012.08.018>

IVEY, D. L.; GRIFFIN, L. I.; NEWTON, T. M.; LYTTON, R. Predicting Wet Weather Accidents. **Accident Analysis and Prevention**, n.13, p.83-91, 1981. DOI: [https://doi.org/10.1016/0001-4575\(81\)90022-1](https://doi.org/10.1016/0001-4575(81)90022-1).

LACERDA, V. M. **Estimação da Velocidade Média em Vias Urbanas com o Uso do Microssimulador VISSIM**. Masters' Thesis. Programa de Pós-graduação em Engenharia de Transportes, Universidade Federal do Ceará. Fortaleza, CE, Brazil, 2016. In Portuguese.

LINDENMANN, H. P. New Findings Regarding the Significance of Pavement Skid Resistance for Road Safety on Swiss Freeways. **Journal of Safety Research**, n. 27, p. 395-400. 2006.

LYON, C.; PERSAUD, B. Safety Effects of Targeted Program to Improve Skid Resistance. **Transportation Research Record: Journal of the Transportation Research Board**, n.2068, p.135–140, 2008. DOI: 10.3141/2068-15.

LYON, C.; PERSAUD, B.; MERRITT, D. Quantifying the safety effects of pavement friction improvements – results from a large-scale study. **International Journal of Pavement Engineering**, Vol. 19(2), p.145-152, 2017. DOI: 10.1080/10298436.2016.1172709

MAIA, R. S., ALECRIM, C. M. C., CASTELO BRANCO, V. T. F., CUNTO, F. J. C. Avaliação do Impacto da Utilização de Revestimentos do Tipo Camada Porosa de Atrito (CPA) no Desempenho da Segurança Viária (Dsv) em Meio Urbano. *In: 33° ANPET - Congresso de Pesquisa e Ensino em Transportes, 2019, Balneário Camboriú - SC. Anais do 33° ANPET - Congresso de Pesquisa e Ensino em Transportes, 2019. In Portuguese.*

MAIA, R. S., ALECRIM, C. M. C., CASTELO BRANCO, V. T. F., ARAUJO, V. M. C., REIS JUNIOR, H. S. Utilização de Revestimentos Drenantes do Tipo Camada Porosa de Atrito (CPA) e de Asfalto Modificado por Polímero (AMP) como Soluções para o Meio Urbano em Fortaleza-CE. *In: 33° ANPET - Congresso de Pesquisa e Ensino em Transportes, 2019, Balneário Camboriú - SC. Anais do 33° ANPET - Congresso de Pesquisa e Ensino em Transportes, 2019. In Portuguese.*

MAIA, R. S., COSTA, S. L., CUNTO, F. J. C., CASTELO BRANCO, V. T. F. Influence of Skid Resistance on Microscopic Simulated Vehicular Conflicts. *In: 99th Annual Meeting of the Transportation Research Board. Washington, D.C., 2020.*

MAYORA, J. M. P.; PIÑA, R. J. An Assessment of the Skid Resistance Effect on Traffic Safety Under Wet-Pavement Conditions. *Accident Analysis and Prevention*, n.41, p.881-886, 2009. DOI: <https://doi.org/10.1016/j.aap.2009.05.004>.

NAJAFI, S.; FLINTSCH, G. W.; MEDINA, A. Linking Roadway Crashes and Tire-Pavement Friction: A Case Study. **International Journal of Pavement Engineering**, 2015. p.1-9, 2015. DOI: <https://doi.org/10.1080/10298436.2015.1039005>.

PERKINS, S. R.; HARRIS, J. I. Traffic Conflict Characteristics – Accident Potential at Intersections. **Highway Research Record**, 1968. N. 225, pp. 35-43.

PTV GROUP. **VISSIM 20 User Manual**. Karlsruhe, Germany, 2020.

PU, L.; JOSHI, R. Surrogate Safety Assessment Model (SSAM): Software User Manual. FHWA Report No. FHWA-HRT-08-050. Virginia, 2008.

RIZENBERGS, R. L.; BURCHETT, J. L.; NAPIER, C. T.; DEACON, J. A. Accidents on Rural Interstate and Parkway Roads and their Relation to Pavement Friction. **Transportation Research Record: Journal of the Transportation Research Board**, n.584, p.22-36, 1976. DOI: <http://dx.doi.org/10.13023/KTC.RR.1972.339>.

TRB – Transportation Research Board. **Highway Capacity Manual**. National Research Council, Washington D. C., United States of America, 2010.

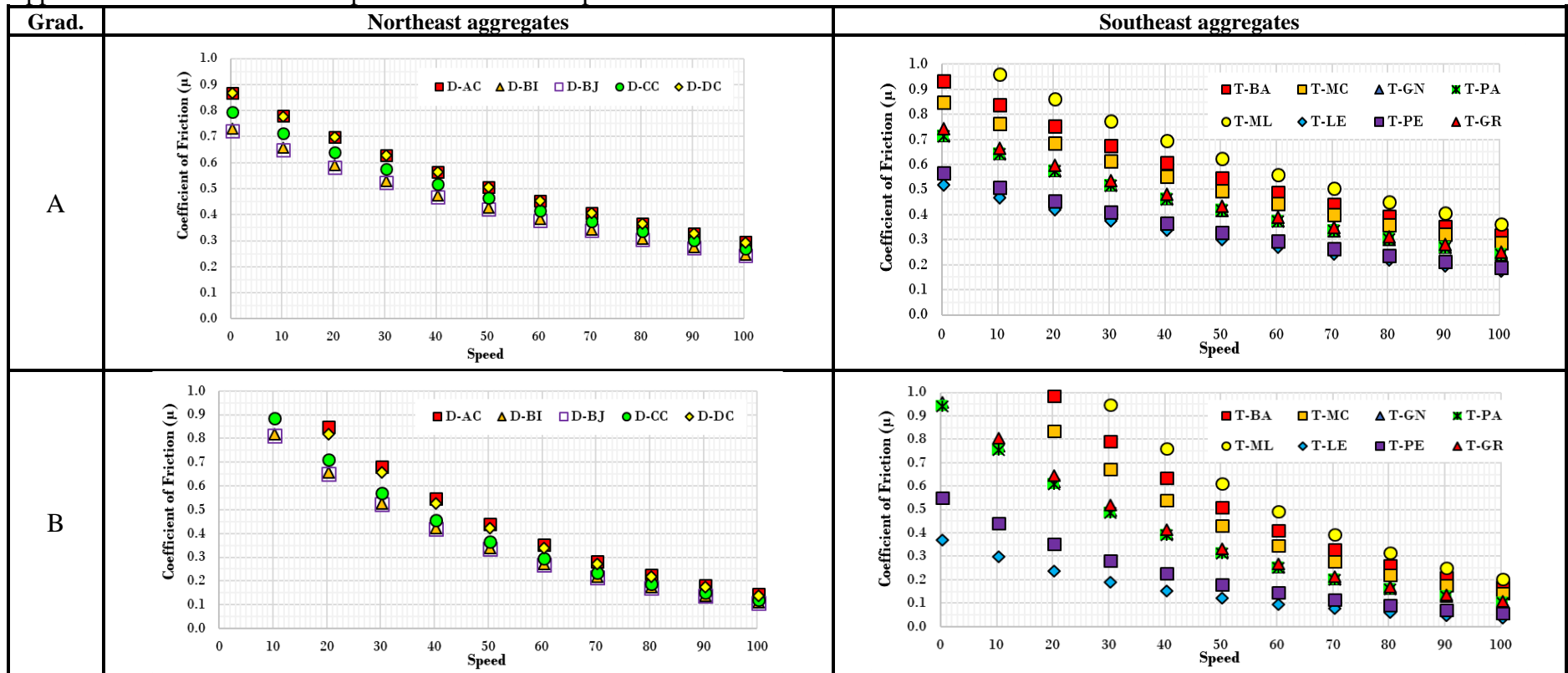
TROTTA, R. P. C. **Quantificação da Degradação Mecânica e Avaliação da Heterogeneidade de Agregados por Processamento Digital de Imagem (PDI)**. Masters' Thesis. Programa de Pós-graduação em Geologia. Instituto de Geociências. Universidade Federal do Rio de Janeiro. Rio de Janeiro, Brazil, 2020. In Portuguese.

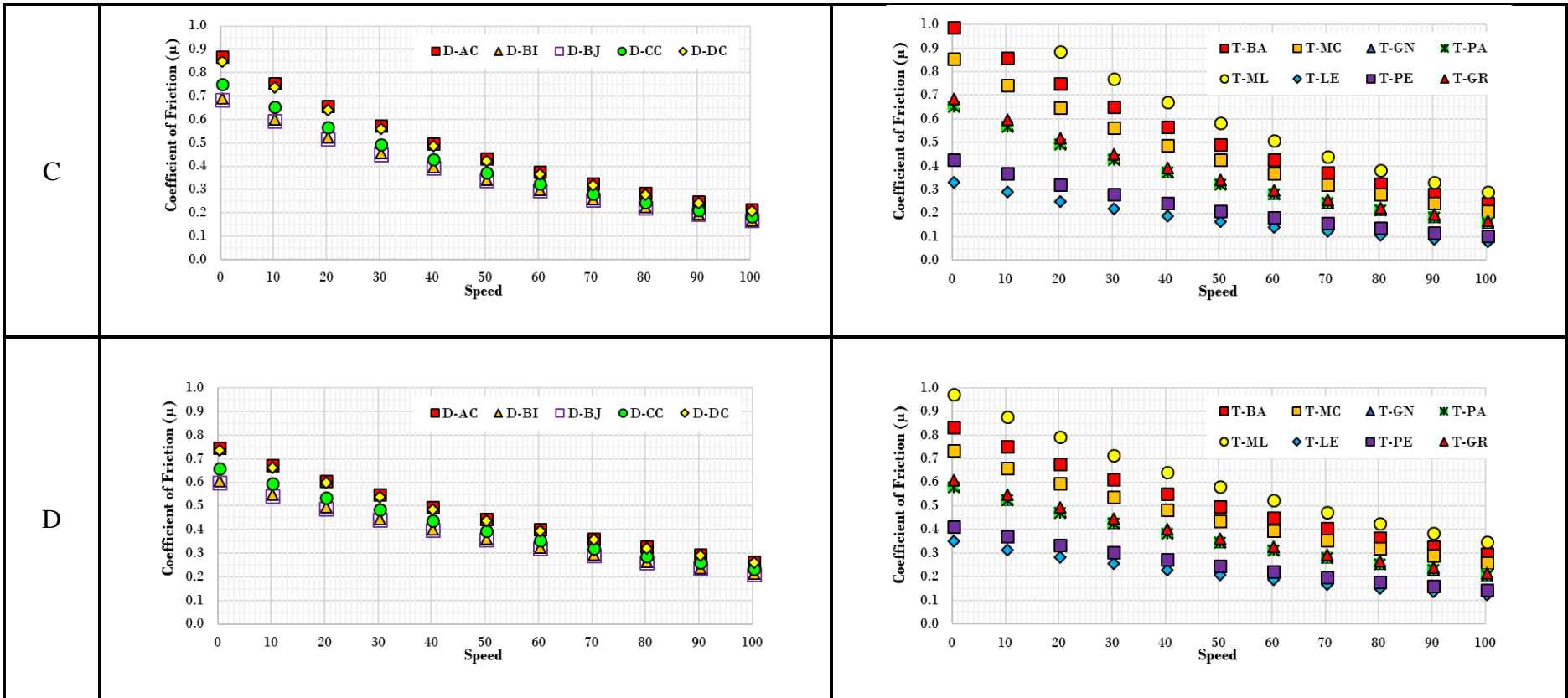
WAMBOLD, J. C.; ANTLE, C. E.; HENRY, J. J.; RADO, Z. International PIARC Experiment to Compare and Harmonize Texture and Skid Resistance Measurements. Paris, France, 1995.

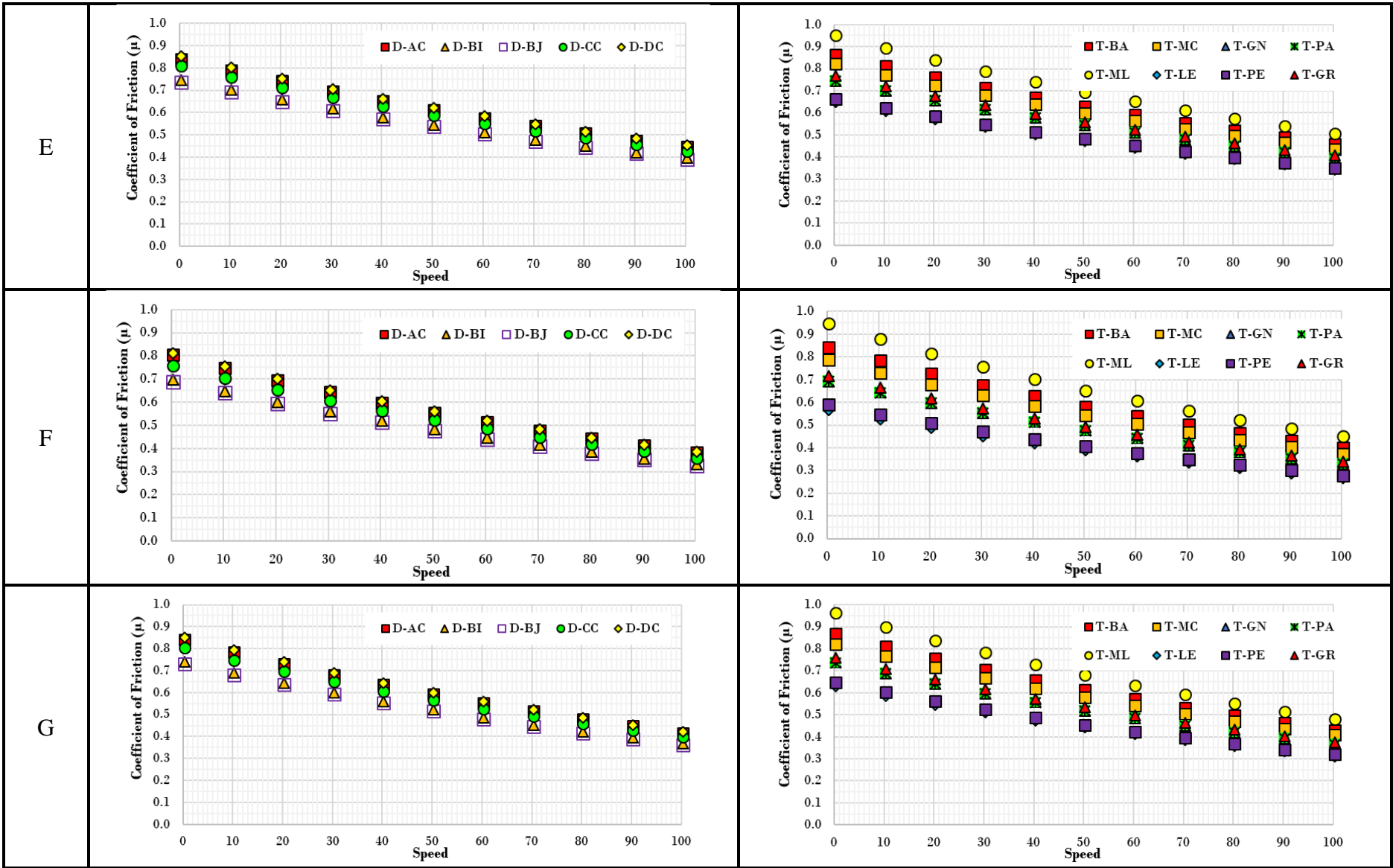
WIEDEMANN, R. **Simulation of road traffic flow**. Technical Report - Institute for Transport and Communication. University of Karlsruhe, Vol. 8, 1974.

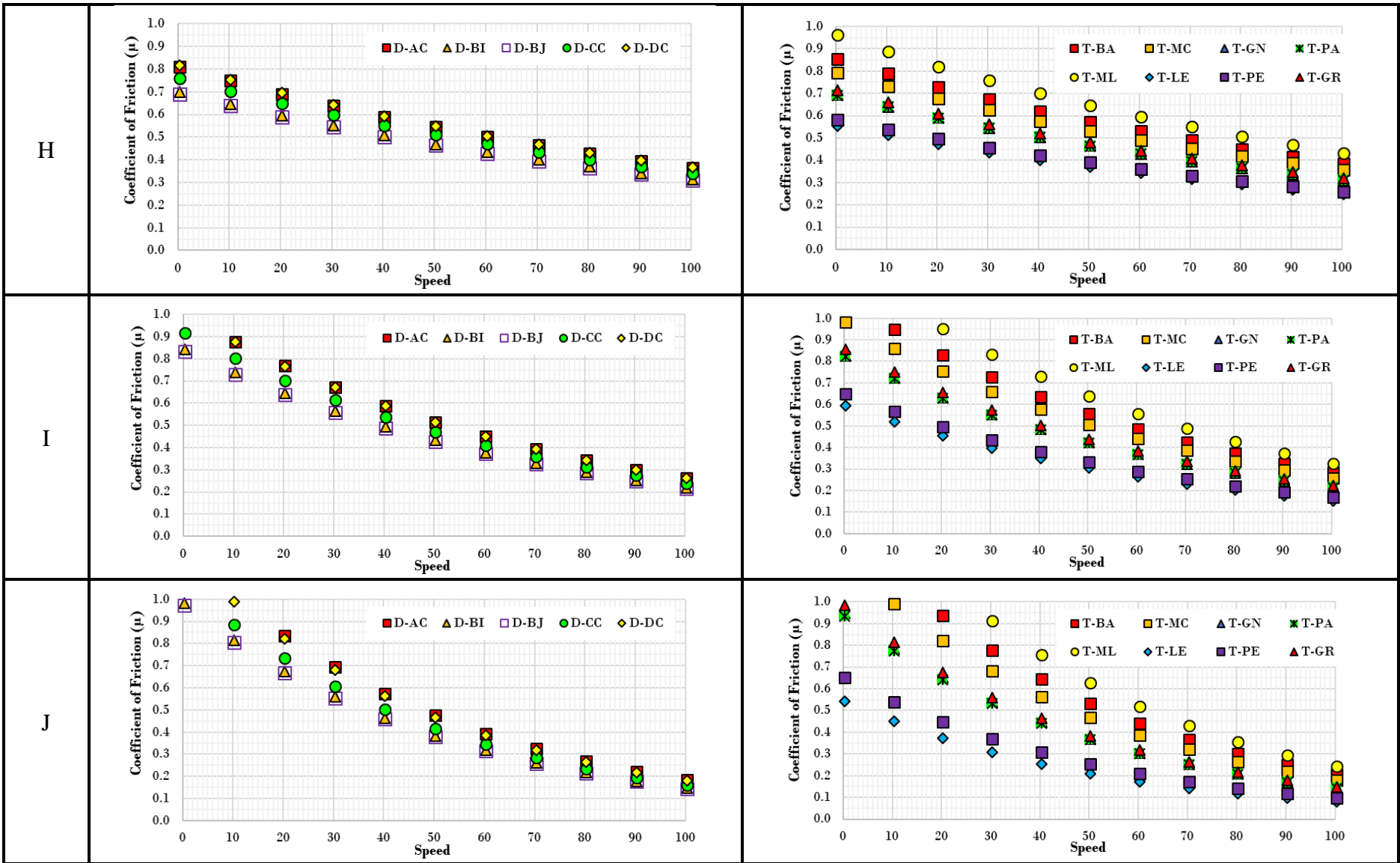
APPENDIX 1 IFI HARMONIZATION

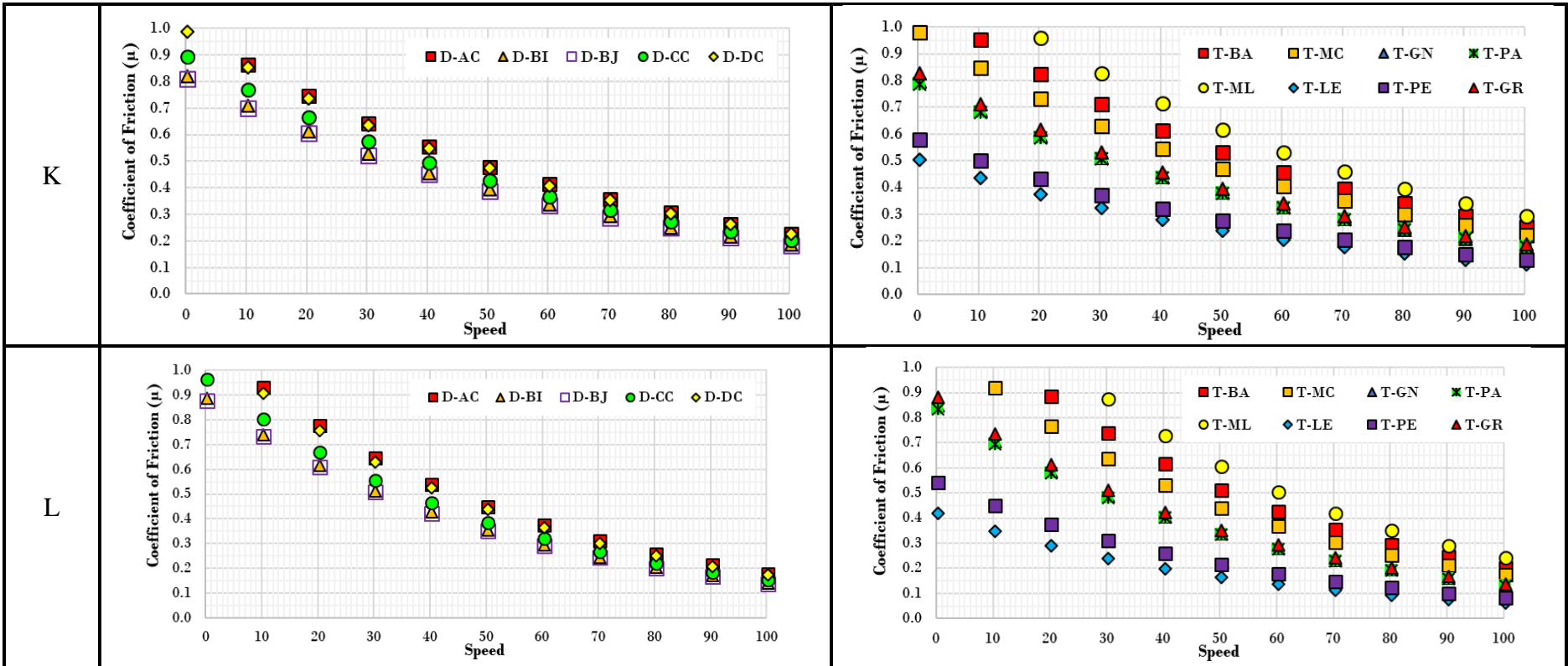
Appendix 1 - Harmonization of predicted IFI *versus* speed.











APPENDIX 2 μ SUGGESTED LIMITS

Appendix 2 - Harmonization of predicted IFI and μ suggested limits.

